The Thesis Committee for Cameron Vitter
Certifies that this is the approved version of the following thesis:

A Generalized Flow Rate Model for Primary Production and an Analysis of Gravity Drainage through Numerical Simulation

APPROVED BY
SUPERVISING COMMITTEE:

Supervisor:

Matthew T. Balhoff

Larry W. Lake

A Generalized Flow Rate Model for Primary Production and an Analysis of Gravity Drainage through Numerical Simulation

by

Cameron Artigues Vitter, BS Chemical Engineering

Thesis

Presented to the Faculty of the Graduate School of

The University of Texas at Austin

in Partial Fulfillment

of the Requirements

for the Degree of

Master of Science in Engineering

The University of Texas at Austin

August 2014

Dedication

I dedicate this thesis to my parents, J. Mark Vitter and Mary W. Vitter.

Acknowledgements

I would like to express my immense gratitude to my advisors, Dr. Matthew T. Balhoff and Dr. Larry W. Lake, for their unbounded enthusiasm and support in the research presented in this thesis. Many brilliant ideas and noteworthy guidance was offered to me in both my times of struggle and my times of success. Throughout this endeavor, I worked alongside members of the Stranded Oil Resources Corporation, especially Phil Lewis, who I would like to thank for their many insights on certain aspects of this work. I would like to express my gratitude to all of those in Department of Petroleum & Geosystems Engineering at The University of Texas at Austin who helped make this effort possible, especially those in Dr. Matthew T. Balhoff's research group and those working on the continued development of the UTCHEM reservoir simulator. Finally, a special thanks goes to Alexis Steger and Joseph Moon, who both helped develop the GFRM during each of their Summer Undergraduate Research Internships (SURI).

Abstract

A Generalized Flow Rate Model for Primary Production & an Analysis of Gravity Drainage through Numerical Simulation

Cameron Artigues Vitter, MS Petroleum Engineering

The University of Texas at Austin, 2014

Supervisors: Matthew T. Balhoff & Larry W. Lake

The age of "easy" oil has steadily declined through the years as many conventional land-based fields have been depleted to residual levels. Novel technologies, however, have reawakened old fields, allowing incremental oil to be added to their recoverable oil in place (ROIP). Underground Gravity Drainage (UGD), an example of one of these technologies, combines improved horizontal and deviated drilling technologies with the longstanding concept of gravity drainage. In this work, a better understanding of gravity drainage has been gained through (1) development of a numerical, three-dimensional, three-phase reservoir simulator (UT-EMPRES), (2) development of a universal, semi-empirical model of production rates through primary depletion, and (3) analysis of the important aspects of gravity drainage through simulation.

UT-EMPRES is a new three-phase, finite-difference reservoir simulator, which utilizes a simple, easy-to-use Microsoft Excel interface to access MATLAB-programmed simulation code. This simulator produces nearly identical results to other well-established simulators, including UTCHEM and CMG. UT-EMPRES has some unique features,

allows for easy post-processing in MATLAB, and has been utilized extensively in the other two areas of this thesis.

The generalized flow rate model (GFRM) is a semi-empirical equation that is used to forecast the dynamic primary production rate of a reservoir with an arbitrary number of wells all operating at the same constant pressure condition. The model is an extension of the classic tank model, which is inherently a single flowing phase development. With the ability to make *a priori* predictions of production figures, users can screen various prospect assets on the basis of economic potential through optimization routines on the GFRM.

Gravity drainage and its approximation through numerical simulation are analyzed. A sensitivity study was conducted on three-phase gravity drainage, leading to the conclusion that small changes in vertical permeability and portions of the relative permeability-saturation relationships can greatly affect production rates. Finally, two-phase (oil and air) and regions of three-phase (water, oil, air) flow simulations were found to exhibit exponential decline in phase production rates, which may enable the GFRM to be applicable to UGD-type processes.

Table of Contents

List of Tables

List of Figures

CHAPTER 1: INTRODUCTION

The need for continued supplies of energy in the form of petroleum fuels has resulted in new methods for exploration and production of oil and gas. New technologies emerge every year to exploit resources at the far ends of the earth and oceans, hydraulically fracture tight formations here in the United States, or flood an existing reservoir with a novel chemical agent. Many of the old, depleted, land-based fields, that formerly fueled much of the nation's energy demands, lack much promise for any traditional further development. Stranded oil in these old reservoirs, which have undergone primary and secondary recovery efforts, amount to an astonishing 400 billion barrels of oil domestically and more than 1.5 trillion barrels world-wide (Kuuskraa, 2004; Moritis, 2006). Fortunately, some of the aforementioned new and improved technologies could be utilized in conjunction with the longstanding concept of gravity drainage to further develop mature fields.

An example of a production scheme in which two technologies, improved deviated drilling techniques and gravity drainage, come together is observed in Laredo Oil's UGD^{TM} – Hyper Down-Spacing^{TM} process. This method takes the form depicted in Figure 1.1. Wells as numerous as hundreds are drilled from beneath the target reservoir up into the payzones. The large exposure surface provided by the great number of wells allows gravity to economically drive remaining mobile oil down through the wells to a collection site. Vent wells are drilled from above the reservoir to permit air to intrude and occupy the pore space that was previously filled with oil and water.

Shale oil and gas and deepwater projects amount to the majority of the new development in the United States; however, gravity drainage production schemes, such as

the UGD™ – Hyper Down-Spacing™ process, could set the stage for a new level of recovery in mature fields here and around the world.

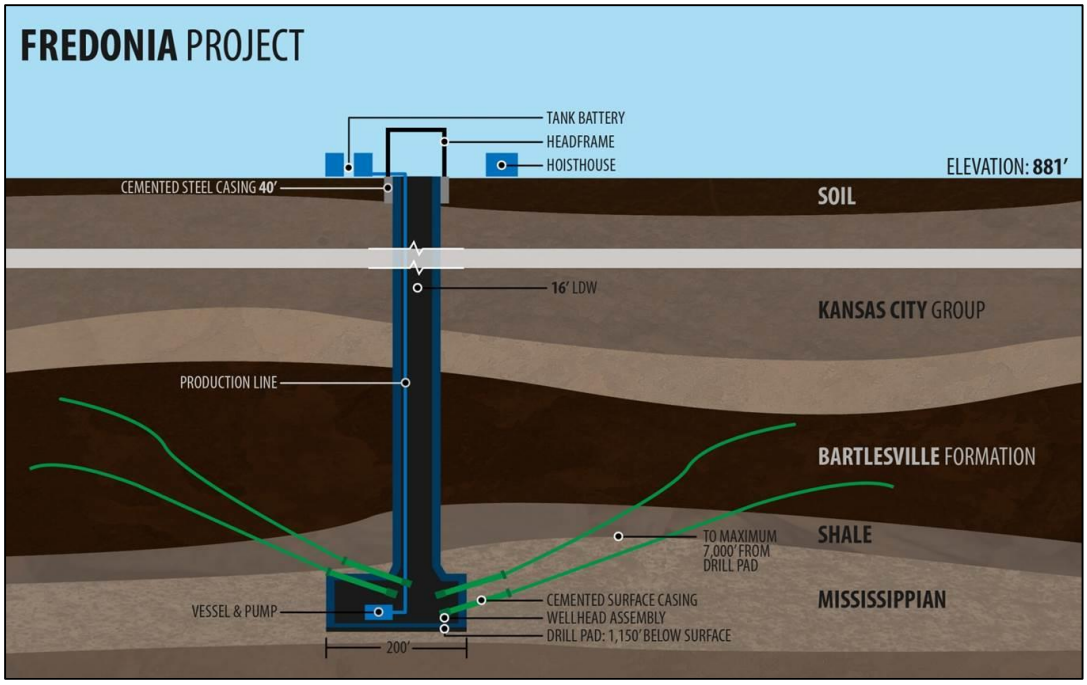

Figure 1.1 Underground Gravity Drainage (UGD) Production Technique, *courtesy Laredo Oil*

Gravity drainage in oil fields has long been recognized as potentially both an important and valuable method of exploiting petroleum reservoirs. Most currently active production schemes in use today do not use gravity to their advantage in propelling fluids from reservoirs. The most difficult and expensive part of extracting hydrocarbons out of the ground, however, is its collection from rigid porous media. Once the petroleum has been released from its confines in the ground, it can easily flow and be processed by engineers. In certain production schemes, the force of gravity can be used to assist in the

drainage process, such as in UGD, which could increase the efficiency and overall success of an asset.

When gravity drainage has been observed in actual oil fields, recovery factors have proven to be exceptionally high compared to most other primary and secondary recovery techniques (Gillham et al., 1996; King and Lee, 1976; Carlson, 1988; Johnston, 1988; Hyatt and Hutchison, 2005). These high ultimate recoveries have drawn much attention to the gravity drainage process and its general applicability to various types of reservoirs.

In order to understand the UGD^{TM} – Hyper Down-Spacing^{TM} process in more detail, three separate research areas were pursued: (1) development of a new numerical reservoir simulator (UT-EMPRES) (2) development of a generalized flow rate model (GFRM) for primary production (3) analysis of important aspects of gravity drainage processes through numerical simulation.

CHAPTER 2: LITERATURE REVIEW

General aspects of primary, secondary, and tertiary recovery are presented in order to place the topics of this thesis. This chapter concludes with a discussion of gravity drainage.

2.1 RESERVOIR DRIVING FORCES

The main three forces acting on the fluids in a reservoir upon production are capillarity, gravity, and the pressure differential imposed at the boundaries of the enclosed reservoir (Leverett, 1940). Capillarity typically has a relatively small impact on production of fluids in a large scale porous medium, such as a field or reservoir. Over smaller dimensions, such as in a rock core, capillary end effect can become very important. Overall movement of fluids in conventional reservoirs, which is the main area of focus in this thesis, typically is not greatly affected by capillarity; however, in using lab experimentation on sand cores, it is necessary to take these forces into consideration in data analysis and transferring information from laboratory scale to field scale.

Gravity is always acting on the fluids in a reservoir in the direction toward the center of the earth. In most petroleum systems, the magnitude of the force of gravity is relatively small in comparison to that levied by imparted internal-external pressure differentials, one reason why gravity is often not considered to enhance production schemes. However, its natural omnipresence makes it potentially appealing as an unconventional recovery method.

Pressure differentials imposed across the boundary of a reservoir are the main driving force used to expel liquids out of rock. Most production schemes make use of either the natural pressure gradients (e.g. solution gas drive, gas cap drive, aquifer drive, etc.) of the reservoir or an artificial anthropogenically-impressed pressure gradient (injected fluids). The utilization of the natural pressure gradient is typically known as pressure depletion in the primary production phase of the lifetime of a field. Reservoir pressure, therefore, occupies a lead role in producing a field, and its maintenance has become an important aspect of production schemes. Pressure maintenance can be executed in many different ways, typically either produced fluid reinjection or introduction of new fluids to a reservoir. The most widely used method of secondary production is the injection of water into a reservoir, which helps increase the pressure of the reservoir and displaces petroleum fluids toward wells.

High reservoir pressure with respect to atmospheric pressure is typically the dominating driving gradient for flow of reservoir fluids out of the reservoir. Even if the reservoir pay thickness is 100 feet, this only amounts approximately to a mere 38 psi head difference from top to bottom of the reservoir, which is relatively small compared to a typical average reservoir. However, when reservoirs have already been depleted to the point that their internal-external pressure gradient is around 100 psi or less, gravity effects in the form of hydrostatic heads begin to assume a more important role in governing flow behavior (Stahl et al., 1942).

2.2 PRIMARY RECOVERY (PRESSURE DEPLETION)

In the primary depletion phase of production, a field typically undergoes four distinct stages of flow behaviors: infinite-acting flow, transitional flow, semi-steady state flow, and depletion flow (Walsh and Lake, 2003). Infinite-acting flow is characterized by inflow into wells as if the reservoir were of infinite extent. When a pressure gradient is imposed on the boundary of a reservoir, a pressure disturbance is felt throughout the reservoir and propagates throughout and to the boundaries of the enclosed reservoir. Infinite-acting flow occurs during the relatively short time in which this pressure disturbance is traveling through the reservoir and its fluids but has not yet reached the boundaries of the reservoir. Typically, this flow stage carries on for a duration of a few days upwards of a few weeks. Infinite-acting flow is well studied and for the simplified case can be described mathematically by an analytical expression. Assuming radial flow, the constant rate of production from an infinite reservoir is described by Equation 2.1 in oilfield units.

$$q = \frac{kh\left(p_e - p_{bhp}\right)}{141.2B\mu\left(\ln\left(\frac{r_e}{r_w}\right) + s\right)} \tag{2.1}$$

In Equation 2.1, k, h, p_e, p_{bhp}, B, μ, r_e, r_w, and s are defined as the permeability, thickness, pressure at the boundary, bottom-hole pressure, formation volume factor, viscosity, radius at the boundary, radius of the well, and well skin, respectively.

After this initial equilibration of the pressure disturbance comes the transitional flow period, in which the pressure profile of the reservoir is evolving toward a semi-steady

flow regime. Transitional flow is not well understood and does not have any simple mathematical description associated with it. The stage of flow behavior that exists between infinite-acting and semi-steady state flow has a duration shorter than that of infinite-acting flow.

The third stage of flow behavior in pressure depletion is semi-steady state flow. This regime is characterized by a continuous movement between a series of pressure profile steady states. Throughout these states, the entire reservoir uniformly decreases in pressure at the same constant rate, which is dictated by a necessary constant rate condition, imposed by a constant rate well. This flow regime has a duration that is only exceeded by the final stage of primary recovery, depletion flow.

Depletion flow is characterized by the well or wells transitioning from a constant rate operation to their minimum bottom-hole pressure, which will remain constant throughout the remainder of the life of the reservoir in the primary production phase of development. The specified minimum bottom-hole pressure of the well is dependent on several factors in the reservoir, especially if artificial influences such as lifting devices are incorporated into the well assembly. Since the majority of the primary production phase of development occurs in the depletion flow regime, it wields the most amount of focus in this study.

Flow of fluids from a porous medium due to internal-external pressure differentials imposed by a point or line source, such as a well, has been studied extensively (Van Everdingen and Hurst, 1949; Matthews et al., 1954; Ramey and Cobb, 1971). For simplicity, a cylindrical geometry is typically chosen with a single vertical well extending

through the entire thickness of the reservoir. It is also assumed at the beginning that only one slightly compressible fluid phase is flowing in a homogeneous reservoir. Due to this selection of petroleum system, a relatively simple mathematical description of transient nature of the fluid flow can be prescribed for infinite-acting and semi-steady state flow regimes (Van Everdingen and Hurst, 1949). The transient solution for a single constant pressure well in the center of a closed cylindrical reservoir was also presented; however, its infinite summation of Bessel functions is of relative complexity.

The constant pressure well solution also does not apply to cases with more than one well in a reservoir, as does the constant rate well solution coupled with the superposition principle. None of this existing theory can be employed since the interest of this thesis lies in a solution to cases with multiple constant pressure wells.

In semi-steady state flow, the reservoir pressure profile has equilibrated into a series of constantly changing steady states known as stabilized flow. This progression through steady states allows mathematical descriptions of the relationship between the fluid flow rate and the pressure drop. Due to this relationship, well models can be developed based on the concept of a well productivity index. Fortunately, semi-steady state flow and depletion flow regimes have very similar dynamic relations, which can be captured through the same well models. These simplifications lay out some of the basic assumptions and methods used in our study of primary production.

In the development of the well productivity index, a traditional derivation begins with the radial diffusivity equation (Equation 2.2).

$$\frac{1}{r}\frac{\partial}{\partial r}\left(r\frac{\partial P}{\partial r}\right)=\frac{\partial P}{\partial t} \tag{2.2}$$

The semi-steady state condition for pressure change (Equation 2.3) is then imposed on the radial diffusivity equation to arrive at Equation 2.4. In Equations 2.2 through 2.4, P, r, t, q, c, r_e, h, and ϕ are variables representing the pressure, radial coordinate, time, volumetric flow rate, compressibility, radial extent to reservoir boundary, thickness of the reservoir, and the porosity, respectively. Manipulations and simplifications are made to transform Equation 2.4 to Equation 2.5. Through the use of the Dietz shape factor, C_A, the Equation 2.5 is generalized for non-cylindrical geometries forming Equation 2.6. Additional variables introduced in Equations 2.5 and 2.6 include $P_{average}$, $P_{bhp,w}$, q_w, μ, k, r_w, s_w, A, and γ, which represent the average reservoir pressure, the bottom-hole pressure at a well, flow rate from a well, viscosity, permeability, radius of a well, skin of a well, areal extent of the reservoir, and the exponential of Euler's constant, respectively.

$$\frac{\partial P}{\partial t}=-\frac{q}{c\pi r_e^2 h\phi} \tag{2.3}$$

$$\frac{1}{r}\frac{\partial}{\partial r}\left(r\frac{\partial P}{\partial r}\right)=-\frac{q}{c\pi r_e^2 h\phi} \tag{2.4}$$

$$P_{average}-P_{bhp,w}=\frac{q_w\mu}{2\pi kh}\left(\ln\left(\frac{r_e}{r_w}\right)-\frac{3}{4}+s_w\right) \tag{2.5}$$

$$P_{average}-P_{bhp,w}=\frac{q_w\mu}{2\pi kh}\left(\frac{1}{2}\ln\left(\frac{4A}{\gamma C_A r_w^2}\right)+s_w\right) \tag{2.6}$$

Simple manipulations and unit conversions of Equation 2.6 are performed to establish the form of the well productivity index in Equation 2.7, which relates the

production rate to the pressure drop of the well (Equation 2.8). In Equations 2. 7 and 2.8, J_w represents the productivity index of a well.

$$J_w = \frac{0.00708hk}{\mu\left(\frac{1}{2}\ln\left(\frac{A}{r_w^2 C_A}\right) + 5.75 + s_w\right)} \tag{2.7}$$

$$q_w = \frac{J_w(P_{average} - P_{bhp,w})}{B} \tag{2.8}$$

Tank models are typically simple, single-cell formulations of entire reservoirs which are used to capture the overall behavior in the depletion stage of production (Walsh and Lake, 2003). These models make use of the radial diffusivity equation with several simplifying assumptions, as have been outlined above, yielding a tractable formulation for production figures. The reservoir is assumed to be isothermal with at most three fluid components in at most two fluid phases at reservoir conditions. If there are two phases in the reservoir, they are completely immiscible and only one of the phases can flow. Finally, the production of fluids from reservoir to surface is described by the deliverability relationship in Equation 2.9, which is based on the formation volume factor, the well productivity index and a difference between the average reservoir pressure and the assigned bottom-hole pressure condition of the well. $B_{average}$ is the average formation volume factor, which in the proceeding development is assumed to hold a value of one.

$$q = \frac{\sum_{w=1}^{N_w} J_w\left(P_{average} - P_{bhp,w}\right)}{B_{average}} \tag{2.9}$$

Based on the simplifying assumptions of the tank model, numerous results ensue. Pressure is predicted to decline exponentially with time. The production rate is proportional to the permeability, the reservoir thickness, the number of wells, and the inverse of the flowing fluid viscosity. The production rate itself declines at a constant rate, known as the decay rate. The decay rate is proportional to the number of wells, the productivity index, the inverse of the pore volume, and the inverse of the total fluid compressibility (Equation 2.10). A given rate is approached at a time inversely proportional to the decay constant. Finally, the volume of fluids recovered through an average reservoir pressure drop is proportional to the reservoir pore volume and total fluid compressibility. Equation 2.11 is a result of pressure declining exponentially and previous equations stated above. In Equations 2.10 and 2.11, N_w, $\lambda_{analytical}$, V_p, c_t, P_i, and q_i represent the number of wells in the reservoir, the analytical expression for the decay rate, the pore volume of the reservoir, the total compressibility, the initial pressure of the reservoir, and the total initial flow rate from the reservoir.

$$\lambda_{analytical} = \frac{\sum_{w=1}^{N_w} J_w}{V_p c_t} \tag{2.10}$$

$$\frac{\sum_{w=1}^{N_w} J_w (P_{average} - P_{bhp,w})}{\sum_{w=1}^{N_w} J_w (P_i - P_{bhp,w})} = \frac{q}{q_i} = \exp\left(-\lambda_{analytical} t\right) \tag{2.11}$$

If a few more assumptions about the hydrocarbon system are made, the equations can collapse to even simpler equations. First, the reservoir is assumed to have homogeneous properties such as porosity and permeability. Second, if more than one well is modeled, all wells are assumed to have identical bottom-hole pressure conditions and are reasonable well-spaced. With these two assumptions, Equations 2.9 through 2.11 further simplify to Equations 2.12 through 2.14, respectively. The variable *J* represents the productivity index of a single well in the reservoir.

$$q = \frac{N_w J \left(P_{average} - P_{bhp} \right)}{B_{average}} \tag{2.12}$$

$$\lambda_{analytical} = \frac{N_w J}{V_p c_t} \tag{2.13}$$

$$\frac{P_{average} - P_{bhp}}{P_i - P_{bhp}} = \frac{q}{q_i} = \exp\left(-\lambda_{analytical} t \right) \tag{2.14}$$

These simplified tank model equations provide us with the foundation for this study of primary production with regard to the flow behavior of the depletion stage of flow. In order to account for the preceding stages of flow, the simplified tank model equation must be modified to obtain a generalized flow model equation.

The tank model has been developed with the underlying assumption of the deliverability relation expressed in Equation 2.12. This relationship between flow rate out of the reservoir and pressure drop is only valid during semi-steady state flow and depletion

flow regimes. Therefore, the deliverability relation is not valid during the stages of flow leading up to depletion flow. Another inherent assumption of the deliverability relation is the well productivity index. The analytical expression for this quantity is a function of a shape factor and a drainage area. If one allows more than one well to flow in a reservoir, the wells interact much like wells interacting with a boundary. Due to this interaction, drainage areas for individual wells effectively become smaller than the entire reservoir. Therefore, the number of wells in a given reservoir serves as an important quantity, which dictates various aspects of the overall flow rate behavior of a primary production system.

2.3 SECONDARY RECOVERY (FLUID DISPLACEMENT)

Aside from the traditional pressure depletion stage of production, there is the approach to production by means of displacement. One fluid, either naturally occurring in a porous medium or injected, is used to displace another fluid phase in hopes of increasing production. The classic and most common type of this production style is seen in waterflooding processes. Naturally occurring fluids, which can serve as displacing agents, can come in the form of an encroaching aquifer or expanding gas cap. The displacement mechanism is the cornerstone of most secondary recovery techniques and therefore warrants attention as a necessary and valuable area to investigate.

The displacement mechanism, as it pertains to porous media, was first explored by Buckley and Leverett with their fundamental theory that mathematically describes the displacement process of one incompressible fluid phase by another incompressible, immiscible phase (Buckley and Leverett, 1941). In this initial assessment of displacement

theory, fractional flow theory is employed as well as a neglect of capillarity. Relative permeability functions for each fluid phase are described in such a way that the saturation is taken as the only variable, which allows the same to be true of the fractional flow variable.

The mathematical formulation developed includes the traditional mass balance of the fluid phases together with the assumptions stated above. A one-dimensional displacement is assumed, and the problem is rendered dimensionless through the use of the reservoir length as well as the pore volume of the reservoir. The method of characteristics is then used to achieve a specific velocity of constant saturation points. Through this quantity, the saturation of one of the phases can be described as a function of the spatial and temporal variables.

A common occurrence in this mathematical formulation is an inflection in the fractional flow curve, which mathematically amounts to a triple-valued region in the saturation profiles. This multi-valued region is not physically valid and must be dealt with in such a way that approximates the actual saturation profiles. The method of characteristics is often used in the study of waves and other similar physical phenomena. This multi-valued region can be described as part of a sharpening wave, whereby a "shock" or discontinuity in the saturation function is placed in space, such that the material balance of the two phases is satisfied. These discontinuities are commonplace in the study of waves and the broader classification of hyperbolic partial differential equations. Discontinuities, however, are never truly seen in these types of systems; rather, dissipative forces, such as capillarity, diffusion, and compressibility, play a role in smoothing out these shocks.

Displacement efficiency can be obtained by subtracting the ratio of average saturation of the displaced fluid at the point in time to the initial saturation from one. In order to get the average saturation, however, it is required that an integration of saturation over distance be performed. A clever approach to this integration was discovered by Welge, which served to broaden Buckley and Leverett's theory (Welge, 1947). The use of wave theory to study Buckley and Leverett's work has elucidated that the traditional shock displacement is a combination of a spreading wave (upstream of the shock) and a sharpening wave (at and downstream of the shock). The use of wave theory has largely broadened and unified the study of EOR displacement processes, in general, from simple immiscible displacements to complex miscible displacements (Lake, 2010).

2.4 Mathematical Development of Tertiary Recovery (Fluid Displacement)

Guzman and Fayers (1997) presented a mathematical analysis of the extension of Buckley-Leverett theory to three immiscible phases. Just as fractional flow theory and method of characteristics was used in Buckley-Leverett's solution (1941), Guzman and Fayers use a generalized form of these principles to extend the solution to three-phase systems. Guzman and Fayers are concerned with the mathematical behavior of the different solutions. These solutions are constructed through using various descriptions of the relative permeability of the separate three phases. Wave equations in their broad form are a subset of the hyperbolic differential equations. Depending on the functional relationship between the relative permeability of each phase and its saturation, solutions to the three-phase Buckley-Leverett problem vary in their hyperbolic behavior. Strict

hyperbolic behavior seems to be valued in the mathematical modeling of hyperbolic-type processes. Most relative permeability models yielded behavior that is not strictly hyperbolic in nature, often elliptic with umbilic points. Guzman and Fayers note that the functional form of the relative permeability model plays a large role in exhibiting the behavior of the solution.

2.5 Gravity Drainage and its Relevance in EOR

Three driving forces dictate the flow of fluids in reservoirs: gravitation, capillarity, and internal-external pressure differentials. This thesis first focuses on internal-external pressure differentials in primary production then moves to the force of gravity and its influence on Enhanced Oil Recovery (EOR) methods.

Gravitation is an omnipresent force during hydrocarbon recovery; however, internal-external pressure differentials typically take the lead role in causing fluids to flow in reservoir rock. In the early history of the petroleum production, the majority of hydrocarbons were exploited through the natural geological pressurization of the fluids within the earth. Most targeted reservoirs were easily accessible and contained rock that allowed fluids to flow easily into wells. As decades passed, the natural pressure in the reservoirs began to deplete causing lower production rates that eventually approached zero. With the technology of the age, petroleum engineers exhausted most of the accessible hydrocarbon systems known at the time. It was well known that fluids still occupied these depleted reservoirs, and the demand for petroleum products continued to grow. Due to this demand, secondary recovery and EOR techniques began to take form. Pressure

maintenance and pumping techniques became popular. The most common forms of displacement-type secondary recovery took the form of injecting water or gases into produced reservoirs. With the internal-external pressure differentials exhausted in these reservoirs, the force of gravity became a more important factor in driving fluid flow.

After fields began to become depleted, EOR techniques took on a large number of styles and production schemes. The types of fluids mainly used are water and a variety of gases. Thermal recovery techniques also played a key role in improved recovery from certain reservoirs. As secondary and EOR displacement-type techniques gained popularity in industry, research interests took hold to mathematically develop the physical phenomena at work in these processes. Buckley and Leverett (1941), as a result, initiated the foundation of displacement theory, which has been further developed ever since.

Displacement techniques involve two or more fluid phases, which naturally tend to segregate due to the force of gravity. Fluid phase interface stability became an important factor in the overall success of displacement processes. Stability research resulted in Dietz stability analysis as well as the vertical equilibrium assumption which simplified a vast number of production scheme configurations. With the concern of stability as well as relative permeability, researchers developed a method to circumvent some of these issues, miscible displacements (Kulkarni, 2006). Potential candidates for miscible fluids are carbon dioxide and light hydrocarbons at the proper pressures and temperatures. Miscible gas displacements have gained vast popularity in industry over immiscible gas displacements and are now used in most gas EOR projects.

The number of projects that utilize injection of immiscible gases, i.e. air, nitrogen, carbon dioxide, and light hydrocarbons, for displacement has declined in the last few decades (Kulkarni, 2004). The advancement of directional drilling techniques has opened up a window of opportunity for different types of EOR projects to become economically feasible. Horizontal wells allowed for greater contact area with the reservoir as well as lower drawdown pressures in the near-wellbore region, which helped to alleviate some stability problems. Higher injectivity and productivity indices also became possible, which increased the maximum stable volumetric rate of injection and production. Immiscible gas displacement processes, therefore, have become more economically viable and warrant further research. Along with an investigation of primary production, the main focus of this thesis involves immiscible gas displacement EOR.

2.6 TRADITIONAL GRAVITY DRAINAGE THEORY

Gravity drainage can be classified as fluid flow through porous media such that gravity is the main driving force. With this definition, gravity drainage can take on two different general types, free gravity drainage and forced gravity drainage. Free gravity drainage is simply fluid flow solely under the influence of gravity. Forced gravity drainage is fluid flow through the influence of gravity as well as another external force, typically in the form of an impressed pressure by a displacing fluid phase. If another phase is displacing the phase of interest under forced conditions, the physical problem ought to be cast in terms of a displacement following the general theory of Buckley and Leverett (1941). On the other hand, free flow gravity drainage is not a true displacement problem

even though another fluid phase is involved. Gas does in fact invade the reservoir; however, it merely fills the voids which were originally occupied by the draining fluid phase. Cardwell and Parsons (1948) have developed a theory of free-flowing gravity drainage for a single draining phase. Both Buckley and Leverett and Cardwell and Parsons assume that the fluid phases involved are incompressible and immiscible. This assumption greatly simplifies the mathematics governing the individual processes. Cardwell and Parsons also have made the assumption that capillarity is not explicitly captured in their model, further simplifying the equations. Many researchers expanded upon the foundational mathematical formulations of these two groups of authors. Terwilliger et al. (1951) have combined the two theories in the hopes of agreement with laboratory steady-state results. Simplifying assumptions include a steady-state relative permeability as well as a constant capillary pressure. Through the work of Terwilliger and his colleagues, a gravity drainage reference rate, or maximum rate, has been established.

Hall (1961) presented a method for calculating gravity drainage performance with the help of an IBM 650 computer program. The program presented is rather elementary compared to present-day numerical reservoir simulation programs; however, Hall made one of the first efforts to understand gravity drainage through simulation practices. Much like Hall's work, results discussed in this thesis were obtained through numerical simulation.

Around the early 1960s, many skeptics were concerned about the validity of modeling counterflows through Darcy's equation and Buckley-Leverett theory. Templeton (1962) put some of these concerns to rest after conducting several counterflow experiments

and monitoring the pressure and saturation profiles with time. He concluded that this method of modeling counterflows was indeed acceptable so long as one knew *a priori* the capillary pressure and relative permeability behavior of the fluids. Although most of Templeton's experiments were conducted in a closed setting, he did touch on gravity drainage in his efforts to form capillary pressure and relative permeability data. Counterflows can be important in characterizing certain gravity drainage process and may play a key role in field development with this recovery technique.

Unlike most researchers who were focused on forced gravity drainage, Dykstra (1978) expanded upon Cardwell and Parsons' theory by including an initial immobile gas saturation as well as incorporating an oil relative permeability, which tends toward a value of zero at residual oil saturation rather than zero saturation. He also used three examples to illustrate how the theory could be put in practice along with his newly-discovered recovery equation, which makes use of his idea of a drainage modulus with a constriction coefficient. His constriction coefficient attempts to capture the productivity constraint of well outflow from wellbores in comparison to the traditional entire reservoir boundary. Dykstra points out that there is much work left to be done but focuses his attention on the variables controlling the drainage rates that can be manipulated by producers: effective oil permeability, viscosity, and well spacing. Based on the assumptions that each well in a field has its own distinct drainage area, an optimum well spacing, based on economics, could be found for free flow gravity drainage field projects.

In 1980, Hagoort attempted to reconcile differences in Buckley-Leverett and Cardwell-Parsons theories by assuming negligible capillarity and that the mobilities of the

gas and oil phases in the shock front were equivalent. These assumptions simplified the fractional flow equation used in Buckley-Leverett theory and allowed Hagoort to formulate an equation equivalent to that found by Cardwell and Parsons (assuming the gas phase is stagnant). With a simple model for relative permeability, Hagoort predicted the cumulative recovery by gravity drainage and found that most of the oil recovered was done so before gas breakthrough. He noted that the crucial variables in this process were the dimensionless time defined, gravity number, and oil relative permeability. Hagoort then goes on to mention the importance of experimentation for calculating relative permeabilities and his distrust in the conventional viscous-displacement method. He holds two reservations toward this technique. He first claims that gas-liquid interfaces inherently yield to instabilities, which would go against the method's inherent flat interface assumption. Second, Hagoort was concerned that the capillary end effect would have adverse effects on the displacement process. With these two objections to the current method, Hagoort devised his own method for measuring relative permeabilities by experimentation through centrifugal force. He goes on to substantiate his method through the Dombrowski-Brownell number, which is defined as the ratio of gravity to interfacial forces on a pore basis (Hagoort, 1980). His insistence on the importance of the relative permeability relations is referenced throughout this thesis.

Dykstra (1992) expanded on his drainage modulus concept with the help of Wade Dickinson. The two researchers compared recovery by gravity drainage through vertical versus horizontal wells. The use of Dykstra's constriction coefficient was again applied for each type of well showing that horizontal wells had a larger constriction coefficient

value than that of vertical wells. Through his study, Dykstra showed that this difference in constriction coefficient value tended to decrease with time for various conditions.

Butler (1992) conducted some work on gravity drainage to horizontal wells. Horizontal wells had become quite popular due to their increased exposure to the reservoir and resulting higher productivity indices as compared to vertical wells. Following his previous work, Butler looked at the effect of well pattern on well rates. He determined that horizontal wells drain at critical rates, depending on the area of the well pattern. Horizontal wells in many cases can produce flow equivalent to a vertical fracture in the same position. When many horizontal wells are placed in close proximity, the overall effect of the wells can tend toward a horizontal fracture in the region that the wells are draining. With this in mind, Butler came up with an approximate economically-optimal well spacing for horizontals: about twice the height of the reservoir. Butler intended much of this research to be applied to heavy oil recovery efforts; however, he commented that there could be great potential for horizontal wells in light oil gravity drainage efforts.

Li and Horne (2003) developed an empirical model for free flow gravity drainage. These two researchers concluded that after over half a century of research on gravity drainage, no analytical model captured the process adequately. Li and Horne started by obtaining the general behavior of the production rate by using a modified version of the empirical model suggested by Aronofsky et al (1958). They utilized some relations governing capillary-gravity equilibrium in the development of their equation. The model must be tuned by individual production data to get reasonable results. The analysis of change in production with both pore size distribution index and capillary entry pressure

was used in the formation of a finalized model, which does a does indeed capture the flow behavior of many different field and laboratory scale processes. Li and Horne note that there are many similarities between the processes of gravity drainage and spontaneous imbibition, for instance, both involve only the forces of gravity and capillarity. The Li and Horne empirical equation is fairly popular in industry; however, further research must be conducted to develop an analytical model for free flow gravity drainage.

Rao et al. (2006) published the results of their work in conjunction with the Department of Energy (DOE) on the gas-assisted gravity drainage (GAGD) process. The authors approached the development of the process through dimensional and mechanistic studies, scaled physical experimentation studies, and conceptual studies. Through dimensional and mechanistic studies, the authors identified several multiphase and fluid dynamic mechanisms governing the overall GAGD process. The majority of the authors' contributions came in the form of scaled experiments. Through laboratory coreflood experiments, the authors showed that GAGD can be superior to more commonplace production schemes, such as continuous gas injection (CGI), water alternating gas (WAG) and Hybrid-WAG. Both miscible and immiscible GAGD were studied, and it was noted that immiscible GAGD can be comparable in performance to miscible GAGD in several applications. Through their studies, the authors noted that reservoir heterogeneity did not affect the performance of GAGD. Through their work with long cores, Rao et al. demonstrated that early gas breakthrough does not affect the ultimate oil recovery such that the injection rate is below the critical injection rate. Conceptual studies by Kulkarni and Rao (2006) touched on modification of existing models as well as development of novel

ideas. The Li and Horne model was modified by including the Z_e* parameter in order to better fit forced GAGD processes. Z_e*, which attempts to account for forced constant pressure injection, is an adjusted version of the original Z_e, which is defined as the depth corresponding to capillary entry pressure (Li and Horne, 2003).

Rao et al. touched on the development of a new mechanistic understanding of post gas breakthrough production in terms of film flow phenomenon and extraction mechanism. Conceptual discoveries from the authors included a new dimensionless number, which can be used to predict overall GAGD performance for both miscible and immiscible GAGD processes. The new dimensionless number is a single function of the capillary, gravity, and viscous forces. Rao et al. have overall increased the knowledge base of the GAGD process.

2.7 Small Scale Phenomena in Gravity Drainage

Dumore and Schols (1974) conducted several two-phase and three-phase drainage experiments in hopes of elucidating a dimensionless capillary pressure function. Three-phase experiments were conducted in water-wet rocks under connate water conditions. After long drainage times, it was observed that oil saturations declined to very low values if capillary pressures between oil and gas phases were relatively high. Experiments were conducted with spontaneously spreading and non-spreading oils, both resulting with similar behavior. Due to these high interfacial tension conditions, a continuous oil phase may result located in between gas and connate water phases. Under the force of gravity, this continuous oil film may flow under "film flow", yielding potentially minute residual

oil saturations. This concept of film flow may play an important part in the recovery efficiency of the gravity drainage process.

Dumore and Schols foundational studies on film flows were repeated in similar experiments by several other researchers. Although often higher recoveries for spontaneously spreading oils were observed, similar results were obtained, and an interest in visualizing the films themselves ensued. Several authors conducted micromodel experiments to directly witness the oil film flow; however, oil films only developed for those which spontaneously spread. This result seemed to contradict those from the rock drainage experiments, especially in Dumore and Schols's work. In 1988, Kantzas et al. set out to display that the high recoveries in gravity drainage could be dependent upon the stability of these oil films as opposed to the spreading nature of the oil between the water and gas phases. Stability of these oil films could, therefore, exist for both spontaneously spreading and non-spreading oils in core experiments due to capillary forces as an oil bank migrates through the rock. The more complicated pore surfaces within the rocks allows for enhanced stability through capillary forces over those seen in glass micromodels. Therefore, the stability of the films was declared as the important variable which dictated the recovery efficiency of the gravity drainage process.

Blunt et al. (1994) further investigated oil film stability and the forces at work in these types of processes. They attempted to look into the intermolecular forces, interaction energy between the three separate phases, and resulting disjoining pressures. Structural forces were found to play an important role in the stability of film thicknesses approaching the size of the molecules themselves. A situation may result in which a non-spreading oil

forms a film at the trailing edge of an oil bank due to a gas flood. The drainage history, therefore, is a critical determinant of film stability for non-spreading oils. The thinning of a thick layer or bank of oil may result in a stable oil film within the gas-invaded zone. This drainage history for non-spreading oils provides another reason why glass micromodels do not allow non-spreading oil films to form. Flow rates through molecular films are typically discarded as negligible. These films, however, allow for the oil phase to be connected and continuous in pressure. Thus, a gas flood may result in oil films swelling, and this swelling phenomenon could yield higher flow rates.

In 1989, Delshad and Pope compared seven different three-phase relative permeability models. The overall analysis of these models, some of which were new and some of which were traditional, shows that most three-phase permeability models do not capture experimental behavior very well. The new models in this paper perform as well or better than the more traditional models. Describing relative permeability for three-phase systems seems to be quite a challenge, which has only been accomplished to an adequate degree. Sufficiently modeling the relative permeability of a three-phase gravity drainage process may amount to an even bigger challenge because of the complexity resulting from the physical processes at hand. The relative permeability model is therefore very important.

2.8 SCALING ANALYSIS

Scaling is the act of extrapolating physical phenomena seen in one system to that of another system of similar yet different size. In 1914, Buckingham published his work

on the theory of dimensional analysis, in which all individual relevant variables of a physical process are grouped into a linearly independent set of dimensionless products. By preserving the value of these dimensionless products from one physical size system to another, one can extrapolate resulting physical phenomena from the first system to the second. This style of scaling physical phenomena is called Buckingham PI Theory. In 1935, Ruark published his theory on inspectional analysis, which extends the theory of Buckingham to mathematical formulations, typically differential equations and their associated boundary and initial conditions. While dimensional analysis does yield a set of linearly independent dimensionless groups, they are not unique. Inspectional analysis, on the other hand, forms unique groups which are typically more physically representative of the process of interest.

The use of scaling in scientific and engineering analysis has become quite popular. Laboratory experimental results can often be extended to predict field scale processes to a reasonable degree of certainty. Since scaling analysis amasses individual parameters into dimensionless groups, sensitivity studies on given physical processes can be carried out in a more efficient manner, whether it be in the laboratory or through numerical simulation. Scaling analysis, therefore, has been utilized extensively in this research.

CHAPTER 3: METHOD

3.1 UT-EMPRES

An Excel-interfaced, MATLAB-based numerical reservoir simulator has been developed using the classic finite difference approach to numerically approximate physical phenomena. Fluid flow and transport in porous media is approximated through a numerical treatment of general conservation equations and auxiliary relationships, such as Darcy's law. The numerical schemes utilized are the classic and improved IMPES formulations, which are implicit in their treatment of solving for pressure and explicit in their treatment of solving for phase saturations (Chen, 2007).

The simulator can be used to solve up to three distinct, immiscible phases. These phases are modeled as slightly compressible fluids with constant viscosities. Relative permeability is an important contributor to the inherent ability of a fluid phase to flow in a reservoir. Relative permeability is modeled empirically through the general model functional form given by Corey and Brooks (Corey, 1954) for two-phase systems and the extended formulation for three-phase systems. Heterogeneous properties of the reservoir and fluid phases can be inputted and used in UT-EMPRES.

UT-EMPRES allows users to run reservoir simulations with the power of MATLAB from a simple Microsoft Excel interface, which is shown in Figure 3.1. UT-EMPRES, which is discussed further in the User's Manual in Chapter 6, was developed by Cameron Vitter and Dr. Matthew T. Balhoff and is the culmination of efforts to fulfill the first objective of this thesis.

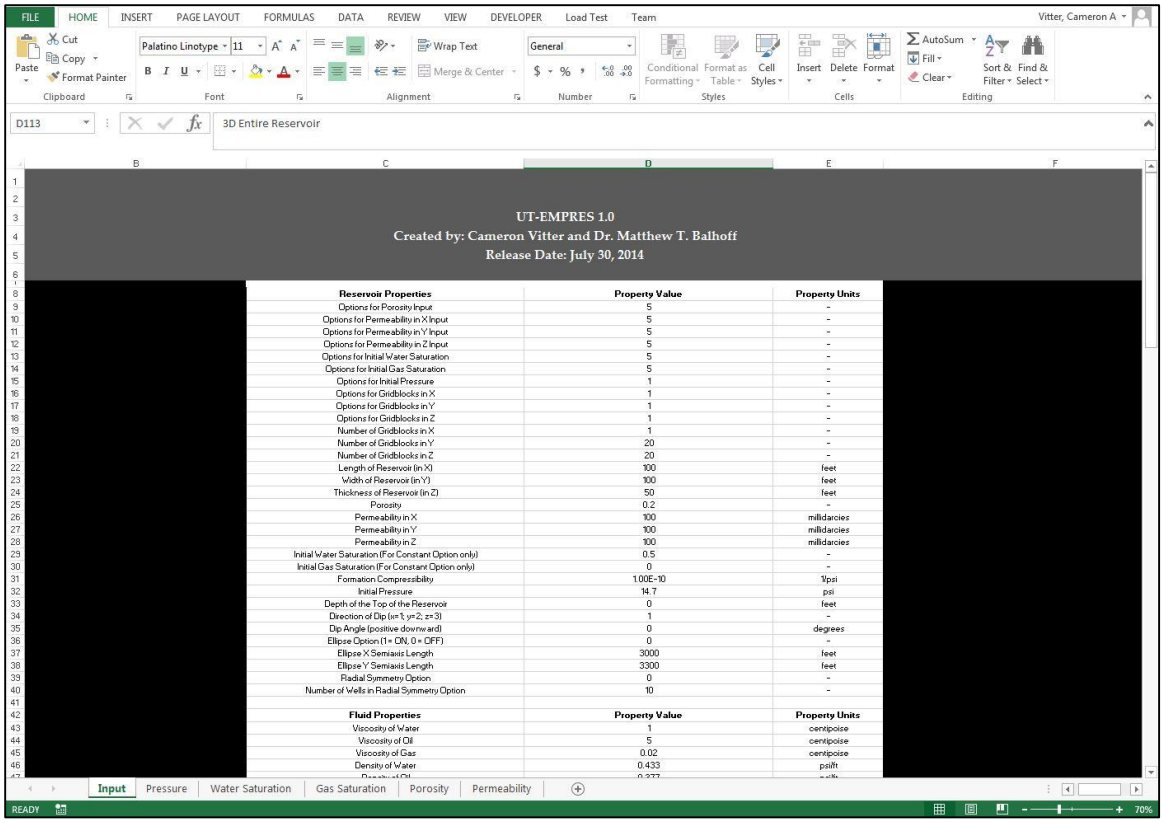

Figure 3.1 Excel interface for the UT-EMPRES simulator

3.2 GENERALIZED FLOW RATE MODEL

The second objective of this thesis is to create a universal, semi-empirical equation which captures the overall production rate from a reservoir with an arbitrary number of wells that operate at the same constant bottom-hole pressure. Figure 3.2 illustrates the general form of the production forecast (rate versus time) on a log-linear plot. The initial stage of production, which encompasses both the infinite-acting and transitional flow regimes, has been deemed the pre-depletion stage, which has no analytical solution for

cases of more than one well. The depletion stage of production is marked by its linear functionality on a log-linear plot, which is attributable to its exponential decline character. The tank model (Equation 2.14) exhibits this exponential functional form and is used as the foundation for the functional form of the depletion phase in the GFRM.

It was first conceived that the two flow stages, pre-depletion and depletion, could be modeled by two separate functional forms, $f_{pre\text{-}dep}$ and f_{dep}, respectively, then linked together at their transition time by damping exponentials. As defined in Equation 3.1, the time variable, t, has been scaled to its dimensionless form, t_D, by the time at which the transition from pre-depletion to depletion stage occurs, t_{dep}. In Equation 3.2, the dimensionless volumetric flow rate, q_D, is formed by scaling the volumetric flow rate, q, by q_{tdep}, which is the flow rate at the transition time. The proposed form of the generalized flow model equation is given in Equation 3.3.

$$t_D = \frac{t}{t_{dep}} \tag{3.1}$$

$$q_D = \frac{q}{q_{t_{dep}}} \tag{3.2}$$

$$q_D = f_{pre-dep} e^{-t_D} + f_{dep}\left(1 - e^{-t_D}\right) \tag{3.3}$$

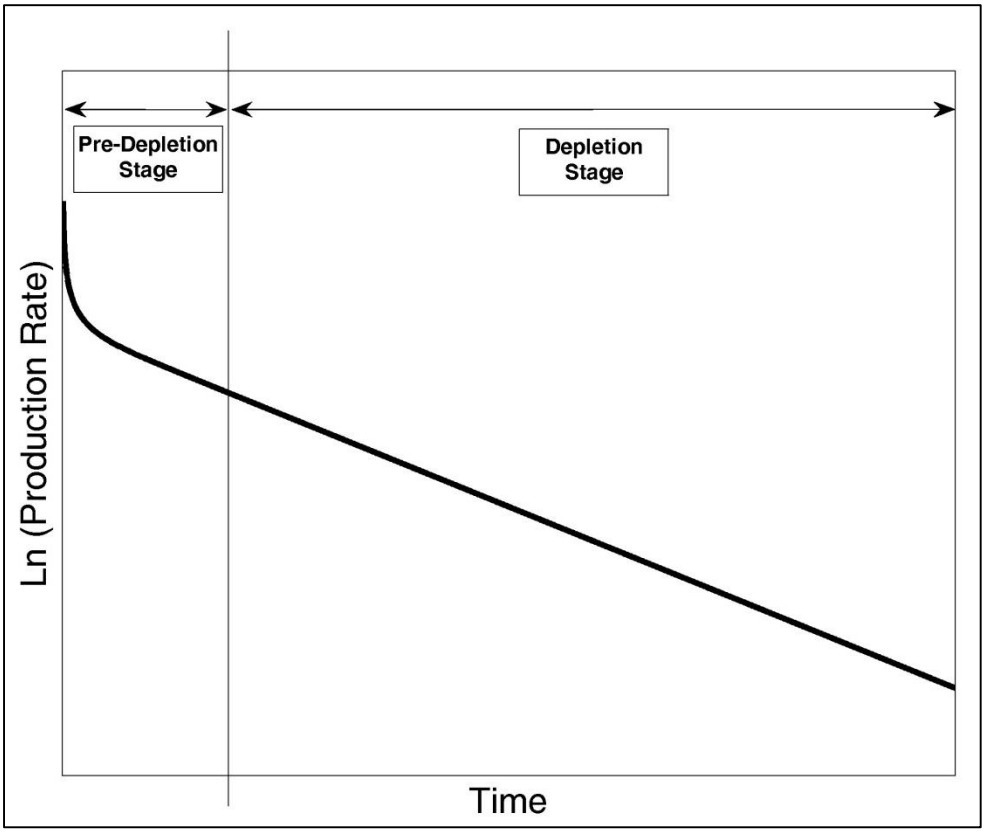

Figure 3.2 General form of primary production forecast for a reservoir with one or more constant pressure production wells

There are several ways to capture the pre-depletion stage of primary production. A decline curve analysis approach has been selected, in which a power law functional form is introduced (Equation 3.4). A modified form of the tank model with a horizontal (Equation 3.5) has been selected to preserve the exponential decline character of the depletion stage of primary production.

$$f_{pre-dep} = t_D^b \tag{3.4}$$

$$f_{dep} = \exp\left(-\lambda\left(t_D - 1\right)t_{dep}\right) \tag{3.5}$$

Equations 3.3, 3.4, and 3.5 are combined to form the functional form of the GFRM (Equation 3.6). The flow regimes that are captured in the model are the infinite-acting, transitional, and depletion regimes. In Equation 3.6, parameters b, λ, t_{dep}, and q_{tdep} represent the pre-depletion parameter, the decay rate, the time at which depletion begins, and the production rate at which depletion begins, respectively.

$$q_D = \left(t_D{}^b\right)e^{-t_D} + \left(\exp\left[-\lambda\left(t_D - 1\right)t_{dep}\right]\right)\left(1 - e^{-t_D}\right) \tag{3.6}$$

Since the generalized flow rate model is only semi-empirical in nature, data must be acquired in order to fit the equation with output parameters b, λ, t_{dep}, and q_{tdep} in order to adequately capture the behavior of a large range of hydrocarbon primary production systems. Many key reservoir and fluid input properties govern the overall flow rate from a given system. Each property must be studied individually in order to elucidate its influence on a given system. By keeping all others constant, one can study the effects of a given property. Since this type of real-world reservoir case study data is not readily available, computer simulations were used to gather data, which serve as close approximations to real-world cases.

The two simulators used were UTCHEM and UT-EMPRES. Through the use of these two simulators, over 2000 single-phase simulations were run by varying reservoir and fluid properties. The model form of Equation 3.6 fit numerical production data well in all simulation cases when b, λ, t_{dep}, and q_{tdep} were treated as fitting parameters.

Due to the general theory on the pressure depletion phase of production, flow behavior is indicative of pressure interactions. In the simplest case, a single well interacts with the boundary of a reservoir, causing flow behavior to transition with time between the main regimes of infinite-acting, transitional, semi-steady state, and depletion flows. Since it has been assumed that all wells operate under constant pressure conditions, only infinite-acting, transitional, and depletion flow regimes are observed. If more than one well or a complicated boundary geometry is introduced to the system, the transitions between flow regimes becomes more complex. After running several simulations, the number of wells in the simulation proved to be the most nonlinear property which caused complexity in the flow behavior. Due to this complexity, the generalized flow rate model has been rendered dimensionless, and the fitting parameters are scaled functions of the number of wells in the system. Therefore, all key input properties were studied individually, holding all others constant with the exception of the number of wells, which allowed for a functional dependence.

The key properties studied are reservoir, fluid, and operational properties. The eight key input properties presented here are viscosity, thickness of the reservoir, total compressibility, difference in initial reservoir and operating pressures, areal extent of the reservoir, porosity, permeability, and the number of wells. The reservoir properties are the thickness of the reservoir, the areal extent of the reservoir, porosity, and permeability. The total compressibility has both reservoir and fluid property character since it is a sum of the formation and fluid compressibilities. The difference in initial and operating pressures has both fluid and operational property character because it is a difference in the initial fluid

pressure and the operating character. Viscosity is a fluid property, and the number of wells is an operational property. All of these key properties influence the behavior of the flow rate from the system in all flow regimes.

The fitting parameters, as mentioned previously, are scaled functions of the number of wells. There are four scaled fitting parameters within the generalized flow rate model, and they are described by Equations 3.7 through 3.10.

$$b \tag{3.7}$$

$$\lambda^* = \frac{\lambda}{\lambda_{analytical}} \tag{3.8}$$

$$t_{dep}{}^* = \frac{t_{dep}}{t_{dep,analytical}} \tag{3.9}$$

$$q_{t_{dep}}{}^* = \frac{q_{t_{dep}}}{q_{t_{dep},analytical}} \tag{3.10}$$

All of the parameters were cast in dimensionless form with careful consideration to the key properties affecting their behavior. The first parameter, b, is used to capture the pre-depletion stage of production. Another two of the four parameters, t_{dep}* and q_{tdep}*, are used to preserve key data at the transition from the pre-depletion stage to the depletion stage. Finally, the parameter λ* is used to capture the decay rate of the depletion stage of production.

The parameter characterizing the pre-depletion stage of production is a constant exponent within the power law functional form of Equation 3.4. These two parameters are purely empirical and are already dimensionless.

There are two parameters preserving information about the transition between pre-depletion and depletion stages. The first, t_{dep}*, is a function of the time at which the depletion stage begins as observed by simulation, which is described in Equation 3.9. This parameter was scaled with a definition (Equation 3.11) of the analytical solution of the approximate time at which the depletion phase of production begins (Ramey and Cobb, 1971).

$$t_{dep,analytical} = \frac{(0.1)\phi\mu A c_t}{(6.33E-3)k} \tag{3.11}$$

The parameter q_{tdep}* is a function of the flow rate at the time when the depletion stage begins, as seen in Equation 3.10. This parameter has been scaled by the analytical solution of the initial flow rate from the tank model, as described in Equation 3.12.

$$q_{t_{dep},analytical} = J_{analytical} N_w \left(P_{initial} - P_{bhp}\right) \tag{3.12}$$

The sole parameter dictating the depletion stage flow behavior, λ*, is a function of the decay rate of the depletion stage of production as observed from simulation. In Equation 3.8, this parameter is scaled by the analytical expression for the decay rate of the tank model, as seen in Equation 3.13.

$$\lambda_{analytical} = \frac{J_{analytical} N_w}{c_t V_p} \tag{3.13}$$

All four fitting parameters are obtained through simulation output of production rate as a function of time. Each simulation is analyzed in a methodical manner. First, the time at which the depletion stage begins is found through the use of the general overall productivity index, *J*, definition (Bertuzzi et al. 1987) in Equation 3.14.

$$J = \frac{q}{\left(P_{average} - P_{bhp}\right)} \tag{3.14}$$

The simulation flow rate, average reservoir pressure, and constant well pressure are used in Equation 3.14. The resulting overall productivity index as a function of time can then be used to find the time at which depletion stage begins. The depletion stage of production is distinguished by a constant productivity index. When plotted versus time, the overall productivity index begins at a relatively high value then asymptotically approaches a final constant value. This final constant value is the overall productivity index of the depletion stage of production. Therefore, in order to obtain the time at which the depletion stage begins, one must approximate the time at which the overall productivity index is equivalent to the constant depletion stage overall productivity index. This is done through an algorithm which selects the data point with the largest value of overall productivity index that is also less than a given tolerance. This tolerance value is set by multiplying the constant depletion stage overall productivity index value by 1.001. Once the approximate time at which the depletion stage of production begins is obtained, the flow rate at this time can easily be acquired from the simulation output data. The fitting parameter which captures the information at the pre-depletion/depletion stage transition can be found through Equations 3.9. The transition point between the pre-depletion and

depletion stages of production has now been marked, and information from each stage can now be gathered.

The pre-depletion stage is described through Equation 3.8, which is linearized to form Equation 3.15. A least-squares regression routine is used to fit the simulation output data within the pre-depletion stage to the functional form of Equation 3.15. The parameter of the pre-depletion stage has now been found.

$$\ln\left(q_D\right) = b \tag{3.15}$$

The depletion stage flow behavior is governed by the exponential decay rate. Simulation output during the depletion stage is used to acquire this value through Equation 3.16. The time at the end of the simulation (any time after the depletion phase has begun) is denoted as t_{end}.

$$\lambda = \frac{\ln\left(\frac{q_{t_{dep}}}{q_{t_{end}}}\right)}{t_{end} - t_{dep}} \tag{3.16}$$

When the exponential decay rate is found, the single parameter of the depletion stage is obtained through Equation 3.8.

Once the values of all four parameters are acquired for all of the simulations in the database, the data for each fitting parameter is regressed to a unique functional form by one or more of the following: (1) the number of wells in the simulations (2) the areal extent of the reservoir (3) the diffusivity. The functional forms are presented in section 4.2.

3.3 GRAVITY DRAINAGE

The investigation of gravity drainage was conducted through numerical simulation in this thesis. The two simulators UTCHEM and UT-EMPRES were used extensively to understand some of the key variables which determine production rates in free fall gravity drainage processes. A validation of Darcy's law was performed through simulation. Many three-phase flow simulations were performed to elucidate interesting three-phase phenomena.

In order to study free fall gravity drainage processes, the initial and boundary conditions of the process must coincide with those of real world problems. Therefore, the initial condition within the reservoir should allow for nothing more than pressurization of the fluids via gravity pressure head. Boundary conditions included well(s) placed at the top and bottom of the reservoirs, all operating at atmospheric conditions. A few cases of forced gravity drainage were simulated by employing a slightly higher constant pressure operating conditions for those wells situated at the top of the reservoir.

Both single dimensional and multidimensional simulations were run to analyze the gravity drainage process. In single dimensional simulations, the only two wells in the reservoir were always situated in vertical alignment. A depiction of the gravity stable pressure distribution from a single dimensional simulation can be seen in Figure 3.3. In multidimensional simulations, however, this alignment was not always achieved, yielding different results.

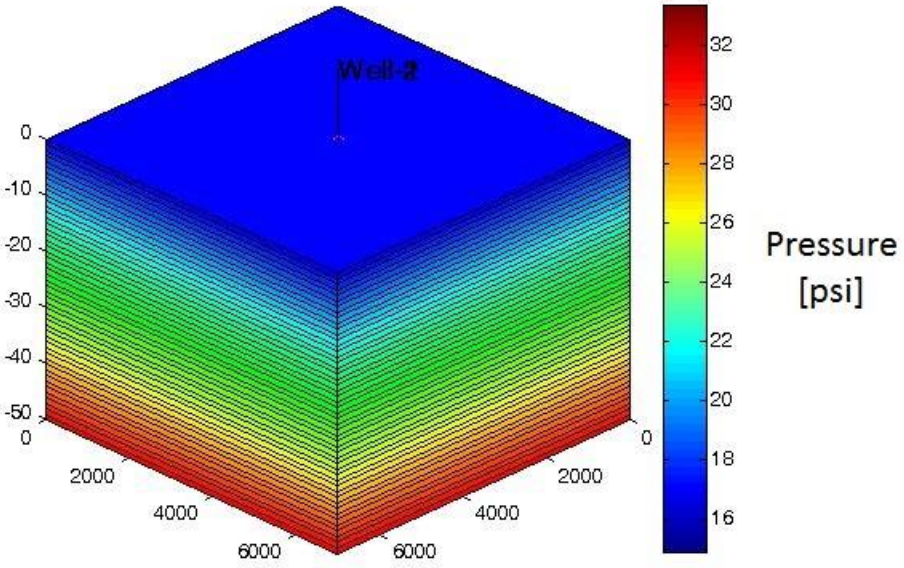

Figure 3.3 Gravity stable pressure distribution in a single-phase UT-EMPRES simulation with an oil density of 0.377 psi/ft and constant pressure wells on top and bottom operating at atmospheric pressure

CHAPTER 4: RESULTS AND DISCUSSION

4.1 UT-EMPRES

UT-EMPRES proved to be a simple, yet accurate form of numerical reservoir simulator, comparable to UTCHEM and CMG for one to three slightly compressible phases in a reservoir. Figure 4.1 depicts an example of comparison between these three simulators for a pressure distribution in a simulation involving two horizontal wells. For this single-phase simulation case, output data between all simulators matched well. Although the color scheme for each simulator's visualization tool are different, the pressure values are identical.

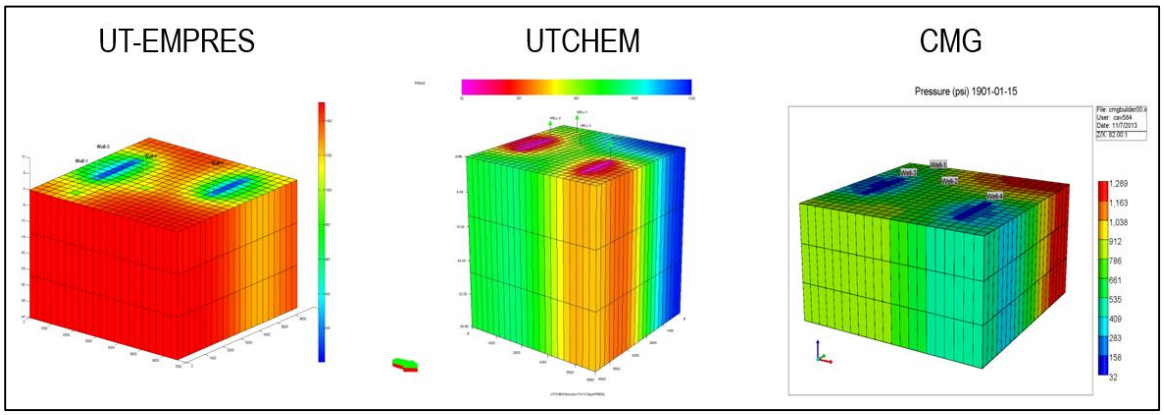

Figure 4.1 Pressure distribution example comparison of results from UT-EMPRES, UTCHEM, and CMG numerical reservoir simulators. Although color schemes are difference among simulators, values of the pressure field displayed are identical.

Another verification simulation involved an immiscible, two-phase, 1D displacement problem. The classic Buckley-Leverett solution is compared to UT-EMPRES, UTCHEM, and CMG. The results of all three simulators replicate the solution to the Buckley-Leverett problem suitably well, considering numerical dispersion effects.

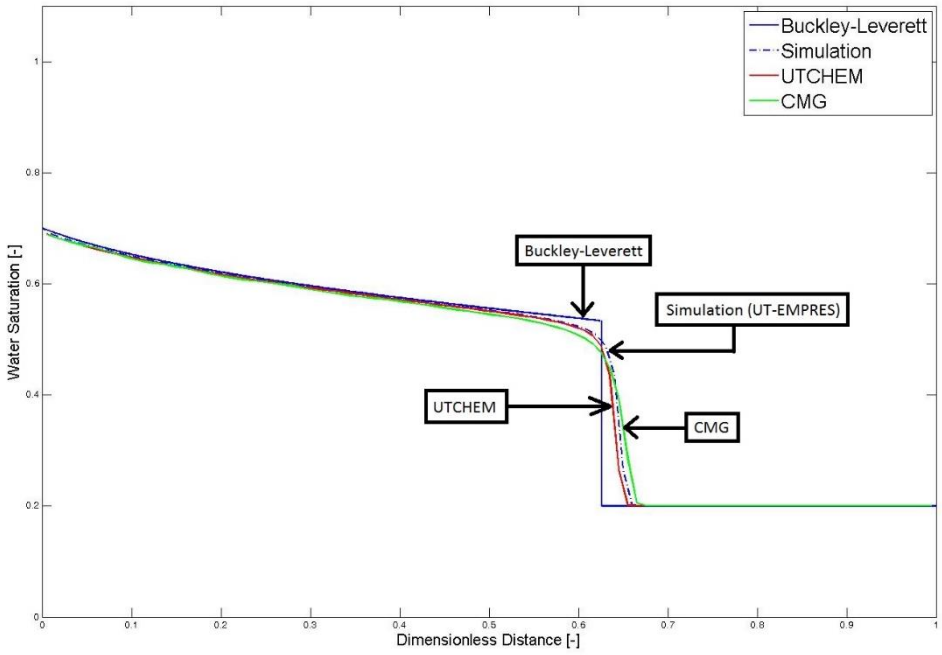

Figure 4.2 Example output of an immiscible displacement problem comparing the classic Buckley-Leverett solution with simulation results from UT-EMPRES, UTCHEM, and CMG

UT-EMPRES was verified through many comparison simulations in multi-dimensions and multiple phases, which gave confidence toward its use as a simulator to collect data for the second and third objective of this thesis.

4.2 GENERALIZED FLOW RATE MODEL

Figure 4.3 shows the production rate data for a small subset of the vast database of over 2000 simulations used to appropriately fit the GFRM. The approach that has been described in Chapter 3 is utilized here, and the resulting fitting parameter expressions are analyzed. The GFRM is finally implemented for a range of reservoir conditions (Table 4.1), and its results are compared to simulation data. Both the success and limitations to

the current version of the model are then addressed. Finally, interests in the behavior of the functional forms of the parameters are explored to conclude this section.

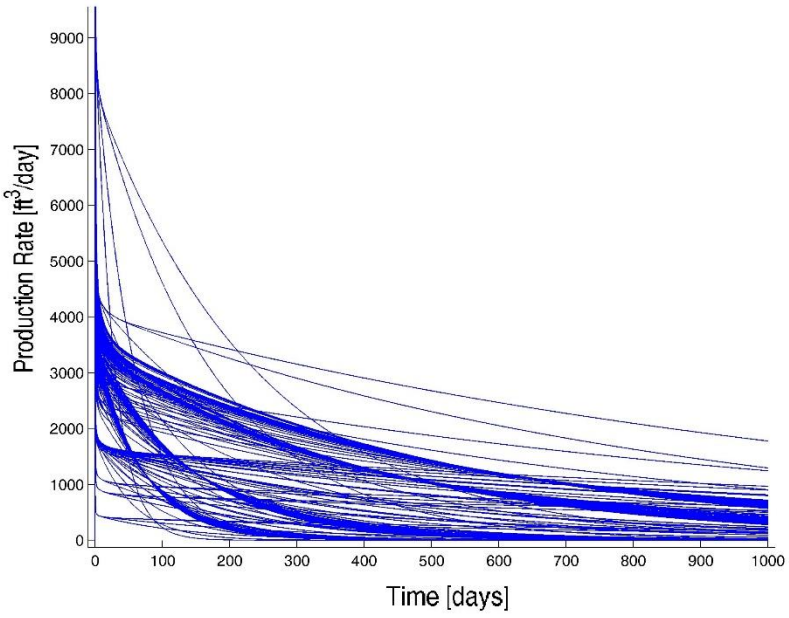

Figure 4.3 Production forecasts from a subset of database simulations

The database used to fit the GFRM (Equation 3.2.6) is composed of more than 2000 simulations with a wide range of values for a variety of different key input properties. It was found that all simulations fit the GFRM accurately when b, λ, t_{dep}, and q_{tdep} were treated as fitting parameters. Table 4.1 provides the minimum and maximum values of each of the key input properties used for simulations in the database.

Table 4.1 Range of key input properties values within the database of simulations used to fit the GFRM

Key Input Property	**Minimum**	**Maximum**
Number of Wells	1	1000
Reservoir Areal Extent [acres]	281.2	2295.7
Porosity	0.1	0.4
Reservoir Thickness [ft]	10	500
Permeability [md]	10	1000
Total Compressibility [psi^{-1}]	2E-6	2.1E-5
Viscosity [cp]	1	30
Initial Pressure [psi]	50	3000
Well Operating Pressure [psi]	14.7	2014.7
Difference in Initial and Well Operating Pressures [psi]	35.3	1985.3

All of the simulations in the database were analyzed to obtain the four parameters that are inputs to the GFRM. To reiterate, there are four key output parameters obtained through post-processing each individual simulation. These parameters are:

1. b : The pre-depletion stage "fitting" parameter
2. λ : The decay rate of the depletion stage
3. t_{dep} : The time at which the depletion stage of flow behavior begins
4. q_{tdep} : The flow rate at time t_{dep}

From these four key output parameters, with the exception of b, the scaled "fitting" parameters can be calculated for each simulation via Equations 3.7 through 3.10. The

scaling of these output parameters was achieved through division by an analytical solution for each parameter. Analytical expressions for both λ and q_{tdep} were found in the tank model, and an expression for an approximate t_{dep} was found in the literature (Ramey and Cobb, 1971).

Initial attempts of scaling the four output parameters included only individual or parts of the analytical expressions in the current version. It was not initially apparent that the output parameters should to be dimensionless; however, after careful plotting of scaled quantities, this became evident. Also, the idea to form a functional relationship between each parameter and the number of wells in the simulations was not part of the initial conceptual model; rather, a "well density" term, the number of wells divided by the areal extent of the reservoir, was used to form a functional relationship. The well density idea may indeed be relevant in the future development of this model, which is explained further in Chapter 5.

Each parameter has been plotted against the number of wells in each simulations of the entire database and can be seen in Figures 4.4 through 4.8. All of the data for each of the four parameters then underwent a nonlinear regression using Microsoft EXCEL's SOLVER to form unique functional relationships in terms of one or more of the three parameters: (1) the number of wells in the simulations, N_w (2) the areal extent of the reservoir, A (3) the diffusivity, α (no other properties were found to affect the parameters). The current functional relationships can be seen in Equations 4.1 through 4.4, which, when paired with 3.6, form an easy-to-use empirical solution to single-phase primary production from a reservoir with an arbitrary number of vertical wells. Initially, all data for each fitting parameter was plotted against the number of wells in the simulations. Functional forms were developed through slightly arbitrary, yet informed trial-and-error attempts of minimizing error routines in Excel. Both λ^* and q_{tdep}^* form strong functions (Equations

4.2 and 4.4) of the number of wells in the simulations, and other variables do not seem to have any substantial effect. The fitting parameter, *b,* on the other hand appears to be a function (Equation 4.1) of not only the number of wells in the simulations, but also the areal extent of the reservoir and the diffusivity. The diffusivity of a reservoir is defined in Equation 4.5. Finally, t_{dep}* does not seem to depend on the number of wells in the simulation, but rather the areal extent of the reservoir and the diffusivity.

$$b = -0.12 + 0.097 N_w^{-0.77} - 0.99 A^{-0.61} - 5E - 10\alpha \tag{4.1}$$

$$\lambda^* = \frac{\lambda}{\lambda_{analytical}} = \frac{1}{0.54 + (1 - 0.54) N_w} \tag{4.2}$$

$$t_{dep}{}^* = \frac{t_{dep}}{t_{dep,analytical}} = 1 + 9.43E3A^{-1.8} + 1.1E - 8\alpha \tag{4.3}$$

$$q_{t_{dep}}{}^* = \frac{q_{t_{dep}}}{q_{t_{dep},analytical}} = \frac{N_w}{0.53 + 0.54 N_w} \tag{4.4}$$

$$\alpha = \frac{k}{\mu \phi c_t} \tag{4.5}$$

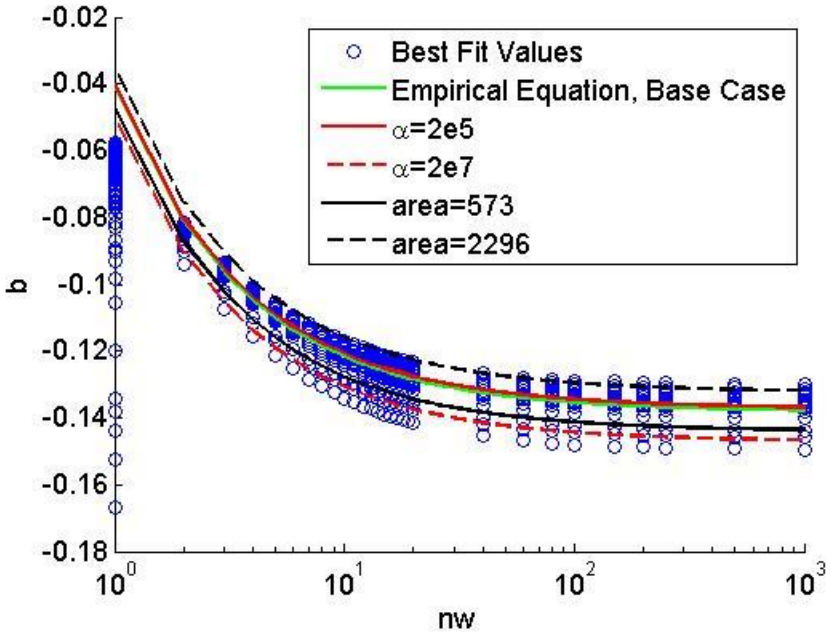

Figure 4.4 Functional plot of all simulation values of *b* versus the number of wells, the areal extent of the reservoir [acres], and the diffusivity [md-psi/cp]

Figure 4.4 shows the functional dependence of *b* by the number of wells in the simulations, the areal extent of the reservoir, and the diffusivity. Initially, there was not one clear functional relationship for all simulations. All data was plotted against the number of wells, and several curves became apparent. Therefore, *b* was dependent on another variable or set of variables. Transient processes, like those in the pre-depletion stage of production, are typically dependent on spatial and diffusive variables. The areal extent of the reservoir is significant because the pressure disturbance incurred by the wells travels toward the boundary within this stage of production. The diffusivity is an important variable in similar dynamic processes. Both the areal extent of the reservoir and the diffusivity proved to be important in forming a functional form of *b*.

For the entire database of simulations, the dimensionless decay rate parameter in Figure 4.5 collapses to one hyperbolic function of the number of wells in a simulation. The

functional expression, as seen in Equation 4.3, fits the data exceptionally well, allowing the GFRM great accuracy in the depletion stage of primary production.

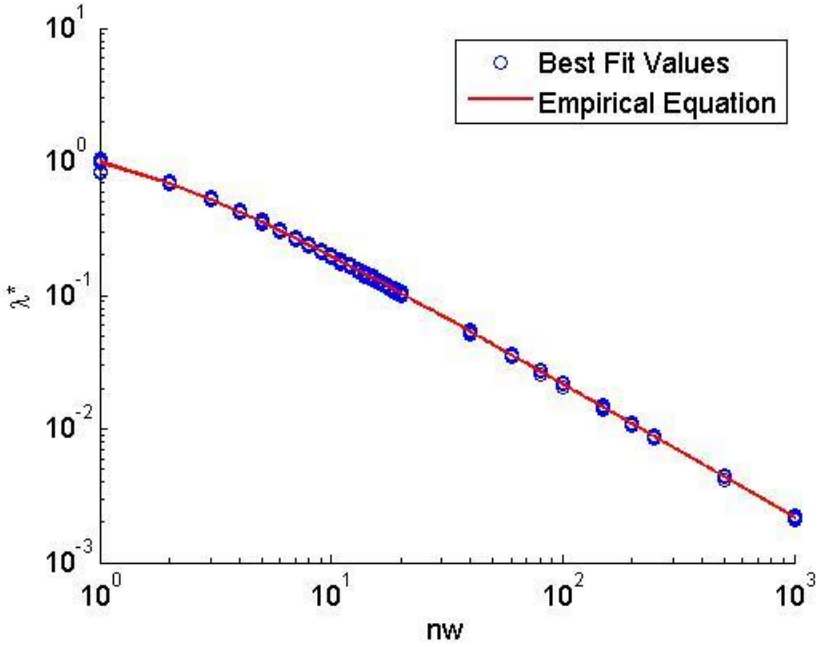

Figure 4.5 Functional plot of all simulation values of λ* versus the number of wells

Figure 4.6 displays all of the simulation results for the scaled parameter for the time at which the depletion stage begins. The parameter t_{dep}* did not exhibit functional dependence on the number of wells, but rather the areal extent of the reservoir and the diffusivity. Just as *b* is dependent upon the pre-depletion stage of production, so too is the time at which the depletion phase occurs.

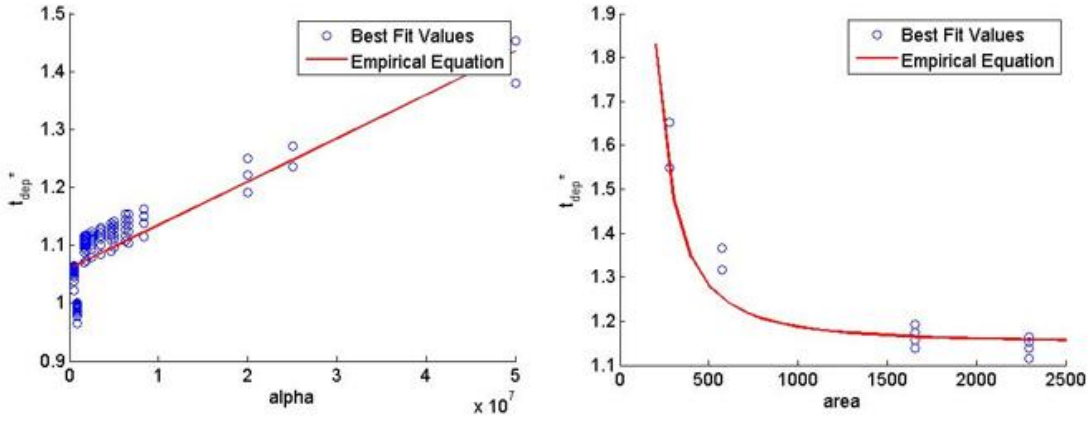

Figure 4.6 Functional plots of all simulation values of t_{dep}* versus the diffusivity and the areal extent of the reservoir. In figure (a), the area was 1000 acres and in (b) diffusivity constant is 2.0E7 md-psi/cp

The data in Figure 4.8 represents the scaled parameter for the production flow rate at which time the depletion stage begins. Just as in the case for the parameter accounting for the decay rate, the functional relationship of all simulations for the scaled flow rate parameter is remarkably accurate with strong dependence on the number of wells in the simulation.

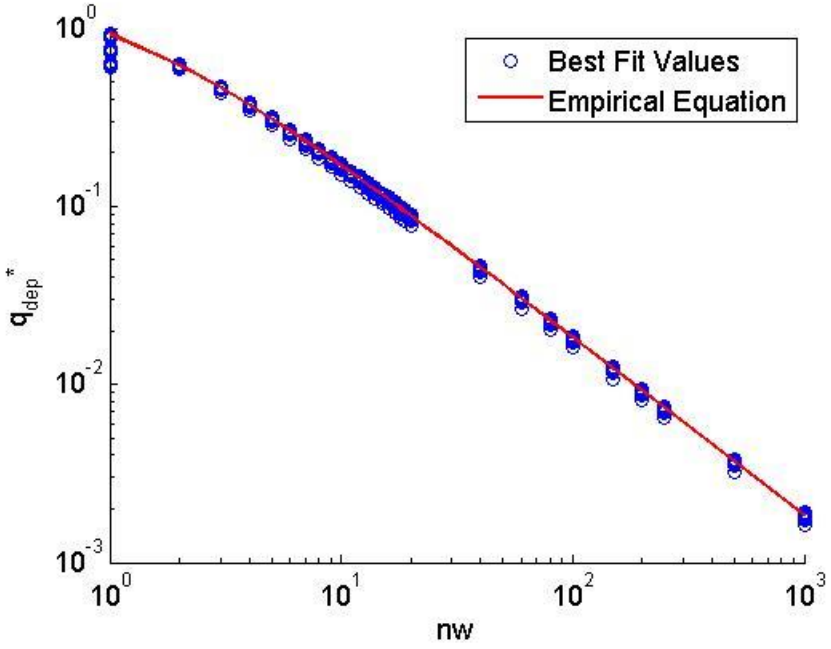

Figure 4.7 Functional plot of all simulation values of q_{tdep}* versus the number of wells

As is shown in the next section, for many cases the predictive results produced from the GFRM are excellent. Other cases show some error in production forecasts in comparison to simulation results; however, many of these predictions are more than sufficient versus those of simulations and within the error of the inherent assumptions associated with the reservoir characterization.

A base case was established from which to evaluate other simulation cases in terms of the functional dependencies of the fitting parameters (N_w, A, and α). The base case was specified to have one well, an area of 1000 acres, and a diffusivity of 2E7 md-psi/cp. The tank model is valid for a single well, which is the reasoning behind using only one well as a basis. The area and diffusivity values used for the basis were selected because they were moderate values from the database of simulations.

In order to critically analyze the predictability of the GFRM in the base case, results of the dimensionless production rate and dimensionless cumulative production were plotted in four combination of scales: linear-linear, logarithmic-linear, linear-logarithmic, and logarithmic-logarithmic, as is shown in Figures 4.8 and 4.9.

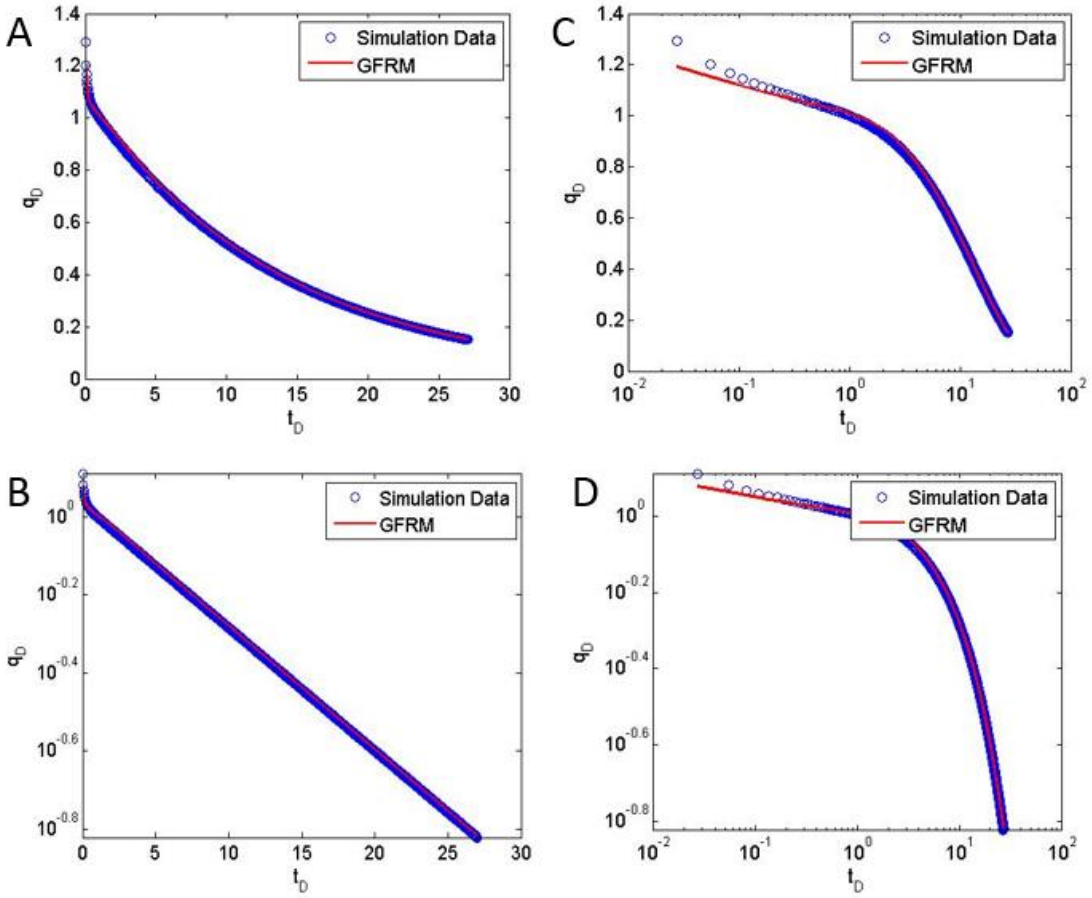

Figure 4.8 Dimensionless plots of base case production rate versus dimensionless time in scales (A) linear-linear (B) logarithmic-linear (C) linear-logarithmic and (D) logarithmic-logarithmic

In Figure 4.8, the GFRM prediction for the base case production rate appears to fit simulation results accurately. Plots A and B, whose dimensionless time is on a linear scale,

illustrate that the GFRM performs exceptionally well in the depletion stage of production. Plots C and D, whose dimensionless time is on a logarithmic scale, highlight the tendency for the pre-depletion stage production rates to be slightly misrepresented at very small dimensionless times.

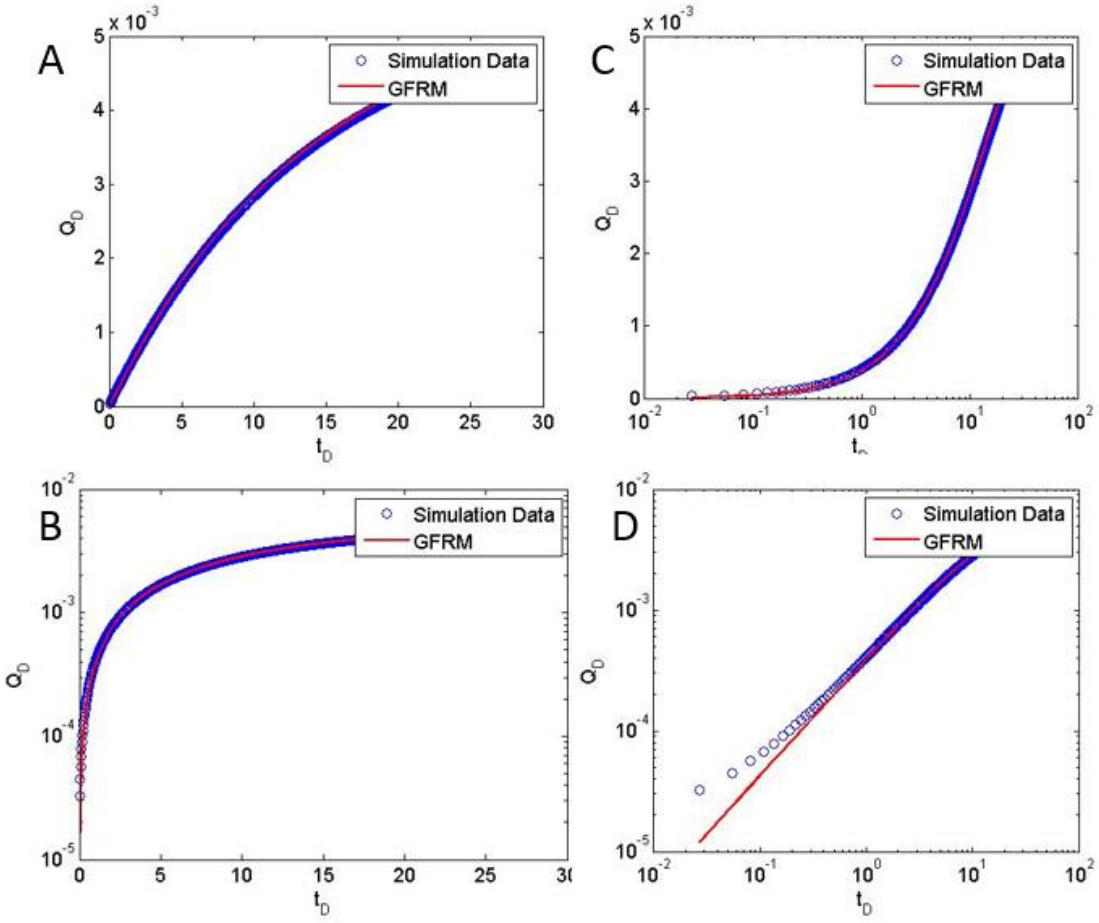

Figure 4.9 Dimensionless plots of base case cumulative production versus dimensionless time in scales (A) linear-linear (B) logarithmic-linear (C) linear-logarithmic and (D) logarithmic-logarithmic

Figure 4.9 shows the comparison between the GFRM prediction and simulation data for the dimensionless cumulative production versus the dimensionless time.

Dimensionless cumulative production, Q_D, is defined as the cumulative production divided by the original oil in place (OOIP). A similar analysis can be given for Figure 4.9 in comparison to Figure 4.8; however, the cumulative production response allows one to hypothesize that the errors at early times in Figure 4.8 do not incur significant error in the cumulative production at moderate to late times.

Now that the base case has been established and analyzed, perturbations of functional dependencies (N_w, A, and α) are made. The resulting predictions of the GFRM are evaluated compared to simulation data.

The base case has been evaluated with a change in the number of wells to both 100 and 1000 wells. The predictions from the GFRM presented in Figure 4.10 prove to be remarkably accurate compared to simulation data. Both of the sets of plots for 100 and 1000 well cases seem to be almost identical, which is a product of the scaling of the equation to dimensionless dependent and independent variables.

The areal extent of the reservoir is the second characteristic to be changed from the base case. In these simulations, the number of wells is set to a value of 1000. The areas of the reservoirs were selected to be 281 acres and 2269 acres. Based on the dimensionless production rate plots in Figure 4.11, both simulations have errors in the GFRM-predicted decay rate values since the slope of the production curves do not match simulation data accurately. The dimensionless cumulative plots, however, show that even a relatively dramatic error in the dimensionless rate plot does not necessarily correlate to a significant error in the overall cumulative production from the reservoir. The accuracy of the GFRM appears to be more sensitive to the area of the reservoir than the number of wells.

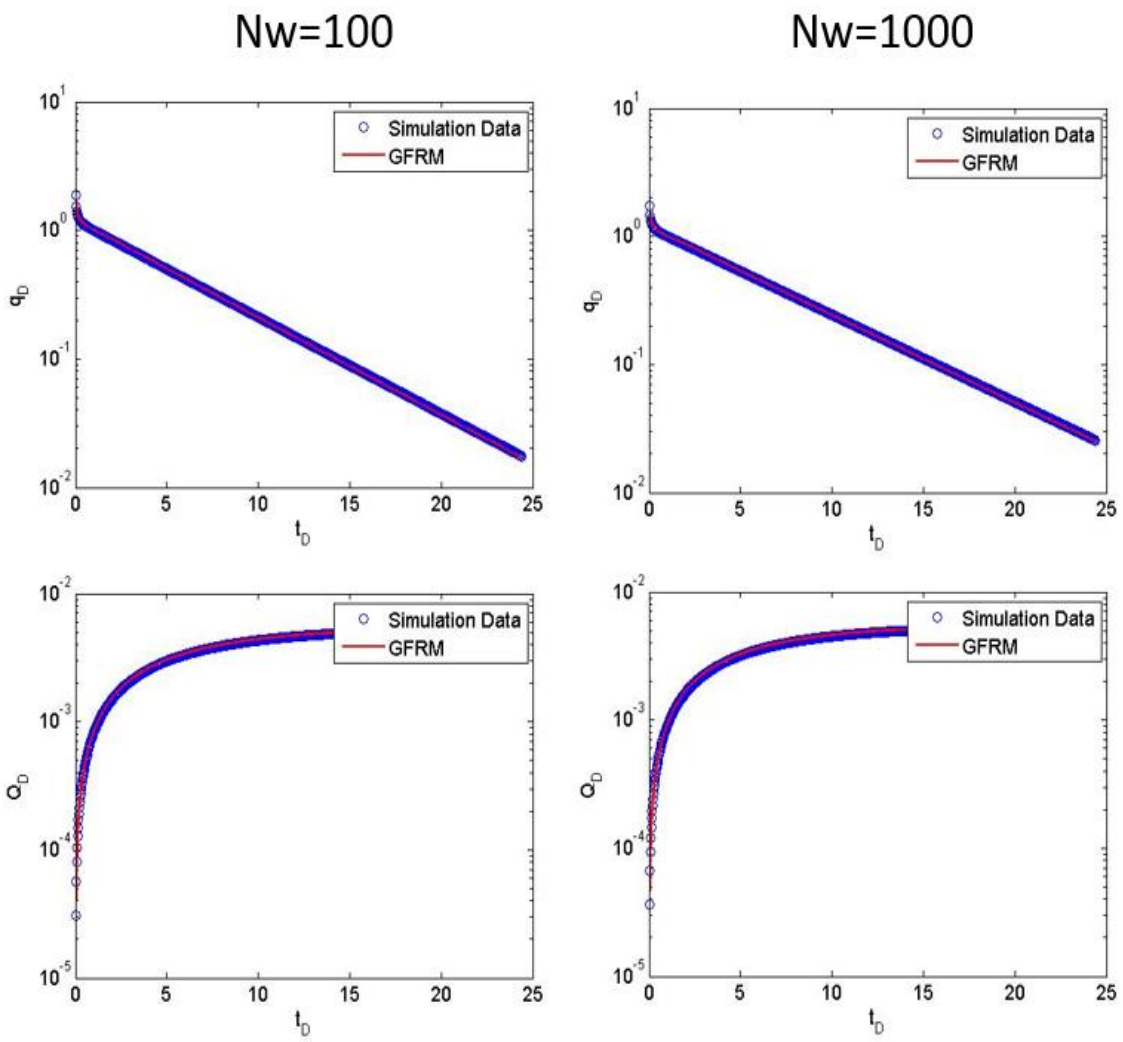

Figure 4.10 Dimensionless production rates and dimensionless cumulative production for 100 and 1000 wells in a reservoir plotted in logarithmic-linear scale. The reservoir is also characterized by an area of 1000 acres and a diffusivity of 2E7 md-psi/cp

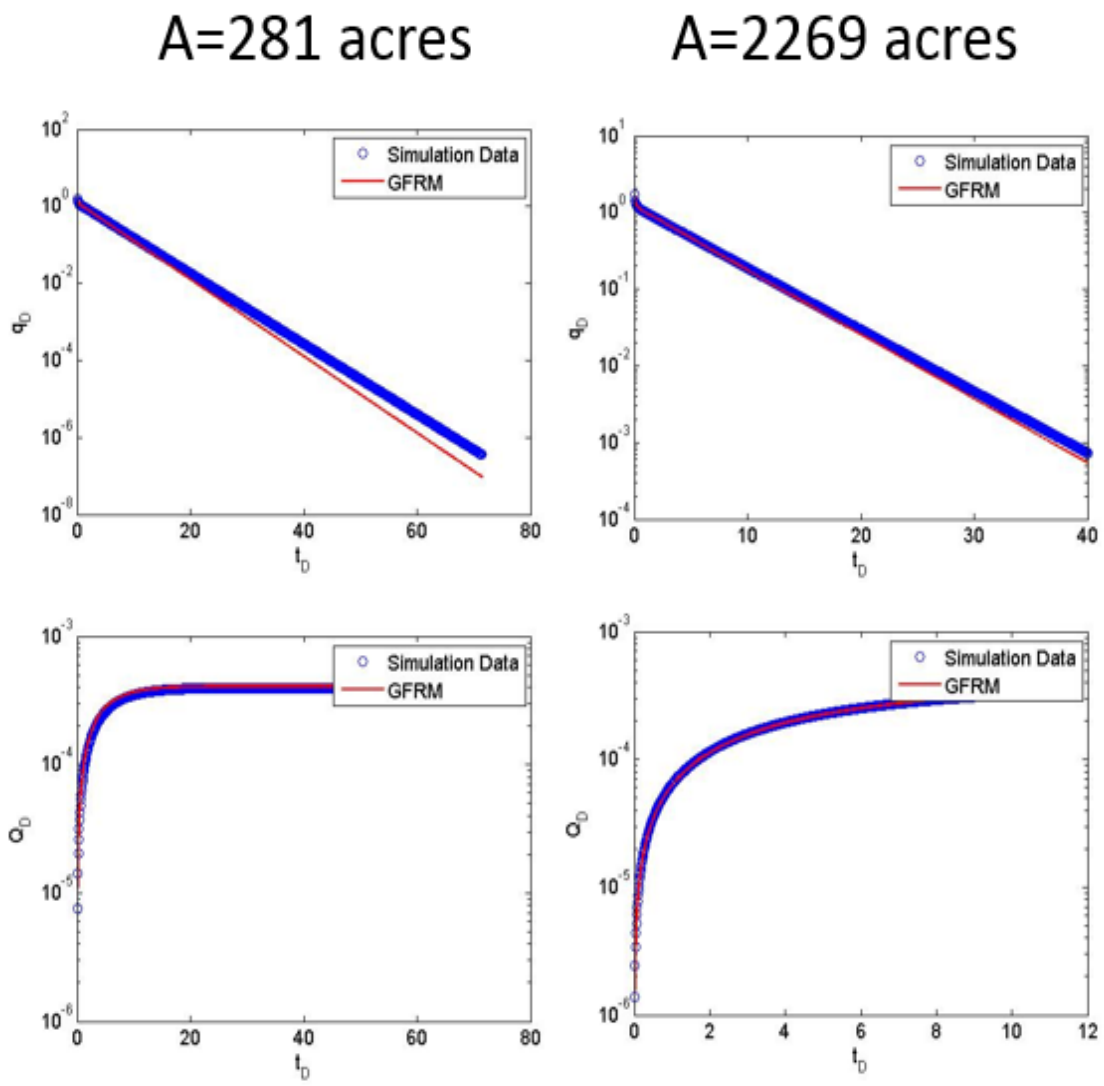

Figure 4.11 Dimensionless production rates and dimensionless cumulative production for reservoirs of area 281 acres and 2269 acres plotted in logarithmic-linear scale. The reservoir is also characterized by 1000 wells and a diffusivity of 2E7 md-psi/cp

Finally, the diffusivity is perturbed from the base case condition to evaluate its sensitivity on the GFRM. Diffusivity values of 5E5 md-psi/cp and 5E7 md-psi/cp are used in comparison simulation cases shown in Figure 4.12. In assessing the accuracy of the GFRM for the 5E5 md-psi/cp case, similar to the comparison of dimensionless rate and dimensionless cumulative plots in Figure 4.11, a relatively large variation in the dimensionless rate does not necessarily translate to inaccuracies in the GFRM-predicted cumulative production values. The GFRM performs well in the case of a 5E5 md-psi/cp value for the diffusivity.

All four of the parameters have been fit to somewhat arbitrary functional forms of the number of wells, area, and diffusivity. Simplifications and modifications in general have been made to the functional forms to make implementation more convenient. More complex correlations could be created in order to produce more accurate results.

The GFRM seems to lose accuracy when the areal extent of the reservoir becomes exceedingly small or the diffusivity becomes immensely large. Figure 4.13 shows an example of a simulation case with 1000 wells, area of 1000 acres, and diffusivity of 2E9 md-psi/cp. Due to the high diffusivity, the production rate declines almost instantaneously, which is not accounted for in the correlations for t_{dep}. The inaccuracy of the GFRM for diffusivity values outside of the range 2E5 to 5E7 when coupled with small areas and large numbers of wells is an obvious limitation in the fitting parameters correlations. All input variables and their associations should be studied to create more complex and robust correlations for the fitting parameters, which empower the GFRM. The GRFM is still useful in these regimes, but only if the better correlations of the fitting parameters are developed.

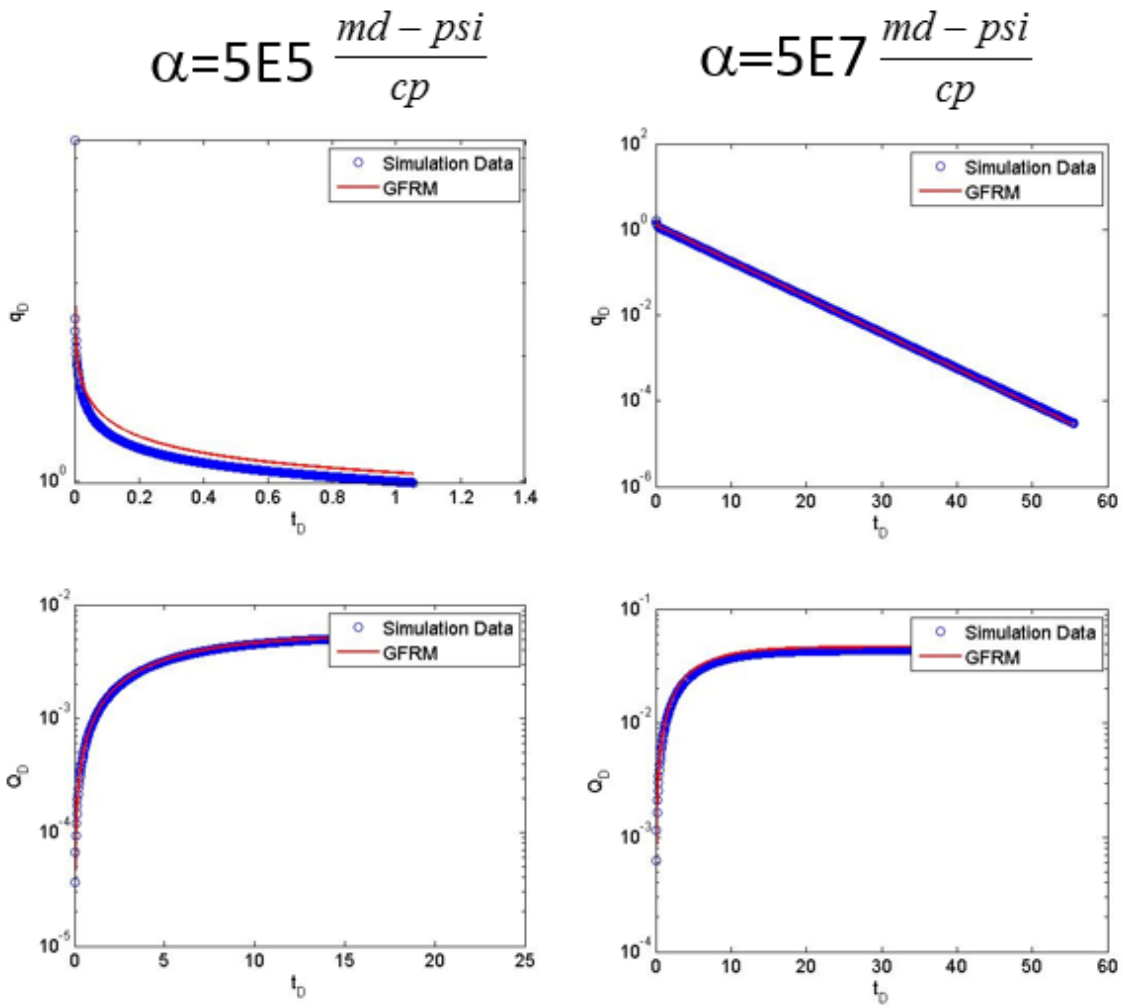

Figure 4.12 Dimensionless production rates and dimensionless cumulative production for reservoirs of diffusivities equal to 5E5 md-psi/cp and 5E7 md-psi/cp plotted in logarithmic-linear scale. The reservoir is also characterized by an area of 1000 acres and 1000 wells

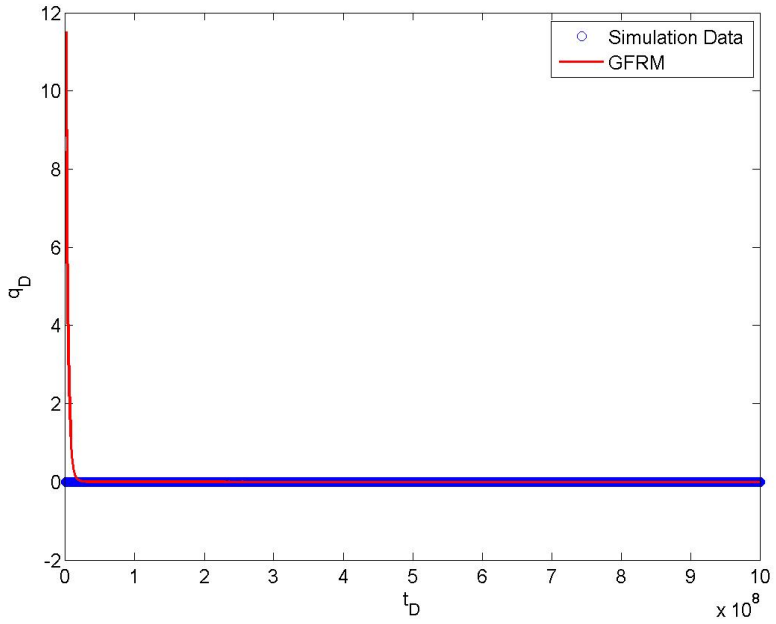

Figure 4.13 Dimensionless production rate versus dimensionless time for a reservoir of 1000 acres, 1000 wells, and a diffusivity of 2E9 md-psi/cp

4.3 GRAVITY DRAINAGE

4.3.1 Darcy's Law in Simulation

In order to gain some confidence in using numerical reservoir simulators to predict gravity drainage flows, the purely gravity-driven flow rate based on Darcy's law is approximated with the help of UT-EMPRES. Single-phase gravity drainage flow rates are described by Darcy's law in Equation 4.6. Henry Darcy (1856) related the flow rate of fluids through a porous media to the properties of the rock, fluids, and potential gradient imposed on the system. Equation 4.6 shows this relationship, which is used in this section to validate a simple case of gravity-driven flow. For a single-phase free-fall gravity

drainage experiment, Darcy found that a constant volumetric rate of fluid was produced. Simulation results show this same constant production rate, which is discussed below.

$$q = \frac{kA}{\mu}\rho g \tag{4.6}$$

In Equation 4.6, the variables q, k, A, μ, ρ, and g are defined as the volumetric flow rate, permeability, areal extent of the reservoir (perpendicular to flow), fluid viscosity, density of the fluid, and the gravitational constant, respectively.

$$q = (6.33E-3)\frac{(50mD)(660\,ft)^2}{(1cp)}(0.377\,psi/\,ft) = 51{,}976\,ft^3/day \tag{4.7}$$

A UT-EMPRES simulation was run with values of 50 mD for permeability, (660 ft)^2 for areal extent, 1 cp for viscosity and 0.377 psi/ft for the product of the density and gravitational constant. These simulation inputs were then utilized in Darcy's law, which is shown in Equation 4.7. The value 6.33E – 3 is a unit conversion factor. Other values considered in the simulation can be found in Table 4.3. This simulation was characterized by only one gridblock in both X- and Y-directions and 50 gridblocks in the Z-direction. Spatial dimensions of the reservoir include 660 ft in both the lateral dimensions and 50 ft in the vertical dimension. Based on the fluid properties, the fluid in this simulation is an approximation of oil.

In order to approximate single-phase flow through simulation, two vertical boundary conditions must be imposed on the system. The lateral boundary conditions are assumed to be no-flow boundaries. The top and bottom boundary conditions both operate under constant atmospheric pressures, just as in a free fall gravity drainage system. Darcy's law (Equation 4.6) assumes that the entire areal extent of the reservoir is the surface through

which fluid enters and leaves the system. The traditional numerical reservoir simulator employs a *well model*, which approximates the relationship among the flow rate of fluids in or out of a well, the operating bottom-hole pressure of the well, and the pressure of the reservoir within the gridblock associated with the well. The traditional well model was formulated by Peaceman (1978) and can be seen in Equation 4.8. $P_{gb\text{-}res}$ is defined as the pressure in the gridblock associated with the well at hand.

$$q = J\left(P_{gb-res} - P_{bhp}\right) \tag{4.8}$$

$$J = \frac{2\pi\sqrt{k_x k_y}\Delta z}{\mu\left(\ln\left(\frac{r_o}{r_w}\right) + s\right)} \tag{4.9}$$

In Equation 4.9, J, kx, ky, Dz, and ro are defined as the productivity index, the x-direction permeability, the y-direction permeability, the length of the gridblock of the well in the z-direction, and the equivalent radius (defined by Peaceman (1978)), respectively.

Since Peaceman's well model approximates an actual well in a reservoir, steps must be taken in order to modify the well model to approximately flow through the areal extent of the reservoir, as is used in Darcy's law (Equation 4.6). In order to do this, the productivity index, *J*, must be modified in such a way that the well approximates flow through the entire areal surface rather than a traditional well. The productivity index is modified by imposing an artificial well skin, *s*, to the wells being modeled. The value of the imposed well skin must be negative in order to increase the value of the productivity index. As is shown in Table 4.2 and Figure 4.14, as the magnitude of the well skin

imposed is increased, the constant flow rate from the reservoir is also increased until the value found from Darcy's law is suitably approximated.

Table 4.2 Well skin and the resulting constant production rates for several simulations

Well Skin	Constant Production Rate [ft^3/day]
0	5050
-1	5922
-2	7159
-3	9048
-4	12292
-4.5	14977
-5	19162
-5.5	26593
-6	43439
-6.12965	51975.99

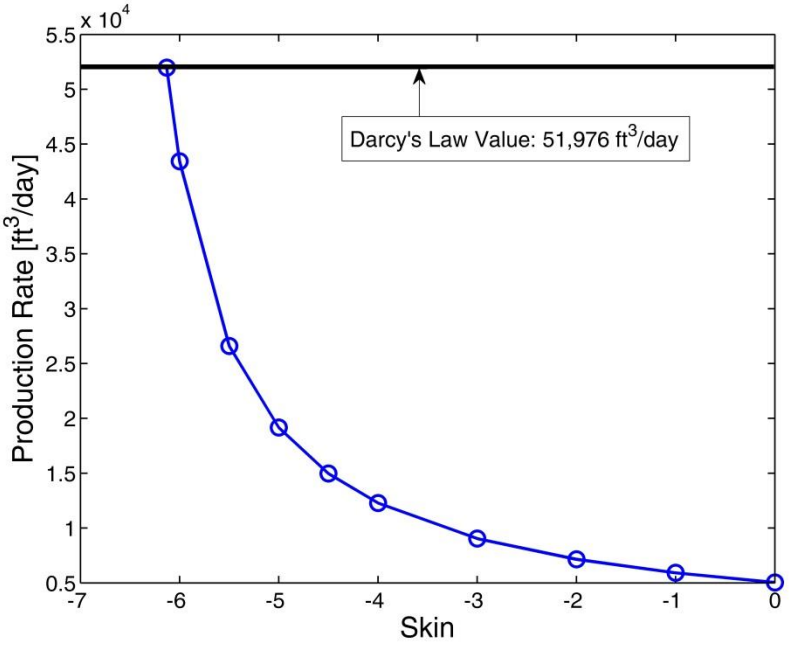

Figure 4.14 Constant production rate versus well skin for simulation compared to Darcy's law value of production rate

The Darcy's law constant flow rate value is best approximated when a well skin is imposed which drives the productivity index toward infinity. Therefore, in general, as the negative skin approaches a magnitude equal to the natural logarithm of the ratio of equivalent radius, r_o, and the well radius, r_w, as is shown in Equation 4.9, the well model approximates fluid flow through the surface of the gridblock normal to the orientation of the well, which in this case is the top and bottom surfaces of the reservoir. The value of the logarithm of the ratio of the equivalent radius and the well radius in this specific example is slightly greater than 6.12965 (See Table 4.2).

$$s \to -\ln\left(\frac{r_o}{r_w}\right) \tag{4.10}$$

For more information concerning the equivalent well radius, please consult Chapter 6. Although the reservoir has boundary conditions of constant pressure, the single-phase flow rate into and out of the reservoir is constant in value, which is attributable to the constant column height of fluid (or pressure head), see Figure 4.15. This validation of Darcy's law provides confidence for more complicated examples of gravity drainage through simulation that are presented in the proceeding sections of this thesis.

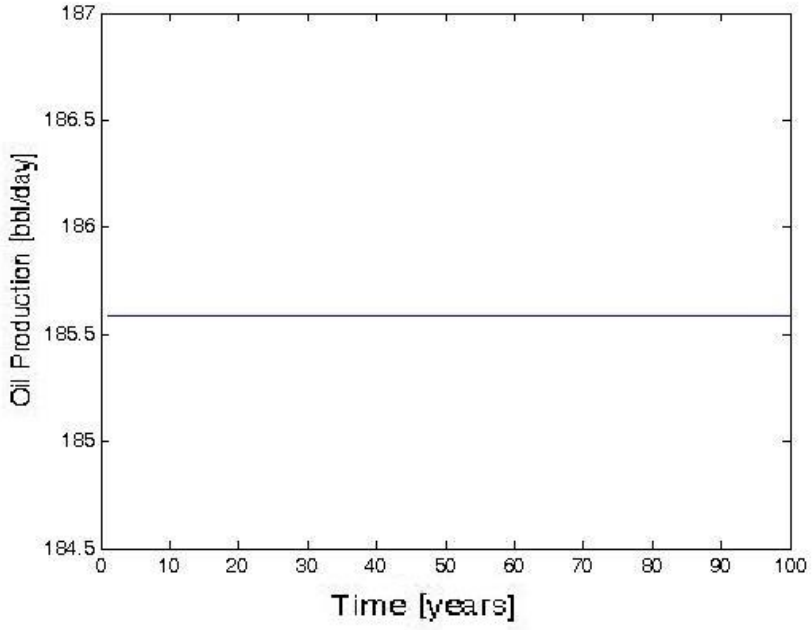

Figure 4.15 Constant oil production rate from a UTCHEM single-phase flow simulation

4.3.2 Saturation Dependence of Multiphase Simulations

For simulations of free fall gravity drainage with only one phase, a constant production rate is observed. This section follows the same general well configuration given in section 4.2.1; however, more than one phase exists in the systems described here. Simulations are characterized by one gridblock in the lateral dimensions and 50 gridblocks in the vertical dimension. The wells in the simulations still operate at constant atmospheric pressures; however, the top well injects a fluid representative of air, and the bottom well produces oil, which initially completely saturates the reservoir. The fluid representative of air is characterized by a fluid density of 0.001 psi/ft, a viscosity of 0.02 cp, and a compressibility of 1E-2 psi^{-1}.

As opposed to the simulations shown in section 4.2.1, simulations with more than one phase produce fluids at rates which are not constant. A depiction of this declining production rate can be seen from an example simulation in Figure 4.16. See Table 4.3 for more information regarding the simulations in this section.

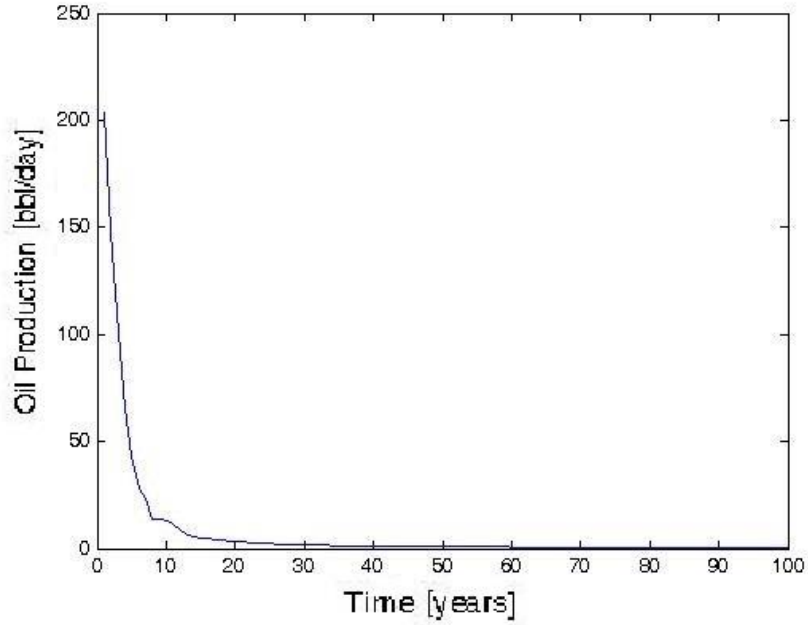

Figure 4.16 Non-constant oil production rate for a UTCHEM two-phase (oil and gas) flow simulation

Once all of the oil that was initially in the reservoir has been produced, the simulation again takes on the single-phase gravity drainage character described by Darcy's law (Equation 4.6) with constant production rates of air. Since production rates of oil decline as the simulation advances through time, the production rates of multiphase gravity drainage experiments are saturation-dependent. The vertical saturation distribution through time is shown in Figure 4.17. If conditions are suitable and stable, the oil production rate tends to decline in an exponential fashion, which may hold interest for its extension to use in the GFRM equation.

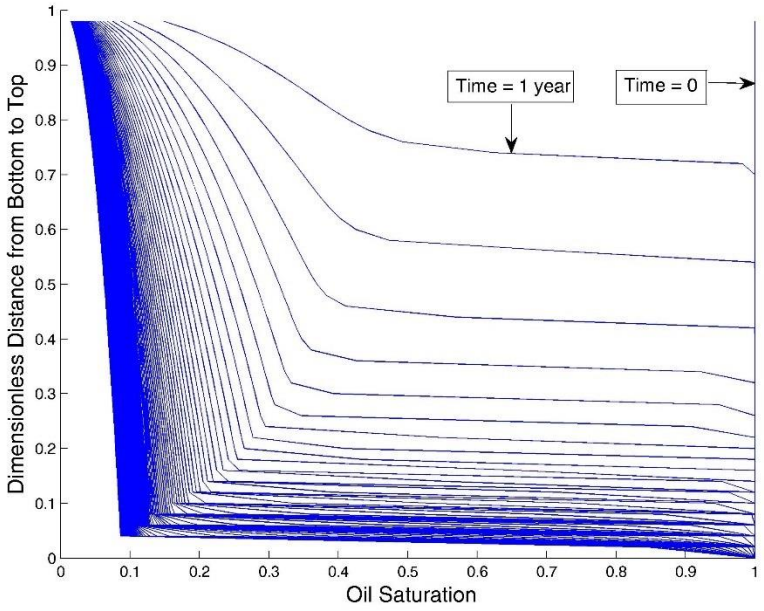

Figure 4.17 Oil saturation profile at each year for a UTCHEM two-phase (oil and gas) flow simulation

The decline of oil production rates is attributable to a loss of pressure head (or height of the oil column). Since the density of the air, 0.001 psi/ft, is so small in comparison to oil, negligible pressure head is added above the oil column. Figure 4.18 depicts the vertical pressure distribution through time, which enables one to see how the oil column height declines with time.

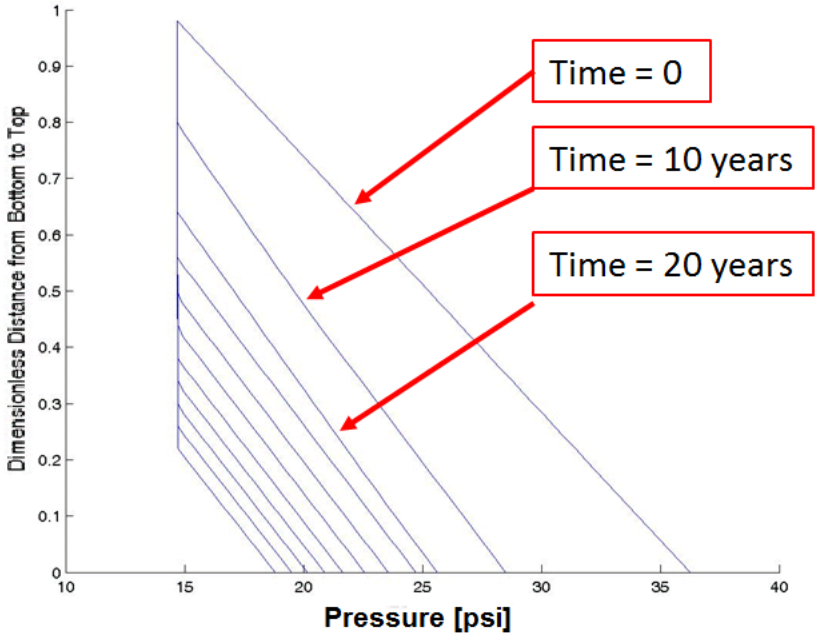

Figure 4.18 Vertical pressure distributions for a UTCHEM two-phase (oil and gas) flow simulation

If three phases exist in a simulation, more interesting saturation-dependent phenomena ensue. As an example, a reservoir is initially saturated homogeneously with 50% oil and 50% water with the same boundary conditions described in the two-phase simulations above. Oil is characterized by a density of 0.377 psi/ft, a viscosity of 5 cp, and a compressibility of 15E-6 psi^{-1}. Water is characterized by a density of 0.433 psi/ft, a viscosity of 1 cp, and a compressibility of 3E-6 psi^{-1}. Air is characterized by a density of 0.001 psi/ft, a viscosity of 0.02 cp, and a compressibility of 1E-2 psi^{-1}. Since water is denser than oil in this case, water tends to move downward, while the more buoyant oil phase remains or even moves upward in the reservoir. Due to the relative buoyancies of the oil and water, at early stages of drainage an oil bank begins to form in the middle and upper portions of the reservoir while a water bank results at the bottom.

Figure 4.19 and 4.20 show these banking phenomena with vertical saturation distributions through time. Figure 4.20 illustrates the oil banking as the oil saturation within regions of the reservoir reaches values greater than the initial value of 0.5.

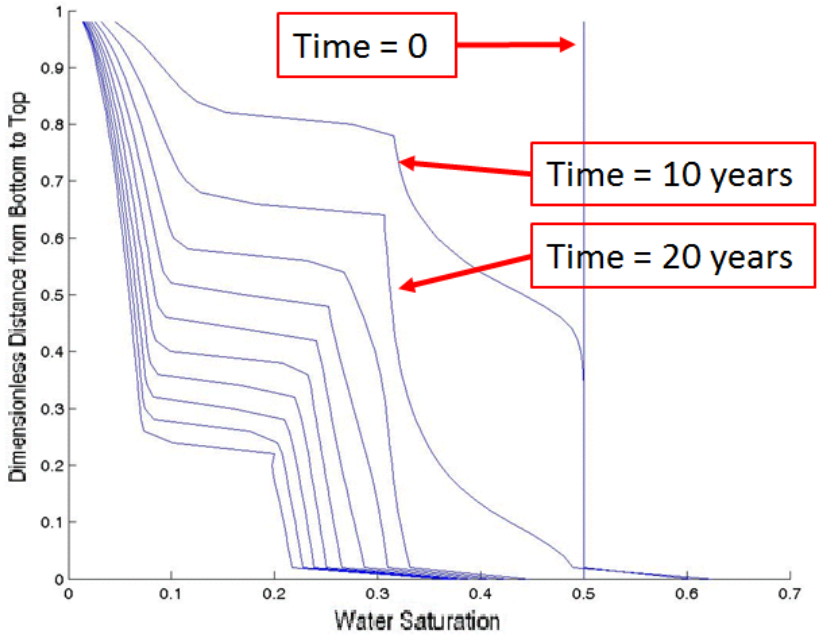

Figure 4.19 Water saturation profiles for a UTCHEM three-phase (water, oil and gas) flow simulation

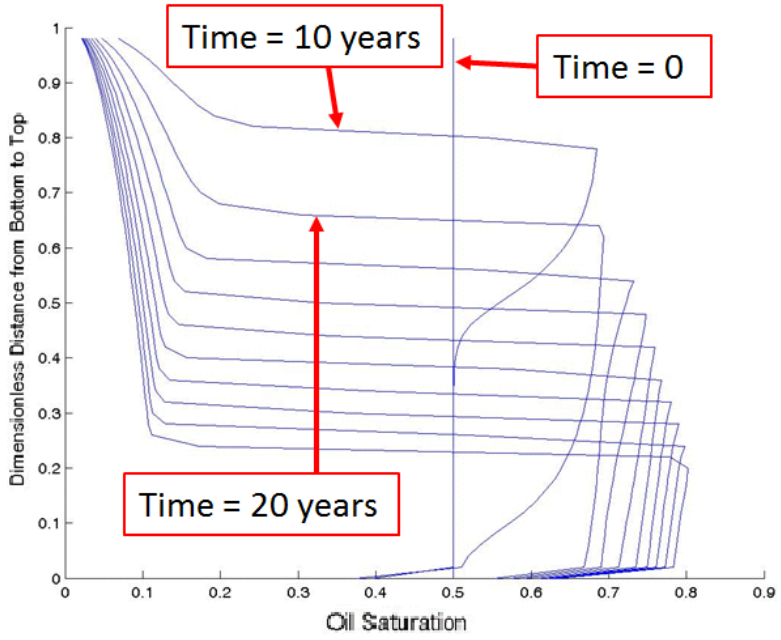

Figure 4.20 Oil saturation profiles for a UTCHEM three-phase (water, oil and gas) flow simulation

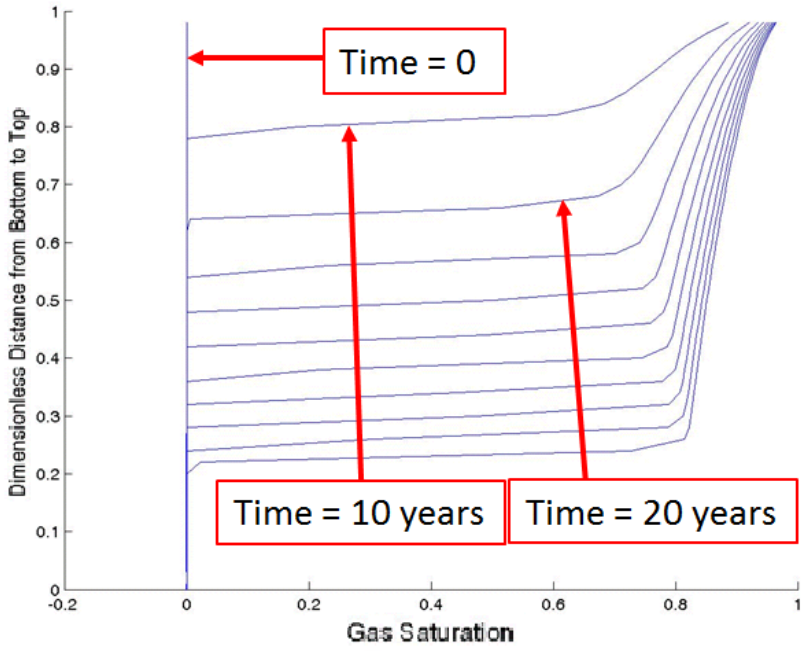

Figure 4.21 Gas saturation profiles for a UTCHEM three-phase (water, oil and gas) flow simulation

Figure 4.21 shows that the gas phase creates a relatively flat interface with the oil phase throughout the simulation.

As shown in the two-phase simulation cases, multiphase simulations result in saturation-dependent dynamics, including production rates. The example three-phase simulation results in phase production rates shown in Figure 4.22.

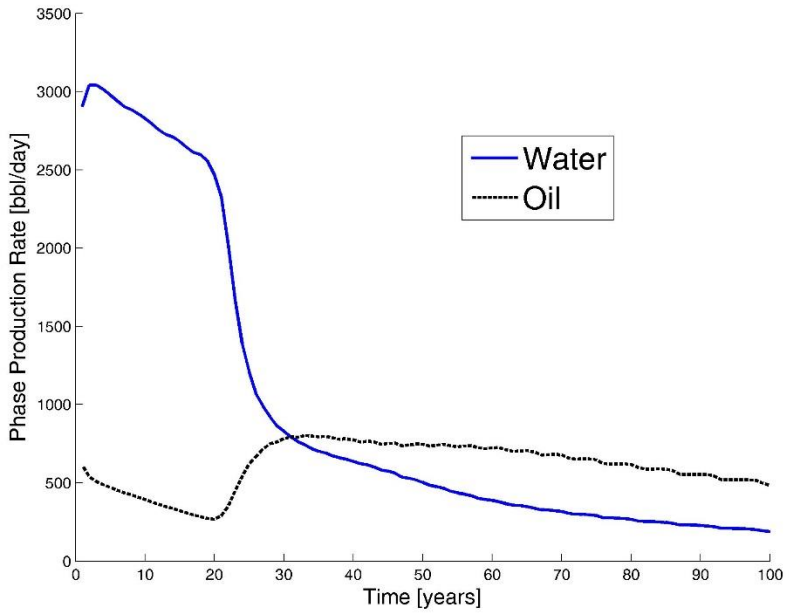

Figure 4.22 Phase Production Rates from a UTCHEM three-phase (water, oil and gas) flow simulation

Since the reservoir is initially homogeneous at 50% oil and 50% water, both water and oil are initially produced. Higher initial water production rates are due to greater mobility in the water phase in comparison to that of oil. As relative buoyancies between the two phases take effect, oil production rates decline as water rushes toward the bottom of the reservoir.

Once most of the water has been produced, the transition zone between water and oil banks begins to be drained from the system. This transition zone is marked by higher

water saturations near its bottom to higher oil saturation at its top. Figure 4.22 shows the production of the transition zone between 20 and 30 years, whereby water production rates decline while oil production rates increase. A similar result ensues when the oil bank is produced and the transition zone to the air phase begins production. These transition zones (water-oil and oil-air) are marked by the existence of more than one phase in the same gridblock. Ternary diagrams are great for illustrating three-phase saturations, and they have been used in this thesis to show how the three phases (water, oil, and air) mix throughout simulations. Each point on the ternary diagrams represent a three-phase saturation value within an individual gridblock at a certain time in the simulation.

Three ternary diagrams are presented here (Figures 4.23-4.25), which are representations of three similar simulations with differences in residual saturations and relative permeability parameters. The simulation example shown in Figure 4.23 is characterized by lateral dimensions of one gridblock with lengths of 660 ft and vertical dimension of 50 gridblocks for total vertical extent of 50 ft. The reservoir is initially homogeneously saturated with 50% oil and 50% water. The densities of water, oil, and air are 0.433 psi/ft, 0.377 psi/ft, 0.001 psi/ft, respectively. The viscosities of water, oil, and air are 1 cp, 5 cp, and 0.02 cp, respectively. The compressibilities of water, oil, and air are 3E-6 psi^{-1}, 15E-6 psi^{-1}, and 1E-2 psi^{-1}, respectively. Two wells operate at atmospheric pressure; one injecting air at the top of the reservoir and one producing fluids at the bottom. All residual saturations are set to a value of zero with the exception of water, whose residual value is 0.2. End-point relative permeabilities of all phases are equal to 0.8. All Corey-Brooks relative permeability model phase exponents are equal to one.

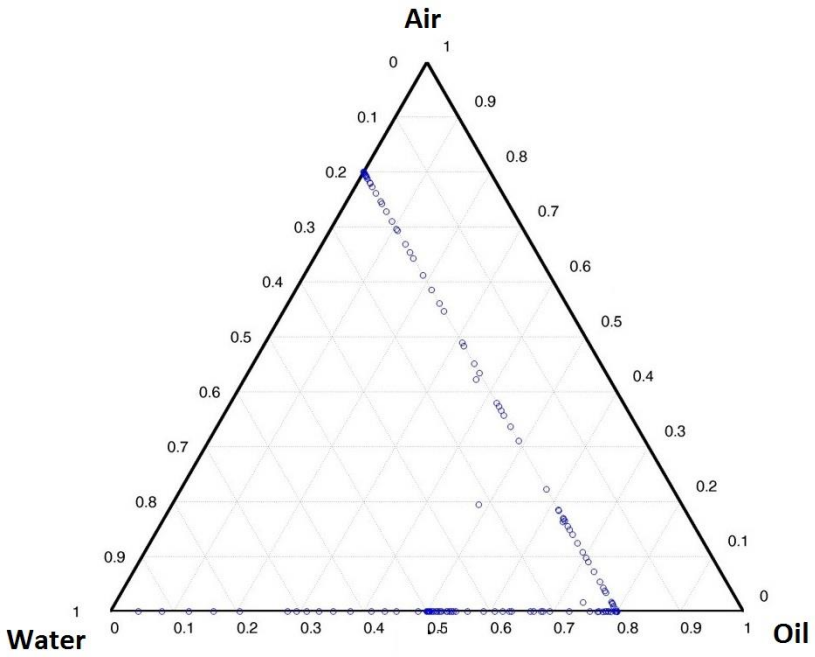

Figure 4.23 Ternary diagram of simulation gridblock phase saturation histories for a three-phase simulation (water, oil and air) with residual water equal to 0.2 and the Corey-Brooks exponents all equal to 1.0

With only few exceptions, the three-phase saturation points form linear trajectories in the ternary diagram. These few points located off the linear trend occur at the beginning of the simulation when three-phase mixing occurs at the top of the reservoir. Points along the air saturation line of zero depict the mixtures of water and oil below the oil-air transition region. The second line of points forms along the water saturation line of 0.2, the residual value of water. These points depict saturation values in regions above the water-oil transition zone where only oil and air are both mixing and flowing.

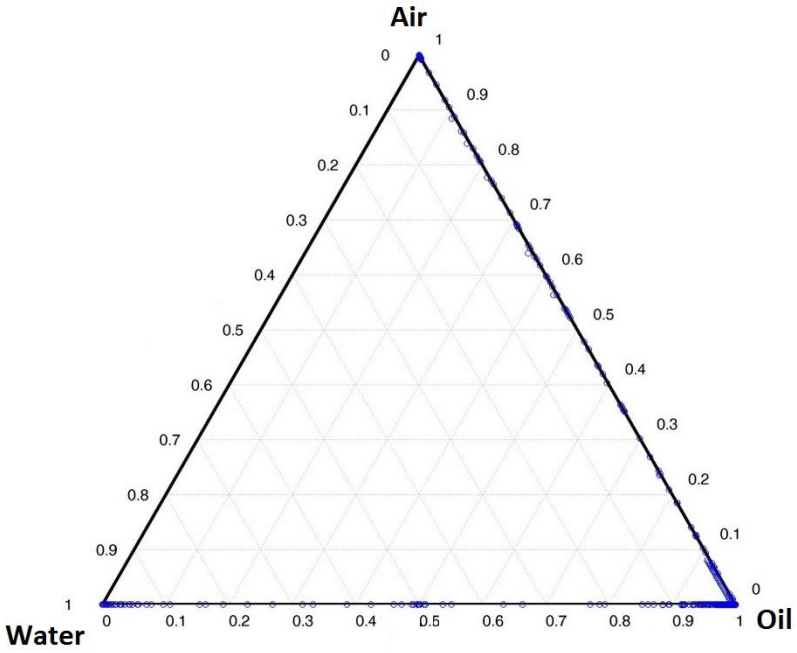

Figure 4.24 Ternary diagram of simulation gridblock phase saturation histories for a three-phase simulation (water, oil and air) with residual water equal to 0.0 and the Corey-Brooks exponents all equal to 1.5

A similar three-phase simulation (Figure 4.24) was performed in which all input properties were identical to the example in Figure 4.23 with two exceptions. The Corey-Brooks relative permeability model exponents were set to 1.5. And the water residual saturation was set to a value of zero. The trajectories of three-phase saturation points are still linear as it was in the previous example; however, a few points along the water saturation of zero line deviate slightly. In the next example simulation, more dramatic deviates occur.

The third example is a simulation that is identical to the one depicted in Figure 4.25 with the exception that the Corey-Brooks relative permeability model exponents were set to a higher value, 2.5. A dramatic difference is observed in Figure 4.25. The three-phase saturation points no longer form a clear linear trajectory parallel to the residual water

saturation line. Due to this scatter, three-phase mixing appears to be prevalent throughout the simulation. Therefore, for an initially unsegregated oil-water reservoir undergoing top gas injection, the degree of mixing may be related to the curvature of the relative permeability functions.

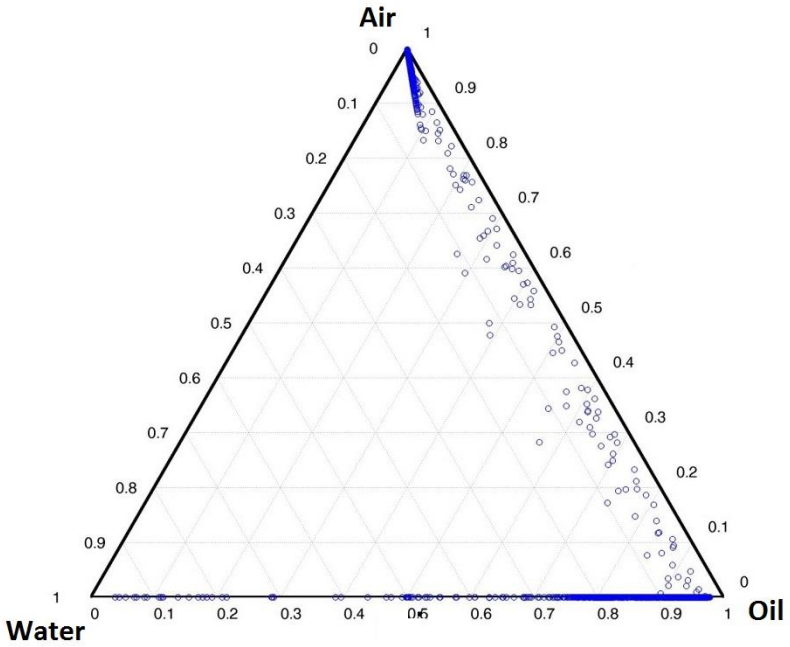

Figure 4.25 Ternary diagram of simulation gridblock phase saturation histories for a three-phase simulation (water, oil and air) with residual water equal to 0.0 and the Corey-Brooks exponents all equal to 2.5

Significant mixing in this simulation may be attributable to intensified lower water relative permeabilities, brought about by the combination of low water saturation regions and the large Corey-Brooks relative permeability model exponent value. These low water saturation regions tend to remain stagnant for longer periods to the point that the front of air reaches them. As is noted in later sections, the relative permeability of the three phases

plays an immense role in governing the behavior of gravity drainage processes. See Table 4.3 for more information about the simulations.

4.3.3 Multidimensional Effects in Simulation

All simulation cases presented thus far have reservoirs which only extend with more than one gridblock in the vertical direction. More than one gridblock is now applied in one of the lateral dimensions. Due to the extra lateral gridblocks, wells on the top and bottom of the reservoir may not necessarily align vertically, which leads to complications in flow patterns.

A UTCHEM simulation was run with 3 gridblocks in the Y-direction (lateral dimension). The number of gridblocks in the X-direction and Z-direction are one and 50, respectively. Initially the reservoir is completely saturated with oil, and air is injected at the top of the reservoir. Two wells were placed in the reservoir and were operated at constant atmospheric pressure. The constant pressure well injector at the top of the reservoir was placed in the first Y-direction gridblock; the constant pressure well producer at the bottom of the reservoir was placed in the third Y-direction gridblock. For more information about the inputs of this simulation, please consult Table 4.3. This simulation differs from previous cases because of the misalignment of the wells at the top and bottom of the reservoir. Figures 4.26 and 4.27 show the change in the vertical oil saturation distributions of the columns in the first and third Y-direction gridblocks, respectively.

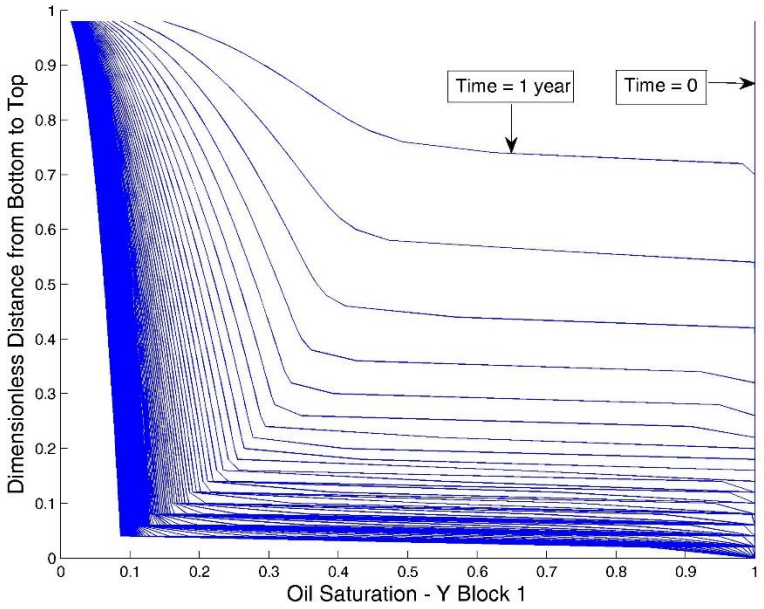

Figure 4.26 Vertical oil saturation profiles at time increments of 1 year along the X-Z plane of the first Y gridblock

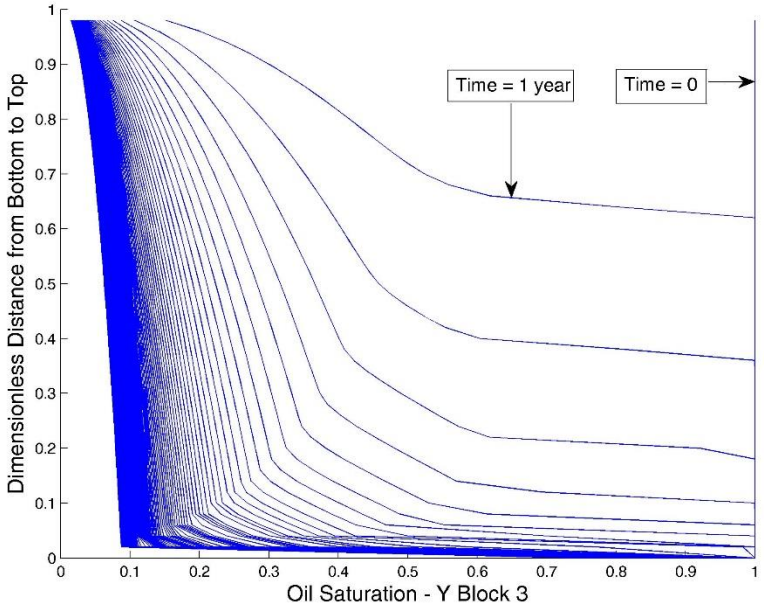

Figure 4.27 Vertical oil saturation profiles at time increments of 1 year along the X-Z plane of the third Y gridblock

Figures 4.26 and 4.27 illustrate the differences in the vertical oil saturation profiles as they evolve both in time and comparatively in the lateral Y dimension. Due to the misalignment of the wells, the oil column drops in height much more quickly in the third Y-direction gridblock than in the first Y-direction gridblock. Since the oil column differs in height laterally throughout the simulation, the oil-air interface is no longer flat.

For gas-assisted gravity drainage projects, this vertical misalignment of wells may cause a lateral difference in the fluid phase saturations. Production rates may be sensitive to the placement of the injection and production wells. High lateral permeability may help smear the effect of vertically misaligned injection and production wells.

4.3.4 General Influence of Input Properties on Production Rates

A variety of input properties were analyzed by their effect on water and oil production rates from gas-assisted gravity drainage simulations. The input properties analyzed were those that controlled the mobility of the fluid phases. The Corey-Brooks formulation for three-phase relative permeability was adopted for all simulations.

The same general set of inputs are used for all simulations presented in section 4.3.4. Some of these input properties are modified based on the property undergoing sensitivity study; however, all others remain equal to those described in the general set of inputs. The general set of inputs proceeds as follows: the number of gridblocks in the X-, Y-, and Z-directions are one, one, and 50, respectively. The lateral dimensions are 660 ft in length, and the vertical dimension extends 50 ft. The lateral permeability is 100 mD, whereas the vertical permeability is 50 mD. Initially the reservoir is homogeneously

saturated with 50% water and 50% oil. Two wells operate at constant atmospheric pressure conditions with the top well injecting air. The densities of water, oil, and air are 0.433 psi/ft, 0.377 psi/ft, 0.001 psi/ft, respectively. Other information concerning these simulations can be found in Table 4.3. Please note that the Corey-Brooks exponent values of all phases are equivalent for all simulations in this sensitivity study.

The first input property analyzed was the end-point relative permeability to oil. Two different values were selected and used in the simulations seen in Figure 4.28. The behavior of the production rate of water is not altered by an appreciable amount when the end-point relative permeability to the oil phase is changed. The oil production rate, however, is affected by this change in value. For the percent change in the value of the end-point relative permeability to oil, the oil production rate initially scaled approximately by the same amount. After the initial surge of oil production, the decline begins to take effect, eventually leading to lower production rates for the simulations with higher end-point relative permeability to oil.

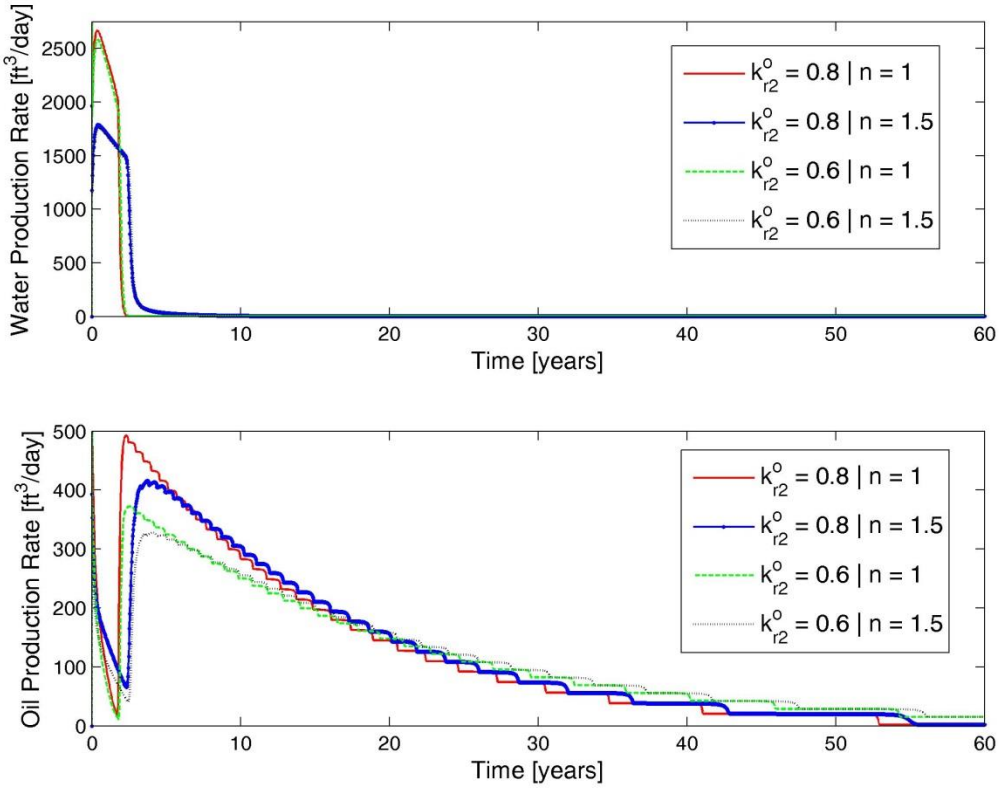

Figure 4.28 Phase production rates sensitivity study to both the end-point relative permeability to oil and the Corey-Brooks exponent

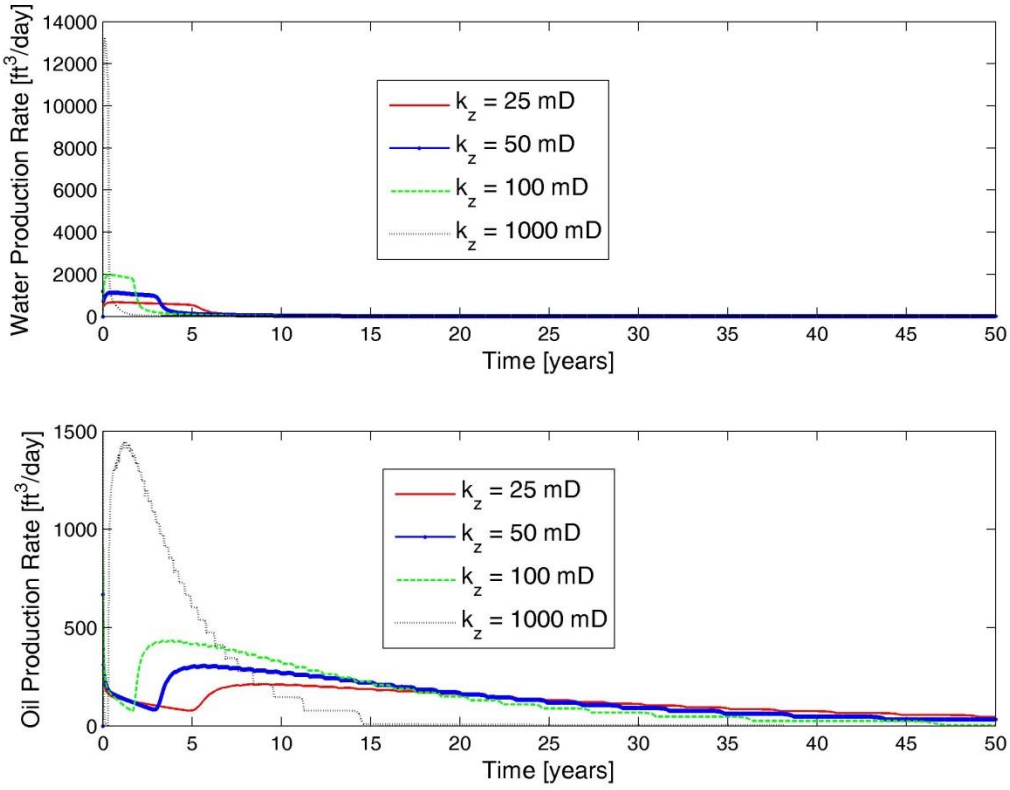

Figure 4.29 Phase production rates sensitivity study to vertical permeability

The absolute vertical permeability was also analyzed. Higher absolute vertical permeability values lead to higher production rates, but the degree to which an increase is observed is not proportional to the change in the permeability. In Figure 4.29, the initial water production rate for simulations with vertical permeability of 1000 mD and 100 mD vary by a multiplying factor of approximately seven. The difference in production rates of oil is even smaller. For the same simulations, the oil production rates only vary by a multiplying factor of approximately three.

A large range of oil viscosities were analyzed through simulations. In Figure 4.30, water production rates are initially higher for lower oil viscosities; however, once the higher saturation oil bank begins to push through, the production rate of water declines much more quickly for the simulation cases with higher oil viscosity. This most likely occurs due to the change in mobility ratio of the two fluid phases. The oil production rates are initially much lower for high viscosity oil, which leads to long, slow-declining oil production rates.

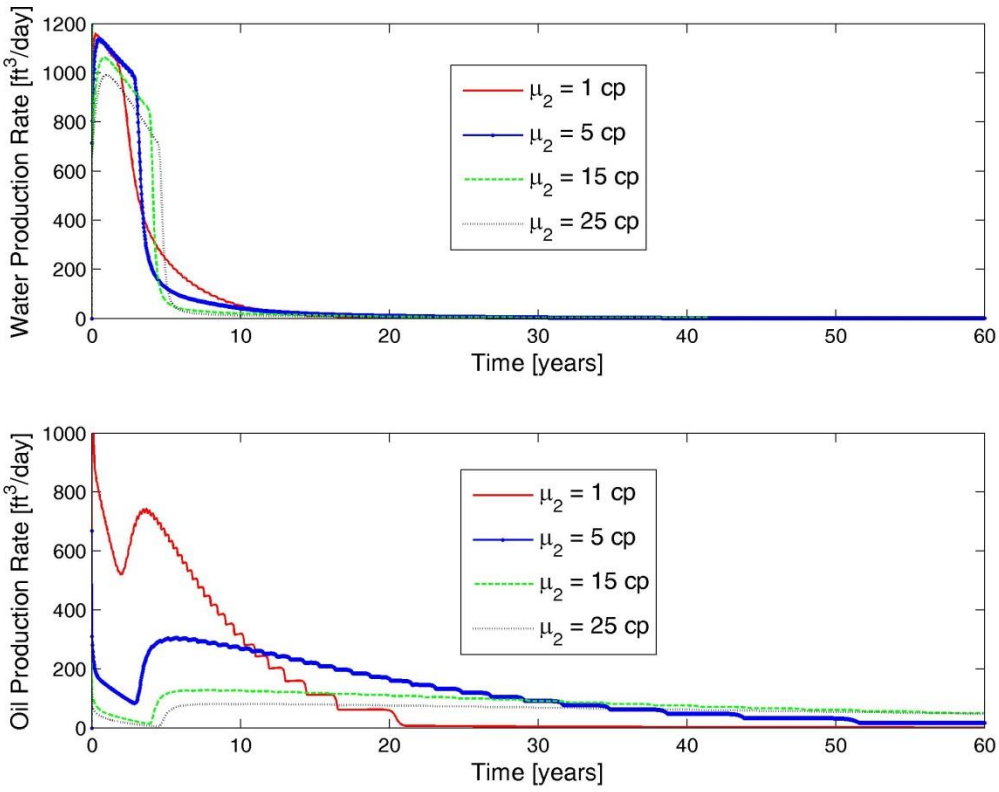

Figure 4.30 Phase production rates sensitivity study to oil viscosity

The curvature of the relative permeability functions also plays a role in flow behavior. The n-exponent in the Corey-Brooks three-phase relative permeability model controls this curvature and plays an important role in production rates. A larger value of the n-exponent for all phases leads to lower initial, yet more prolonged and steady, production rates of each phase as is illustrated in Figure 4.31.

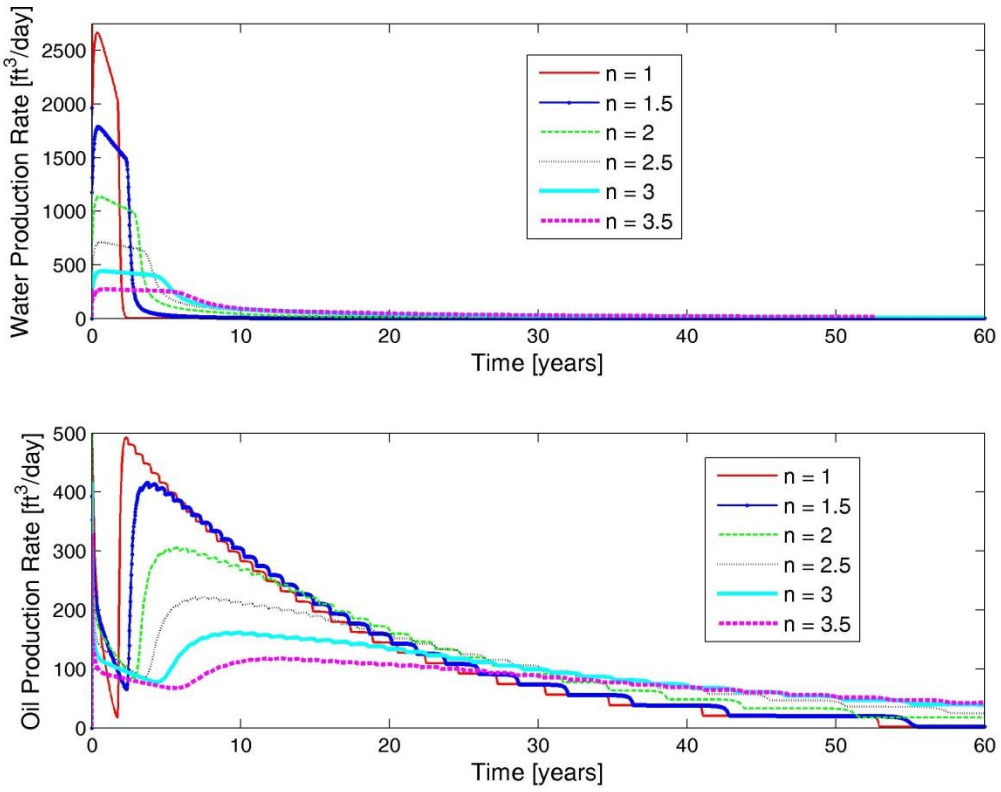

Figure 4.31 Phase production rates sensitivity study to Corey-Brooks exponent for all phases

The last two input properties that were investigated were the initial and residual water saturations. These two properties play a key role in the relative permeability model for both phases. Figure 4.32 shows the effect of the initial water saturation throughout the reservoir. These simulations were conducted with an assumed residual water saturation of 0.2. Therefore, when the initial saturation of the reservoir is 0.2, no water flows or is produced, and the oil production rate follows a steady decline with no banking character. As the initial water saturation is set to higher values, the water production rate is initial higher, which is paired with a decrease in the oil production rate once the oil bank is produced.

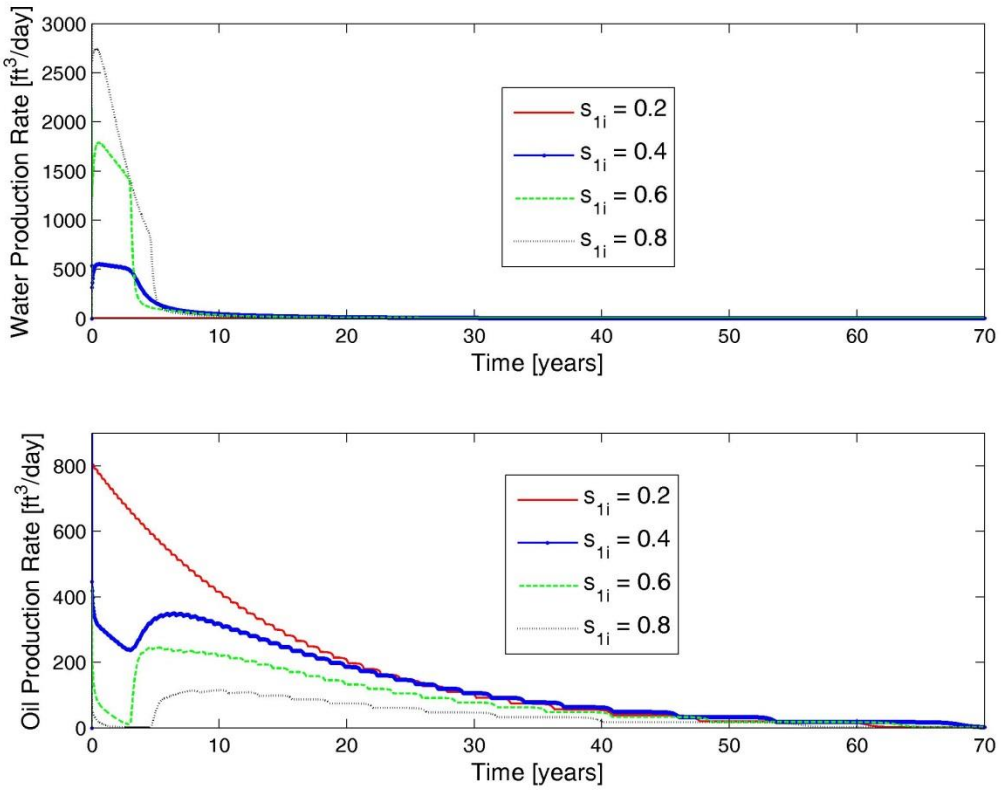

Figure 4.32 Phase production rates sensitivity study to initial water saturation

In Figure 4.33, the residual water saturation is varied while holding the initial water saturation at 0.5 throughout the entire reservoir. Higher residual water saturation yielded lower water production rates and higher oil production rates initially which declined more quickly.

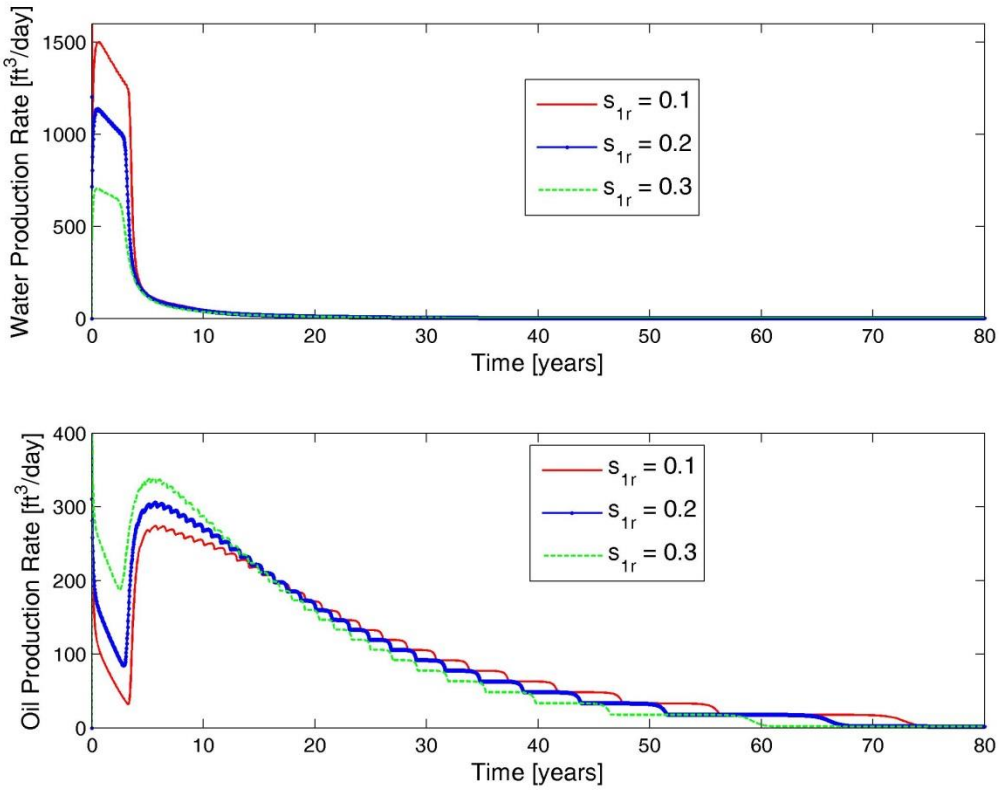

Figure 4.33 Phase production rates sensitivity study to residual water saturation

The relative mobilities of the different phases and their ratios play a key role in the dynamics of the flow behavior in three-phase systems, such as gas-assisted gravity drainage processes. Although the values of the factors which influence the relative permeability of

each phase are typically assumed to be filled with uncertainty in reservoir studies, they play a major role in the dynamics of the flow behavior in such multiphase systems.

4.3.5 Further Insights and Potential Development of Gravity Drainage Processes

Three simulations have been selected to illustrate three general cases of three-phase gravity drainage. These cases are described as follows: (1) Free fall gravity drainage with water saturation initially at residual, (2) Forced gravity drainage with water saturation initially at residual, (3) Free fall gravity drainage with water saturation initially above residual.

In general, simulations which initially are characterized by water saturations at residual values exhibit no flow of water in the reservoir because of a lack of mobility in the water phase. Three-phase free fall gravity drainage simulations which are initially characterized by residual water saturation result in oil production rates that decline exponentially with time, as is shown in Figure 4.34.

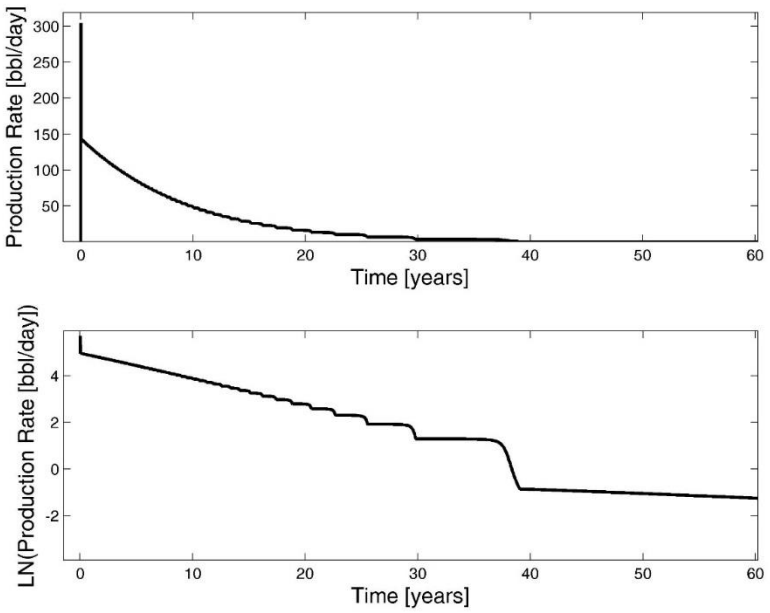

Figure 4.34 Linear-linear and log-linear plots of oil production rate versus time for a three-phase UT-EMPRES free fall gravity drainage simulation with water initially at residual saturation

From the plot of the logarithm of the oil production rate in Figure 4.34, it is clear that there are a series of stepwise declines in the production rate; however, the overall trend of the oil production rate declines exponentially.

Figure 4.35 shows a similar simulation with the exception that this gravity drainage is forced by an imposed pressure difference between the injector and production well of 10 psi. The same exponential decline of the oil production rate ensues with a dramatic reduction in the step-like nature of the decline. Instead, after a certain point in the simulation, oil production rates dramatically decline and take on another functional form.

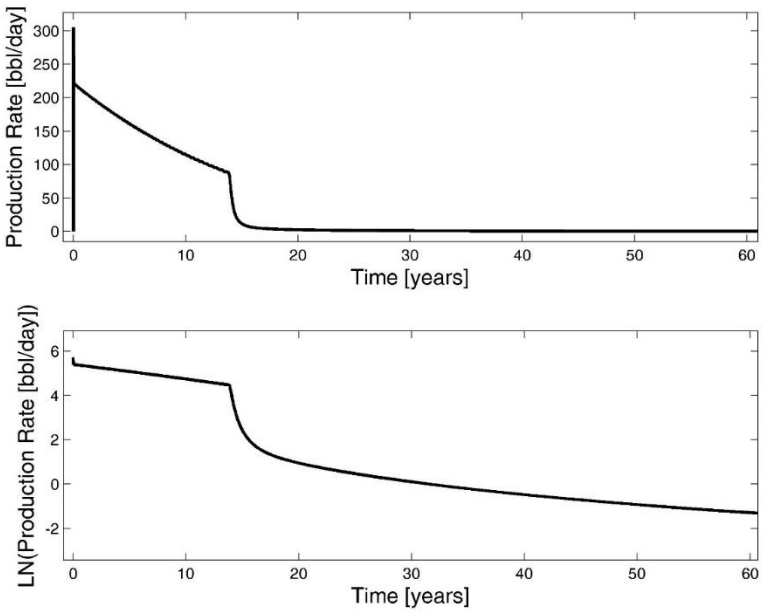

Figure 4.35 Linear-linear and log-linear plots of oil production rate versus time for a three-phase UT-EMPRES forced gravity drainage simulation with water initially at residual saturation

The last example case of three-phase gravity drainage is similar to the first type described in that it is free fall in character; however, in this case, initial saturations of water to be greater than residual levels. Since water levels are above residual values initially, water flows and is produced from the reservoir as is shown in Figure 4.36. Production rate behavior of the water and oil appear to be quite exponential in character at certain regions of the simulation. Between years 0 and approximately 3, a water bank structure has formed and is being produced, which results in exponential decline of both phases. A similar result occurs when the oil bank is formed and produced between years 18 and 60. The non-exponential declines of phase production rates occur when the transition zone between water and oil is being produced between years 3 and 18.

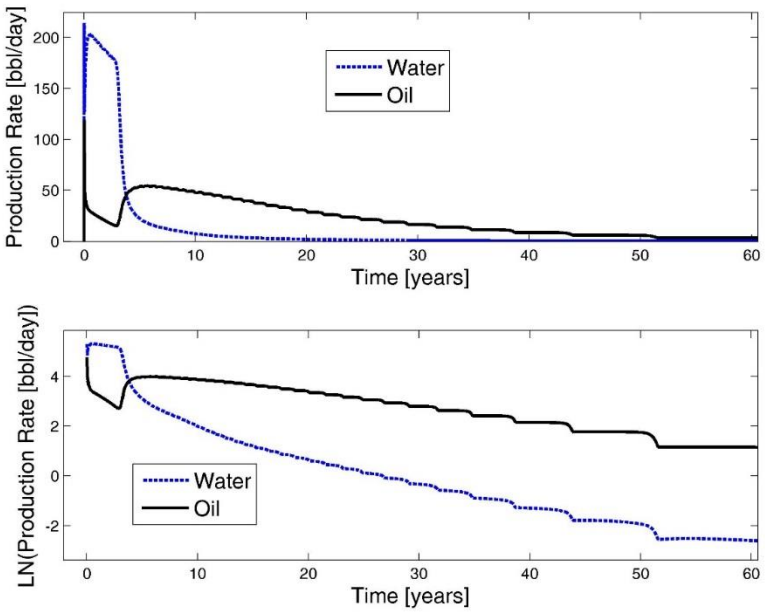

Figure 4.36 Linear-linear and log-linear plots of oil and water production rates versus time for a three-phase UT-EMPRES free fall gravity drainage simulation with water initially above residual saturation

General single-phase primary depletion simulations prove to be fit well by the generalized flow rate model (GFRM). These single-phase primary depletion cases exhibit exponential decline in the depletion stage of production. From these three cases presented in section 4.3.5, exponential decline of phase production rates appear when a banking structure of one phase is produced. Since only oil is produced when water is initially at residual levels, these types of three-phase gravity drainage simulations are great candidates for modeling through the GFRM. A more complicated version of the GFRM would ensue if attempts to capture the type of simulation seen in Figure 4.36.

Table 4.3 Simulation input data for various figures in section 4.3

Simulator Used	**UT-EMPRES**	**UTCHEM**	**UTCHEM**	**UT-EMPRES**	**UTCHEM**
Input Property	**Figure 4.15**	**Figures 4.16-18**	**Figures 4.19-22**	**Figs. 4.3.23-25,28-33**	**Figs. 4.26-27**
I.NX	1	1	1	1	1
I.NY	1	2	2	1	5
I.NZ	50	50	50	50	50
I.LX	660	200	7000	660	200
I.LY	660	200	7000	660	200
I.LZ	100	200	50	50	200
I.phi	0.25	0.25	0.2	0.25	0.25
I.kx	100	50	25	100	50
I.ky	100	50	25	100	50
I.kz	50	50	5	50	50
I.sat1i	0	1	0.5	0.5	1
I.sat3i	1	-	0	0	-
I.cf	0.00E+00	0.000003	0.000003	1.00E-09	0.000003
I.Pinit	14.7	14.7	14.7	50	14.7
I.top_depth	0	0	0	0	0
I.ddir	1	-	-	1	-
I.angle	0	-	-	0	-
I.ellipse	0	-	-	0	-
I.xsemi	3000	-	-	3000	-
I.ysemi	2500	-	-	2500	-
I.RadSym	0	-	-	0	-
I.RadSym_nw	10	-	-	10	-
I.mu1	1	2	1	1	2
I.mu2	5	0.002	2	5	0.002
I.mu3	1	-	0.002	0.02	-
I.rho1_ref	0.377	0.38	0.44	0.433	0.38
I.rho2_ref	0.377	0.0005	0.38	0.377	0.0005
I.rho3_ref	0.377	-	0.0005	0.001	-
I.rho1_pref	14.7	14.7	14.7	14.7	14.7
I.rho2_pref	14.7	14.7	14.7	14.7	14.7
I.rho3_pref	14.7	-	14.7	14.7	-
I.s1r	1	0	0	0.2	0
I.s2r1	1	0	0	0	0
I.s2r3	1	-	0	0	-
I.s3r	0	-	0	0	-
I.kr1ep	0	1	1	0.8	1
I.kr2ep	0	1	1	0.8	1
I.kr3ep	1	-	1	0.8	1
I.n1	0	3	3	1	3
I.n2	0	3	3	1	3
I.n3	0	-	3	1	-
I.c1	0	0.00006	0.000003	0.000003	0.00006
I.c2	0	0.0014	0.000015	0.000015	0.0014
I.c3	0	-	0.0014	0.01	-
I.options.setup	1	-	-	1	-
I.options.constraints	0	-	-	0	-
I.nw	2	2	2	2	2
I.orientation	1*ones(1,2)	2*ones(1,2)	2*ones(1,2)	1*ones(1,2)	1*ones(1,2)
I.rw	0.16667*ones(1,2)	0.5*ones(1,2)	0.5*ones(1,2)	0.16667*ones(1,2)	0.5*ones(1,2)
I.skin	0*ones(1,2)	0*ones(1,2)	-6.5*ones(1,2)	0*ones(1,2)	0*ones(1,2)
I.type	[3 2]	[3 2]	[3 2]	[3 2]	[3 2]
I.condition	14.7*ones(1,2)	14.7*ones(1,2)	14.7*ones(1,2)	14.7*ones(1,2)	14.7*ones(1,2)
I.constraint_min	0*ones(1,2)	-	-	0*ones(1,2)	-
I.constraint_max	0*ones(1,2)	-	-	0*ones(1,2)	-
I.origin	1*ones(1,2)	1*ones(1,2)	1*ones(1,2)	1*ones(1,2)	1*ones(1,2)
I.terminus	1*ones(1,2)	2*ones(1,2)	2*ones(1,2)	1*ones(1,2)	1*ones(1,2)
I.tcoord1	1*ones(1,2)	1*ones(1,2)	1*ones(1,2)	1*ones(1,2)	[1 3]
I.tcoord2	[1 50]	[1 50]	[1 50]	[1 50]	[1 50]

CHAPTER 5: CONCLUSIONS AND RECOMMENDATIONS

5.1 CONCLUSIONS

5.1.1 UT-EMPRES

- The three-dimensional, finite-difference numerical reservoir simulator yielded results nearly identical to analytical solutions and other simulators (UTCHEM and CMG) for modeling slightly compressible phases for all cases tested.
- Numerical instabilities can form in the simulator if the assumption of slightly compressible phases is not followed. In this work, it was assumed in the gas phase (air) was slightly compressible because of the relatively small pressure changes.
- UT-EMPRES provides the user with a novel easy-to-use Microsoft Excel interface, which accesses the powerful MATLAB simulation code.

5.1.2 Generalized Flow Rate Model

- The semi-empirical GFRM equation (3.6 and 4.1-4) has been developed and can be used to adequately fit virtually any primary depletion reservoir production scheme with any number of wells of identical constant pressure operating condition when four parameters, b, t_{dep}^{*}, q_{dep}^{*}, and λ^{*} are treated as fitting parameters .
- The production scheme of using vertical wells was fitted through over 2000 simulations in order to develop a predictive form of the GFRM.
- The key parameters that were fit by over 2000 simulations are only functionally dependent on the number of wells and sometimes the diffusivity and the areal extent of the reservoir.

- The GRFM assumes a very simple model for the pre-depletion stage, but nonetheless gives could predictions especially at late times for most cases studied here. A more complicated pre-depletion model could be implemented in the GFRM for more accuracy.
- Correlation equations (4.1-4) are developed for the four key parameters as a function of number of wells, reservoir area, and diffusivity constant for homogeneous, isotropic reservoirs. The correlations are simple (and could be improved), but are adequate in the range of properties studied here.
- Predictability of the GFRM for vertical wells is very good for the vast majority of simulation inputs and acceptable for most errant cases. However, combinations of input variables outside of the range investigated can prove to be too extreme for the GFRM to model accurately. This GRFM could be improved by developing more rigorous equations for the four fitting parameters.
- The GRFM is expected to work for horizontal wells, gravity, and in some cases even multiphase flow. However, the functionality of the four model parameters would likely be unique.

5.1.3 Gravity Drainage

- Darcy's law for a purely gravity-driven flow can be approximated through simulation by imposing an artificial well skin on the traditional Peaceman well model.
- Vertical permeability and phase saturation quantities, including those involved in the relative permeability relations, are extremely important in the gravity drainage process.

- The curvature of the relative permeability relations can play a role in the amount of three-phase mixing occurring for initially non-segregated gas-assisted gravity drainage (GAGD) simulations.
- Due to the inherent resistance in porous media, vertical misalignment of top injection wells and bottom producing wells for GAGD systems can alter pressure and saturation profiles in the lateral dimension, which can dramatically affect production curves.
- For free fall (and in some cases forced) three-phase gravity drainage simulations, exponential decline of phase production rates are observed when phase bank structures undergo production – which may open up the opportunity to fit the GFRM for these processes.

5.2 RECOMMENDATIONS

5.2.1 UT-EMPRES

- UT-EMPRES could be improved upon by adding several capabilities for three phase flow, such as compressible fluids, capillary pressure, other relative permeability models, etc.
- Interactions between Excel and MATLAB could be more efficient.
- As expected, the simulations are relatively slow for multiple dimensions and phases compared to commercial and academic simulators CMG and UTCHEM. Significant effort was put into improving the speed and robustness, but additional vectorization and code optimization could improve the speed.

5.2.2 Generalized Flow Rate Model

- The functionality of the fitting parameters for the case of vertical wells could be improved in order to improve the predictability of the GFRM for a broader range of input values.
- The GFRM could be extended to include different production schemes which include horizontal wells, gravity, uncentered wells (with help of the Dietz shape factor)
- Three-phase gravity drainage simulations, especially those characterized by initial residual water levels, could be used to extend the GFRM to GAGD processes.
- Although the GFRM works for all primary recovery simulations tested when the four fitting parameters are treaded as best fits, the empirical equations for the parameters do not apply when wells are not relatively uniformly spaced. Improved correlations for non-uniform spacing should be developed.
- The GRFM should be extended to horizontal wells, gravity, and in some cases even multiphase flow; new functionality of the four model parameters would need to be developed. For the case of gravity, it is recommended to add the constant gravity hydrostatic head to the pressure drawdown in equations 2.11-2.14

5.2.3 Gravity Drainage

- The three-phase relative permeability relationships for gravity drainage processes could be improved.
- Specific gravity drainage production schemes could be modeled through the GFRM.

- Capillary pressure effects on GAGD should be investigated because the order of magnitude of the value of capillary pressure may be near or equivalent to the overall pressure of the fluid phases.
- Small-scale processes drive gravity drainage in its late stages. These processes are not well studied and should be further developed and eventually implemented into numerical simulation in some manner.

CHAPTER 6: USER'S MANUAL FOR UT-EMPRES

UT-EMPRES
The University of Texas at Austin – Excel-interfaced MATLAB-based Petroleum Reservoir Simulator

Version 1.0 (Release July 2014)

By

The Department of Petroleum & Geosystems Engineering
The University of Texas at Austin
Austin, Texas 78712

Primary Author: Cameron A. Vitter (M.S. 2014)
Principal Advisor: Dr. Matthew T. Balhoff
Co-advisor: Dr. Larry W. Lake

Table of Contents

Section 1: Introduction

This MATLAB-based numerical reservoir simulator is built upon the classic finite difference approach to numerically approximate physical phenomena. Fluid flow and transport in porous media is approximated through a numerical treatment of general conservation equations and auxiliary relations (as can be seen in the Mathematical Formation in Section 7). The numerical schemes utilized are the classic and improved IMPES formulations, which are implicit in their treatment of solving for pressure and explicit in their treatment of solving for phase saturations.

The simulator can be used to solve up to three distinct, immiscible phases. These phases are modeled as slightly compressible fluids with constant viscosities. Relative permeability is an important contributor to the inherent ability of a fluid phase to flow in a reservoir. Relative permeability is modeled empirically through the general model functional form given by Corey and Brooks (Corey, 1954) for two-phase systems and the extended formulation for three-phase systems. Other relative permeability models, such as the Stone models (Stone, 1973) and others, could easily be incorporated into the code, which should be a future additional capability.

External influences on the reservoir can be taken in the form of either a well or a boundary condition. Vertical and horizontal wells can be incorporated into a given simulation with trajectories parallel to any of the principal coordinate axes. These wells can exhibit constant rate or pressure conditions. Constant pressure wells can be constrained to operate within a given pressure range. Well productivity indices are incorporated

through Peaceman's traditional formulation (Peaceman, 1978) and its extension to multiphase flows. Wells may be incorporated in one of two ways: either in a manual or an automatically-spaced method. Additional well capabilities, such as scheduling, arbitrarily-declared well perforations for a given well, and Babu's productivity formulation (Babu et al., 1989), should be incorporated into the code in the future. Boundaries conditions are the second form of external influences on the reservoir. These can currently be employed in the form of no flow conditions or constant pressure conditions on any boundary. These boundary conditions capabilities should be extended to incorporate constant rate conditions as well in the future. It may also be wise to introduce a spatially-varying constant pressure along a boundary due to the presence of gravity and its contribution to a hydrostatic head of fluids.

Numerically, a given simulation marches through time and saves data in a constant, linear fashion. Log-scale time advancement was used in a previous, single-phase case of the code; however, it is important to note that this code only solved for pressure and did this in an implicit manner (always stable). Since the current version of the code is written in such a manner that solves for phase saturations explicitly (IMPES), the log-scale time advancement method is not an option for a wide range of stable simulations. Alternatively, an automatic time-step selector could be incorporated into the code in a traditional manner based on the CFD number (Courant et al., 1928).

Other capabilities of this simulator include reservoir characterization. Porosity, directional permeabilities, phase saturations, and pressure may all be set as constant values throughout the entire reservoir, constant values by reservoir layer, or individually for each

gridblock. There is also the capability of automatic generation of a pseudo-simulation of an elliptically-shaped reservoir as well as a circular section of a reservoir. These geometries are discussed in the proceeding sections. Variable gridblock dimensions could be incorporated as an option in this code.

This simulator does not account for capillary pressures between phases – which should be a future development of the code. Also, there is no option to automatically introduce a capillary-gravity equilibrated system at the beginning of a simulation (other than using data obtained from running the simulation for long times at high permeabilities with no external influences).

Section 2: Using UT-EMPRES

Since this simulator has been written in MATLAB, it can be run through a few different paths, but the use of the MATLAB Command Window and Editor and Excel-based interface are explained below. There are a few key files which the user can manipulate to access the full capabilities of the simulator. These files can be seen in Table 6.1 and are explained in more detail in Section 4:

Table 6.1 Key files associated with the UT-EMPRES

Quantity Described	Associated External File Name
Majority of Input Data	Input.m
Porosity	phi.txt
X-Direction Permeability	permx.txt
Y-Direction Permeability	permy.txt
Z-Direction Permeability	permz.txt
Initial Phase-1 Pressure	pres1.txt
Initial Phase-1 Saturation	sat1.txt
Initial Phase-3 Saturation	sat3.txt
Majority of Input Data (Using Excel)	UTEMPRES.xlsm

The explanation for the use of the simulator is introduced based on the file Input.m (for Matlab-based interfacing) or UTEMPRES.xlsm (for Excel-based interfacing). All other files in the table above are optional based on the data in Input.m or UTEMPRES.xlsm. Many input quantities must be introduced in the Input.m or UTEMPRES.xlsm file in a certain format. These are mentioned in the following paragraphs. Also, please note that all Input.m or UTEMPRES.xlsm variables are more extensively explained in Section 6.

Although only the Input.m file is discussed below, the same input items are available through the Input tab of UTEMPRES.xlsm under column A.

The first section of the main input file, Input.m, accounts for reservoir properties. If any external *.txt files are declared to be used (through manipulating the I.options.* quantity in Input.m to be a value of 2 or 3), the constant values for the associated quantities do not need to be incorporated as part of the Input.m file since they are not be relevant to the simulation.

In order to run the simulation, the Input.m file must first be completed with the necessary input lines, then the Main.m file can be called from the Matlab Command Window simply by typing Main then pressing the Enter key. The simulation then begins and shows completion status with a bar. When the simulation is complete, the status bar closes and an alert window appears stating that the simulation has run to completion.

Section 3: List of Necessary Files and Simulation Progression

Below is a list of files that are necessary to run this simulator:

If Matlab-based interface is being used:

get_wells.m
Input.m
Main.m
Plot_Matlab.m
Postprocess.m
Preprocess.m
Process.m
set_upstream.m

If Excel-based interface is being used:

UTEMPRES.xlsm
UTEMPRES.exe
UTEMPRES_PLOT.exe

Description of necessary files:

get_wells.m

This function file reads data from the Input.m and subsequent Preprocess.m files then calculates various properties of all wells assigned in Input.m.

Input.m

This script file is used by the user to input necessary input data for the desired simulation to be run.

Main.m

This script file is executed by the user to run the prepared simulation.

Plot_Matlab.m

This function file reads data from several sources as well as user inputs then plots a three-dimensional visualization of the specified attribute at the designated point in the simulation.

Postprocess.m

This script file uses data from the simulation run and performs various calculations as well as plotting if selected in Input.m.

Preprocess.m

This function file reads data from Input.m and uses it to numerically build and initialize the reservoir as well as critical data structures used in the simulation of the reservoir.

Process.m

This script file uses data from previous files and performs the calculations associated with time-varying properties (the IMPES routine).

set_upstream.m

This function file reads data from various sources and performs an update on relative permeability, relative mobility, upwinding of mobilities, and recalculations of the necessary transmissibility matrices.

UTEMPRES.xlsm

This Excel file is used by the user to input necessary input data for the desired simulation to be run.

UTEMPRES.exe

This executable file is used by the "Run Simulation" macro button on the Input tab of UTEMPRES.xlsm. The "Run Simulation" macro button runs the simulation with the inputs specified on the Input tab.

UTEMPRES_PLOT.exe

This executable file is used by the "Plot" macro button on the Input tab of UTEMPRES.xlsm. The "Plot" macro button plots a 3-dimensional visualization of the specified output field on the Input tab.

SIMULATION PROGRESSION

Key: **bold =** main simulation subroutine or function
italics = subfunction

All of the below are contained within the Main.m file.

Input.m
Preprocess.m
get_block_props
init_grid_setup

get_corners
modify_grid_center
modify_grid_corners
get_faces
get_interfaces
get_const_trans
get_bound_cont
get_wells.m

Process.m

set_upstream.m

Postprocess.m

Plot_Matlab.m

Section 4: Optional Input Files/Tabs

Below is a list of optional input files/tabs that can be used to more easily input certain data. Data from these files are extracted in a particular format.

Data for all gridblocks is extracted and assigned to each gridblock assuming the numbering of each gridblock is in accordance with a nested looping scheme for the x-direction, y-direction, and z-direction (positive downward), respectively, such that the x-direction is the most inner loop.

Data constant for each layer is read in order of layers starting with the top layer and working downward (the z-direction is positive downward).

phi.txt / "Porosity" Tab – porosity data
UNITS: dimensionless

If I.options.phi = 1, then the constant input I.phi is used.
If I.options.phi = 2, then the phi.txt is used assuming a value for all gridblocks.
If I.options.phi = 3, then the phi.txt is used assuming a value for each layer.
If I.options.phi = 4, then the "Porosity" Tab is used assuming a value for all gridblocks.
If I.options.phi = 5, then the "Porosity" Tab is used assuming a value for each layer.

permx.txt / "Permeability" Tab – x-direction permeability data
UNITS: millidarcy

If I.options.permx = 1, then the constant input I.kx is used.
If I.options.permx = 2, then the permx.txt is used assuming a value for all gridblocks.
If I.options.permx = 3, then the permx.txt is used assuming a value for each layer.
If I.options.permx = 4, then the "A" column of the "Permeability" Tab is used assuming a value for all gridblocks.
If I.options.permx = 5, then the "A" column of the "Permeability" Tab is used assuming a value for each layer.

permy.txt / "Permeability" Tab – y-direction permeability data
UNITS: millidarcy

If I.options.permy = 1, then the constant input I.ky is used.
If I.options.permy = 2, then the permy.txt is used assuming a value for all gridblocks.

If I.options.permy = 3, then the permy.txt is used assuming a value for each layer.
If I.options.permy = 4, then the "B" column of the "Permeability" Tab is used assuming a value for all gridblocks.
If I.options.permy = 5, then the "B" column of the "Permeability" Tab is used assuming a value for each layer.

permz.txt / "Permeability" Tab – z-direction permeability data
UNITS: millidarcy

If I.options.permz = 1, then the constant input I.kz is used.
If I.options.permz = 2, then the permz.txt is used assuming a value for all gridblocks.
If I.options.permz = 3, then the permz.txt is used assuming a value for each layer.
If I.options.permz = 4, then the "C" column of the "Permeability" Tab is used assuming a value for all gridblocks.
If I.options.permz = 5, then the "C" column of the "Permeability" Tab is used assuming a value for each layer.

pres1.txt / "Pressure" Tab – initial pressure data
UNITS: psi

If I.options.pres = 1, then the constant input I.Pinit is used.
If I.options.pres = 2, then the pres1.txt is used assuming a value for all gridblocks.
If I.options.pres = 3, then the pres1.txt is used assuming a value for each layer.
If I.options.pres = 4, then the "Pressure" Tab is used assuming a value for all gridblocks.
If I.options.pres = 5, then the "Pressure" Tab is used assuming a value for each layer.

sat1.txt / "Water Saturation" Tab – initial saturation of phase 1 data
UNITS: dimensionless

If I.options.sat1 = 1, then the constant input I.sat1i is used.
If I.options.sat1 = 2, then the sat1.txt is used assuming a value for all gridblocks.
If I.options.sat1 = 3, then the sat1.txt is used assuming a value for each layer.
If I.options.sat1 = 4, then the "Water Saturation" Tab is used assuming a value for all gridblocks.
If I.options.sat1 = 5, then the "Water Saturation" Tab is used assuming a value for each layer.

sat3.txt / "Gas Saturation" Tab – initial saturation of phase 3 data
UNITS: dimensionless

If I.options.sat3 = 1, then the constant input I.sat3i is used.
If I.options.sat3 = 2, then the sat3.txt is used assuming a value for all gridblocks.
If I.options.sat3 = 3, then the sat3.txt is used assuming a value for each layer.
If I.options.sat3 = 4, then the “Gas Saturation” Tab is used assuming a value for all gridblocks.
If I.options.sat3 = 5, then the “Gas Saturation” Tab is used assuming a value for each layer.

Section 5: Keywords in Input.m File

Below is a list of keywords in the Input.m file

I.options.phi
Input option flag for porosity values
UNITS: [dimensionless]
Note: I.options.phi = 1 allows constant input via I.phi
I.options.phi = 2 allows variable inputs for all gridblocks via phi.txt
I.options.phi = 3 allows variable inputs for each layer via phi.txt

I.options.permx
Input option flag for x-direction permeability values
UNITS: [dimensionless]
Note: I.options.permx = 1 allows constant input via I.kx
I.options.permx = 2 allows variable inputs for all gridblocks via permx.txt
I.options.permx = 3 allows variable inputs for each layer via permx.txt

I.options.permy
Input option flag for y-direction permeability values
UNITS: [dimensionless]
Note: I.options.permy = 1 allows constant input via I.ky
I.options.permy = 2 allows variable inputs for all gridblocks via permy.txt
I.options.permy = 3 allows variable inputs for each layer via permy.txt

I.options.permz
Input option flag for z-direction permeability values
UNITS: [dimensionless]
Note: I.options.permz = 1 allows constant input via I.kz
I.options.permz = 2 allows variable inputs for all gridblocks via permz.txt
I.options.permz = 3 allows variable inputs for each layer via permz.txt

I.options.sat1
Input option flag for initial phase 1 saturation values
UNITS: [dimensionless]
Note: I.options.sat1 = 1 allows constant input via I.sat1i
I.options.sat1 = 2 allows variable inputs for all gridblocks via sat1.txt
I.options.sat1 = 3 allows variable inputs for each layer via sat1.txt

I.options.sat3
Input option flag for initial phase 3 saturation values
UNITS: [dimensionless]
Note: I.options.sat3 = 1 allows constant input via I.sat3i
I.options.sat3 = 2 allows variable inputs for all gridblocks via sat3.txt
I.options.sat3 = 3 allows variable inputs for each layer via sat3.txt

I.options.pres

Input option flag for initial phase 1 pressure values
UNITS: [dimensionless]
Note: I.options.pres = 1 allows constant input via I.Pinit
I.options.pres = 2 allows variable inputs for all gridblocks via pres1.txt
I.options.pres = 3 allows variable inputs for each layer via pres1.txt

I.NX

Number of gridblocks in the x-direction
UNITS: [dimensionless]

I.NY

Number of gridblocks in the y-direction
UNITS: [dimensionless]

I.NZ

Number of gridblocks in the z-direction
UNITS: [dimensionless]

I.LX

Total length of reservoir in the x-direction
UNITS: [feet]

I.LY

Total length of reservoir in the y-direction
UNITS: [feet]

I.LZ

Total length of reservoir in the z-direction
UNITS: [feet]

I.phi

Constant porosity value for entire reservoir (if applicable)
UNITS: [dimensionless]

I.kx

Constant x-direction permeability value for entire reservoir (if applicable)
UNITS: [millidarcy]

I.ky

Constant y-direction permeability value for entire reservoir (if applicable)
UNITS: [millidarcy]

I.kz

Constant z-direction permeability value for entire reservoir (if applicable)
UNITS: [millidarcy]

I.sat1i

Constant phase 1 initial saturation value for entire reservoir (if applicable)
UNITS: [dimensionless]

I.sat3i

Constant phase 3 initial saturation value for entire reservoir (if applicable)
UNITS: [dimensionless]

I.cf

Constant formation compressibility value for entire reservoir

UNITS: [1/psi]

I.Pinit

Constant initial pressure value for entire reservoir (if applicable)
UNITS: [psi]

I.top_depth

Depth to the top of the first (1, 1, 1) gridblock
UNITS: [feet]

I.ddir

Direction of reservoir dip
UNITS: [dimensionless]
Note: I.ddir = 1 allows for dip in the x-direction
I.ddir = 2 allows for dip in the y-direction

I.angle

Angle of reservoir dip
UNITS: [degrees (positive downward)]
Note: I.angle = 0 allows for a horizontal reservoir

I.ellipse

Input option flag for elliptical reservoir (simulated by reducing the porosity and permeability values of non-ellipse containing gridblocks)
UNITS: [dimensionless]
Note: I.ellipse = 1 allows for elliptical reservoir option to be turned on
I.eelipse = 0 allows for elliptical reservoir option to be turned off

I.xsemi

X-direction semi-axis length of ellipse
UNITS: [feet]
Note: For I.ellipse = 1 only.

I.ysemi

Y-direction semi-axis length of ellipse
UNITS: [feet]
Note: For I.ellipse = 1 only.

I.RadSym

Input option flag for radially symmetric approximated wells (only one production well truly simulated) ….
UNITS: [dimensionless]
Note: I.RadSym =1 allows for RadSym option to be turned on
I.RadSym = 0 allows for RadSym option to be turned off

I.RadSym_nw

Number of wells to be approximated by constrained grid.
UNITS: [dimensionless]
Note: For I.RadSym = 1 only.

I.mu1

Viscosity of phase 1
UNITS: [centipoise]

I.mu2
Viscosity of phase 2
UNITS: [centipoise]
I.mu3
Viscosity of phase 3
UNITS: [centipoise]
I.rho1_ref
Density of phase 1 at reference pressure I.rho1_pref
UNITS: [psi/foot]
I.rho2_ref
Density of phase 2 at reference pressure I.rho2_pref
UNITS: [psi/foot]
I.rho3_ref
Density of phase 3 at reference pressure I.rho3_pref
UNITS: [psi/foot]
I.rho1_pref
Reference pressure for density of phase 1
UNITS: [psi]
I.rho2_pref
Reference pressure for density of phase 2
UNITS: [psi]
I.rho3_pref
Reference pressure for density of phase 3
UNITS: [psi]
I.s1r
Residual saturation of phase 1
UNITS: [dimensionless]
I.s2r1
Residual saturation of phase 2 to phase 1
UNITS: [dimensionless]
I.s2r3
Residual saturation of phase 2 to phase 3
UNITS: [dimensionless]
I.s3r
Residual saturation of phase 3
UNITS: [dimensionless]
I.kr1ep
End-point relative permeability of phase 1
UNITS: [dimensionless]
I.kr2ep
End-point relative permeability of phase 2
UNITS: [dimensionless]
I.kr3ep

End-point relative permeability of phase 3
UNITS: [dimensionless]

I.n1

Corey-Brooks relative permeability model exponent for phase 1
UNITS: [dimensionless]

I.n2

Corey-Brooks relative permeability model exponent for phase 2
UNITS: [dimensionless]

I.n3

Corey-Brooks relative permeability model exponent for phase 3
UNITS: [dimensionless]

I.c1

Compressibility of phase 1
UNITS: [1/psi]

I.c2

Compressibility of phase 2
UNITS: [1/psi]

I.c3

Compressibility of phase 3
UNITS: [1/psi]

I.options.setup

Input option flag for type of well setup
UNITS: [dimensionless]
Note: I.options.setup = 1 allows for the wells to be placed manually by user
I.options.setup = 2 allows for the wells to be placed automatically by code

I.options.constraints

Input option flag for operating constraints on wells
UNITS: [dimensionless]
Note: I.options.constraints = 1 allows for the operating constraints on the wells to be turned on
I.options.constraints = 0 allows for the operating constraints on the wells to be turned off

I.nw

Number of wells
UNITS: [dimensionless]

I.orientation

Orientations of well trajectories
UNITS: [dimensionless]
Note: I.orientation = 1 allows for a well to be drilled in the x-direction
I.orientation = 2 allows for a well to be drilled in the y-direction
I.orientation = 3 allows for a well to be drilled in the z-direction

I.rw

Radius of wellbores

UNITS: [feet]

I.skin

Skin of wells
UNITS: [dimensionless]

I.type

Type of operation of wells
UNITS: [dimensionless]
Note: I.type = 1 allows for an injection well to be operated at constant rate
I.type = 2 allows for a production well to be operated at constant pressure
I.type = 3 allows for an injection well to be operated at constant pressure
I.type = 4 allows for a production well to be operated at constant rate

I.condition

Operating condition of wells
UNITS: [ft^3/day or psi]
Note: For I.type = 1, injection rate is positive valued with units of ft^3/day
For I.type = 2, bottomhole pressure is positive valued with units of psi
For I.type = 3, bottomhole pressure is positive valued with units of psi
For I.type = 4, production rate is negative valued with units of ft^3/day

I.constraint_min

Minimum operating constraint on constant pressure wells.
UNITS: [psi]
Note: For I.options.constraints = 1 only.

I.constraint_max

Minimum operating constraint on constant pressure wells.
UNITS: [psi]
Note: For I.options.constraints = 1 only.

I.origin

Gridblock coordinate of well trajectory's origin
UNITS: [dimensionless]
Note: Gridblock coordinate in the direction of I.orientation

I.terminus

Gridblock coordinate of well trajectory's terminus
UNITS: [dimensionless]
Note: Gridblock coordinate in the direction of I.orientation

I.tcoord1

Orthogonal gridblock coordinate of well in second coordinate direction
UNITS: [dimensionless]
Note: If I.orientation = 1, I.tcoord1 is the y-direction coordinate
If I.orientation = 2, I.tcoord1 is the x-direction coordinate
If I.orientation = 3, I.tcoord1 is the x-direction coordinate

I.tcoord2

Orthogonal gridblock coordinate of well in third coordinate
UNITS: [dimensionless]

Note: If I.orientation = 1, I.tcoord2 is the z-direction coordinate
If I.orientation = 2, I.tcoord2 is the z-direction coordinate
If I.orientation = 3, I.tcoord2 is the y-direction coordinate

I.t_final

Total amount of time of simulation
UNITS: [days]

I.dt

Constant linear time-step
UNITS: [days]

I.NumSatSubInt

Integer number of subinterval steps for explicit phase saturation solving
UNITS: [dimensionless]
Note: When I.NumSatSubInt > 1, improved IMPES routine is used.

I.t_save

Constant time increment for saving data into output variables
UNITS: [days]
Note: This value must be a multiple of I.dt

I.bound_type

Type of boundary condition
UNITS: [dimensionless]
Note: I.bound_type = 0 allows for no flow boundaries
I.bound_type = 1 allows for constant pressure boundaries
I.bound_type must be declared as a 1x6 vector with an entry corresponding to a given face of the reservoir such that [-x, +x, -y, +y, -z, +z]

I.bound_cond

Boundary condition for constant pressure boundaries [-x, +x, -y, +y, -z, +z]
UNITS: [psi]
Note: If I.bound_type = 0, I.bound_cond is not relevant to the simulation
If I.bound_type = 0, I.bound_cond is in units of psi
I.bound_cond must be declared as a 1x6 vector with an entry corresponding to a given face of the reservoir such that [-x, +x, -y, +y, -z, +z]

I.SheetName

Name assigned to the particular simulation run
UNITS: [dimensionless]

I.SaveSimData

Input option flag to automatically save simulation data in a *.mat file
UNITS: [dimensionless]
Note: If I.SaveSimData = 1, the simulation data are automatically saved
If I.SaveSimData = 0, the simulation data are not automatically saved

I.PlotOutput

Input option flag to automatically plot some of outputted data
UNITS: [dimensionless]
Note: If I.PlotOutput = 1, plots are created automatically

If I.PlotOutput = 0, plots are not created automatically

I.PlotOutputByWell

Input option flag to automatically plot some of the outputted data by well
UNITS: [dimensionless]
Note: If I.PlotOutputByWell = 1, plots by well are created automatically
If I.PlotOutputByWell = 0, plots by well are not created automatically

I.SaveFigs

Input option flag to automatically save the figures plotted by I.PlotOutput and I.PlotOutputByWell
UNITS: [dimensionless]
Note: If I.SaveFigs = 1, all output plots are saved automatically
If I.SaveFigs = 0, all output plots are not saved automatically

I.FigFormat

File format for saving plots.
UNITS: [dimensionless]
Note: For I.SaveFigs = 1 only.
File formats available: 'fig', 'jpg', 'bmp', 'png', 'tif', 'eps', 'emf', 'pcx', 'pbm', 'pdf', 'pgm', 'ppm'

I.KeepFigsOpen

Input option flag to keep figures open that were plotted by I.PlotOutput and I.PlotOutputByWell.
UNITS: [dimensionless]
Note: If I.KeepFigsOpen = 1, all plots are left open after simulation is complete
If I.KeepFigsOpen = 0, all plots are closed after simulation is complete

I.Excel

Input option flag to export standard suite of output data to a new Excel Tab within the Excel file Matlab_Simulator_20140630.xlsm.
UNITS: [dimensionless]
Note: The Excel file Matlab_Simulator_20140630.xlsm must allow other users to edit it. This can be done through changing the setting under Review -> Changes -> Share Workbook -> Editing. Once this is done, the simulation is run and export data to a tab named after the simulation name (specified by I.SheetName). The exported data in the tab may not appear immediately, so simply save the file, and the data appears. Caution: The exporting process does not delete old data that may still be present in an existing tab of the same name.

Section 6: Keywords within Simulation Code & Output

Below is a list of keywords within the simulation code and output.

A
Sparse "A" matrix used in the pressure equation

B
Sparse "B" matrix used in the pressure equation

Cum1Inew
Temporary variable used to store new cumulative injection data for phase 1

Cum1Pnew
Temporary variable used to store new cumulative production data for phase 1

Cum2Inew
Temporary variable used to store new cumulative injection data for phase 2

Cum2Pnew
Temporary variable used to store new cumulative production data for phase 2

Cum3Inew
Temporary variable used to store new cumulative injection data for phase 3

Cum3Pnew
Temporary variable used to store new cumulative production data for phase 3

G
Gravity "G" vector used in the pressure equation

I
Data structure for storing all inputs from Input.m as well as various other variables:

toggle_input_source: Flag used to toggle between input sources (Matlab=0 versus Excel=1)
N: Total number of gridblocks
por: Vector of porosity values
permx: Vector of x-direction permeability values
permy: Vector of y-direction permeability values
permz: Vector of z-direction permeability values
dx: Vector of length values of gridblocks in the x-direction
dy: Vector of length values of gridblocks in the y-direction
dz: Vector of length values of gridblocks in the z-direction
centerx: Vector of spatial x-direction coordinates of gridblock centers
centery: Vector of spatial y-direction coordinates of gridblock centers
centerz: Vector of spatial z-direction coordinates of gridblock centers
corner: 3-D array of the x-, y-, and z-coordinates of the 8 corners of gridblocks

faces: 4-D array of the x-, y-, and z-coordinates of the 4 corners of the 6 faces of gridblocks
porvol: Vector of pore volumes of gridblocks
cfv: Vector of formation compressibility of gridblocks
NI: Total number of interfaces between gridblocks themselves and exterior
l: Vector enumerating each gridblock (1 to I.N)
IX: 2-D array of all positive x-direction interfaces containing a row entry for each interface with column entries defining the reference gridblock in the first column and the interfacing gridblock in the second column. If the interfacing "gridblock" is an exterior boundary, then the value of the second column entry is set to 0.
IXB: Vector of all x-direction interfaces marked as either 0 (interior boundary), 1 (negative x-direction face boundary), or 2 (positive x-direction face boundary).
IY: 2-D array of all positive y-direction interfaces containing a row entry for each interface with column entries defining the reference gridblock in the first column and the interfacing gridblock in the second column. If the interfacing "gridblock" is an exterior boundary, then the value of the second column entry is set to 0.
IYB: Vector of all y-direction interfaces marked as either 0 (interior boundary), 1 (negative y-direction face boundary), or 2 (positive y-direction face boundary).
IZ: 2-D array of all positive z-direction interfaces containing a row entry for each interface with column entries defining the reference gridblock in the first column and the interfacing gridblock in the second column. If the interfacing "gridblock" is an exterior boundary, then the value of the second column entry is set to 0.
IZB: Vector of all z-direction interfaces marked as either 0 (interior boundary), 1 (negative z-direction face boundary), or 2 (positive z-direction face boundary). Note: z-direction is positive downward.
Ivect: 2-D array concatenation of all interfaces [I.IX;I.IY;I.IZ]
IBvect: Vector concatenation of all boundary interfaces [I.IXB;I.IYB;I.IZB]
Ivect_i: 2-D array of all interior interfaces
Ivect_it: 2-D array of all interior interfaces and their opposites (for transmissibility matrix)
Ivect_itl: Vector of linear indices which define the position of each interior interface entry within transmissibility matrices.
Tdiagl: Vector of linear indices which define the position of the main diagonal entries within transmissibility matrices.
t: Temporal interaction counter
n: Iteration counter
s: Saved data entry position counter
status: Vector of length I.N showing the status of well operation
rho1: Vector of density of phase 1 in gridblocks
rho2: Vector of density of phase 2 in gridblocks
rho3: Vector of density of phase 3 in gridblocks
kr1: Vector of relative permeability of phase 1 in gridblocks
kr2: Vector of relative permeability of phase 2 in gridblocks

kr3: Vector of relative permeability of phase 3 in gridblocks
lr1: Vector of relative mobility of phase 1 in gridblocks
lr2: Vector of relative mobility of phase 2 in gridblocks
lr3: Vector of relative mobility of phase 3 in gridblocks
lrt: Vector of total mobility in gridblocks
kr1v: Vector of single-point upstream-weighted relative permeability values of phase 1 corresponding to each entry of I.Ivect_itl.
kr2v: Vector of single-point upstream-weighted relative permeability values of phase 2 corresponding to each entry of I.Ivect_itl.
kr3v: Vector of single-point upstream-weighted relative permeability values of phase 3 corresponding to each entry of I.Ivect_itl.
ct: Vector of total compressibility in gridblocks

J

Sparse matrix of constant portion of well productivity indices along main diagonal. J is used in the pressure equation.

Jv

Vector form of J

O

Data structure for storing most outputs from simulations:

status: 2-D array of saved W.status at time increments I.t_save
Q1I: 2-D array of saved I.Q1Inew at time increments I.t_save
Q2I: 2-D array of saved I.Q2Inew at time increments I.t_save
Q3I: 2-D array of saved I.Q3Inew at time increments I.t_save
Cum1I: 2-D array of saved I.Cum1Inew at time increments I.t_save
Cum2I: 2-D array of saved I.Cum2Inew at time increments I.t_save
Cum3I: 2-D array of saved I.Cum31Inew at time increments I.t_save
Q1P: 2-D array of saved I.Q1Pnew at time increments I.t_save
Q2P: 2-D array of saved I.Q2Pnew at time increments I.t_save
Q3P: 2-D array of saved I.Q3Pnew at time increments I.t_save
Cum1P: 2-D array of saved I.Cum1Pnew at time increments I.t_save
Cum2P: 2-D array of saved I.Cum2Pnew at time increments I.t_save
Cum3P: 2-D array of saved I.Cum3Pnew at time increments I.t_save
t: Vector of saved times at time increments I.t_save
P1avg: Vector of average pressure saved at time increments I.t_save
S1avg: Vector of average phase 1 saturation saved at time increments I.t_save
S2avg: Vector of average phase 2 saturation saved at time increments I.t_save
S3avg: Vector of average phase 3 saturation saved at time increments I.t_save

Q

Source vector used in pressure equation

Q1Inew

Temporary variable used to store new injection rate data for phase 1

Q1Pnew

Temporary variable used to store new production rate data for phase 1

Q2Inew

Temporary variable used to store new injection rate data for phase 2

Q2Pnew

Temporary variable used to store new production rate data for phase 2

Q3Inew

Temporary variable used to store new injection rate data for phase 3

Q3Pnew

Temporary variable used to store new production rate data for phase 3

Q_b

Vector for constant part of boundary contribution of source term

Q_w1

Vector of source terms for well of I.type = 1

Q_w14

Vector of source terms for well of I.type = 1 and I.type = 4

Q_w2

Vector of productivity portion of source terms for well of I.type = 2

Q_w2c

Vector of well conditions portion of source terms for well of I.type = 2

Q_w23

Vector of productivity portion of source terms for well of I.type = 2 and I.type = 3

Q_w3

Vector of productivity portion of source terms for well of I.type = 3

Q_w3c

Vector of well conditions portion of source terms for well of I.type = 3

Q_w4

Vector of source terms for well of I.type = 4

T

Sparse matrix of constant portion of transmissibility

T1

Sparse matrix of transmissibility of phase 1 used in pressure equation

T2

Sparse matrix of transmissibility of phase 2 used in pressure equation

T3

Sparse matrix of transmissibility of phase 3 used in pressure equation

T_b

Sparse matrix of constant portion of transmissibility of boundary conditions

T_b1

Sparse matrix of transmissibility of phase 1 for boundary conditions used in pressure equation

T_b2

Sparse matrix of transmissibility of phase 2 for boundary conditions used in pressure equation

T_b3

Sparse matrix of transmissibility of phase 3 for boundary conditions used in pressure equation

Tnd

Sparse matrix of constant portion of transmissibility with main diagonal entries equal to 0

W

l: Vector of linear index of all well perforations
type: Vector of well type (I.type) of each well perforation
IDN: Vector of well ID number associated with each perforation
condition: Vector of well condition (I.condition) associated with each perforation
status: Vector of well status associated with each perforation
J: Vector of constant portion of well productivity index associated with each perforation
constraint_min: Vector of minimum well operating constraint of each perforation
constraint_max: Vector of maximum well operating constraint of each perforation
i1: Vector of logical flag for all perforations of W.type = 1
i2: Vector of logical flag for all perforations of W.type = 2
i3: Vector of logical flag for all perforations of W.type = 3
i4: Vector of logical flag for all perforations of W.type = 4
i1f: Vector of indices of W.type for which W.type is equal to 1
i2f: Vector of indices of W.type for which W.type is equal to 2
i3f: Vector of indices of W.type for which W.type is equal to 3
i4f: Vector of indices of W.type for which W.type is equal to 4
il1: Vector of linear index of all well perforations of W.type = 1
il2: Vector of linear index of all well perforations of W.type = 2
il3: Vector of linear index of all well perforations of W.type = 3
il4: Vector of linear index of all well perforations of W.type = 4
perfsbywell: Logical 2-D array of perforations by well within vector W.l

pres1

2-D array of phase 1 pressure values saved at time increment I.t_save

pres1_new

Temporary vector used to store new values of phase 1 pressures

pres1_old

Temporary vector used to store old values of phase 1 pressures

sat1

2-D array of phase 1 saturation values saved at time increment I.t_save

sat1_new

Temporary vector used to store new values of phase 1 saturations

sat1_old

Temporary vector used to store old values of phase 1 saturations

sat3
2-D array of phase 3 saturation values saved at time increment I.t_save
sat3_new
Temporary vector used to store new values of phase 3 saturations
sat3_old
Temporary vector used to store old values of phase 3 saturations
t_prep
Time taken to run through all part of simulation up to Process.m
t_recur
Time taken to run through initial iteration of Process.m
waitbarh
Handle for simulation completion status waitbar

Section 7: Mathematical Formulation

The development of the model is based on the foundational equations of the mass balance and Darcy's law. As seen in Equation 6.1, Darcy's law describes the flow of fluid in porous media and is characterized by relating the superficial velocity, $\bar{u}$, and the potential spatial gradients of pressure and gravity. It should be noted that variables with one and two bars above them denote that these quantities are vectors and tensors, respectively.

$$\bar{u}_j = -\frac{k_{rj}}{\mu_j}\bar{\bar{k}} \cdot \bar{\nabla}\left(P_j + \rho_j g D\right) \tag{6.1}$$

In Equation 6.3.1, viscosity, relative permeability, permeability, pressure, density of fluid, gravitational constant, and the vertical depth in the fluid are denoted as μ_j, k_{rj}, $\bar{\bar{k}}$, P_j, ρ_j, g, and D, respectively. The alignment of the coordinate axes of the system is assumed to have been oriented in line with the three principle directions of permeability in the system, thus diagonalizing the permeability tensor to form Equation 6.2.

$$\begin{bmatrix} u_x \\ u_y \\ u_z \end{bmatrix}_j = -\frac{k_{rj}}{\mu_j}\begin{bmatrix} k_x & 0 & 0 \\ 0 & k_y & 0 \\ 0 & 0 & k_z \end{bmatrix}\begin{bmatrix} \frac{\partial P_j}{\partial x} + \rho_j g \frac{\partial D}{\partial x} \\ \frac{\partial P_j}{\partial y} + \rho_j g \frac{\partial D}{\partial y} \\ \frac{\partial P_j}{\partial z} + \rho_j g \frac{\partial D}{\partial z} \end{bmatrix} \tag{6.2}$$

The mass balance of the system, as seen in generalized, weak form is shown in Equation 6.3.

$$\frac{d}{dt}\left(\int W_i dV\right)+\int\left(\bar{N}_i\cdot\bar{n}\right)dA=\int R_i dV \tag{6.3}$$

Above, the time, overall concentration of component i, volume, flux of component i, outward normal vector from the surface, area of flux, and source/sink term of component i are described by the quantities t, W_i, V, $\bar{N}_i$, $\bar{n}$, A, R_i, respectively. Three flowing phases are considered. Phase pressures and saturations must be accounted for throughout the simulations; one phase pressure and two phase saturations require solution in order to obtain the other phase pressures and saturations. It is assumed that water pressure and both water and gas saturations are solved for within the simulator, so the accompanying equation hence forward is set up to solve for water pressure and both water and gas saturations. Water is denoted with a subscript "1"; oil is marked by the subscript "2"; and gas is marked by the subscript "3".

Consider the first term of Equation 6.3, the temporal derivative of total concentration. The general definition for W_i is provided in Equation 6.4.

$$W_i=\phi\sum_{j=1}^{N_p}S_j\rho_j\omega_{ij}+\left(1-\phi\right)\rho_s\omega_{is} \tag{6.4}$$

It is assumed there is no interaction of either of the fluid components with the solid, thus the term involving ω_{is} becomes irrelevant. It is also assumed that the three phases are completely immiscible, thus:

$$\omega_{1j} = \begin{Bmatrix} 1, \, for \ldots j = 1 \\ 0, \, for \ldots j = 2 \\ 0, \, for \ldots j = 3 \end{Bmatrix} \tag{6.5}$$

$$\omega_{2j} = \begin{Bmatrix} 0, \, for \ldots j = 1 \\ 1, \, for \ldots j = 2 \\ 0, \, for \ldots j = 3 \end{Bmatrix} \tag{6.6}$$

And

$$\omega_{3j} = \begin{Bmatrix} 0, \, for \ldots j = 1 \\ 1, \, for \ldots j = 2 \\ 1, \, for \ldots j = 3 \end{Bmatrix} \tag{6.7}$$

Therefore, $W_1 = \varphi S_1 \rho_1$, $W_2 = \varphi S_2 \rho_2$ and $W_3 = \varphi S_3 \rho_3$. Since we is be using the weak form over finite gridblock volumes, the integral over the volume is simply yield a volume of the gridblock within the simulator and the saturation, density, and porosity is be assumed homogeneous throughout a given gridblock at a particular point in time. Also, the adoption of a slightly compressible fluid with regards to three flowing phases uncovers what we define as the total compressibility,c_t, defined in Equation 6.8.

$$c_t = c_1 + c_2 + c_3 + c_f = \frac{1}{\rho_1}\frac{d\rho_1}{dP} + \frac{1}{\rho_2}\frac{d\rho_2}{dP} + \frac{1}{\rho_3}\frac{d\rho_3}{dP} + \frac{1}{\phi}\frac{d\phi}{dP} \tag{6.8}$$

Equation 6.9 is used for all three phases, and the time derivative is expanded through product rule. Through some mathematical manipulation of the time derivative term, the following equation for component i can be found:

$$\frac{d}{dt}\left(\int W_i dV\right) = V\rho_i\phi\left(\left[S_i c_f + S_i c_i\right]\frac{\partial P_i}{\partial t} + \frac{\partial S_i}{\partial t}\right) \tag{6.9}$$

Dividing the water accumulation and the oil accumulation terms by their respective densities then adding these terms yields (neglecting the capillary pressure change with time):

$$\begin{aligned}&\frac{\frac{d}{dt}\left(\int W_1 dV\right)}{\rho_1} + \frac{\frac{d}{dt}\left(\int W_2 dV\right)}{\rho_2} + \frac{\frac{d}{dt}\left(\int W_3 dV\right)}{\rho_3} \\ &= V\phi\left(\begin{array}{l}\left[\left(S_1+S_2+S_3\right)c_f + S_1c_1 + S_2c_2 + S_3c_3\right]\frac{\partial P_1}{\partial t} \\ + \frac{\partial S_1}{\partial t} + \frac{\partial S_2}{\partial t} + \frac{\partial S_3}{\partial t}\end{array}\right)\end{aligned} \tag{6.10}$$

The simple relationships $S_1 + S_2 + S_3 = 1$ and $\frac{\partial S_1}{\partial t} + \frac{\partial S_2}{\partial t} + \frac{\partial S_3}{\partial t} = 0$ should be remembered in order to arrive at the final expression for the accumulation term in the balance:

$$\frac{\frac{d}{dt}\left(\int W_1 dV\right)}{\rho_1} + \frac{\frac{d}{dt}\left(\int W_2 dV\right)}{\rho_2} + \frac{\frac{d}{dt}\left(\int W_3 dV\right)}{\rho_3} = V\phi c_t \frac{\partial P_1}{\partial t} \tag{6.11}$$

Now we turn to the flux term (the second term) of Equation 6.3. It is first necessary to define the flux, $\bar{N}_i$:

$$\bar{N}_i = \sum_{j=1}^{N_p} \left(\rho_j \omega_{ij} \bar{u}_j - \phi \rho_j S_j \bar{\bar{K}}_{ij} \cdot \bar{\nabla} \omega_{ij} \right) \tag{6.12}$$

Since ω_{ij} equals either 1 or 0 and are therefore constants, the gradient of ω_{ij} becomes zero, and the dispersive term in the flux definition becomes irrelevant. Therefore, $\overline{N_1} = \rho_1 \bar{u}_1$, $\overline{N_2} = \rho_2 \bar{u}_2$ and $\overline{N_3} = \rho_3 \bar{u}_3$. Dividing the water flux and the oil flux terms by their respective densities then adding these terms yields:

$$\begin{aligned} &\frac{\int \left(\bar{N}_1 \cdot \bar{n} \right) dA}{\rho_1} + \frac{\int \left(\bar{N}_2 \cdot \bar{n} \right) dA}{\rho_2} + \frac{\int \left(\bar{N}_3 \cdot \bar{n} \right) dA}{\rho_3} \\ &= \frac{\int \left(\rho_1 \bar{u}_1 \cdot \bar{n} \right) dA}{\rho_1} + \frac{\int \left(\rho_2 \bar{u}_2 \cdot \bar{n} \right) dA}{\rho_2} + \frac{\int \left(\rho_3 \bar{u}_3 \cdot \bar{n} \right) dA}{\rho_3} \end{aligned} \tag{6.13}$$

Darcy's law Equation 6.1 is then submitted into the flux terms. In order for the integral to be solved for a gridblock, the integrand must be evaluated over each interblock connection then summed for a complete evaluation of the integral.

Finally, the source term (right hand side of Equation 6.3) remains as the source rate of mass of q_i integrated the volume. Now after adding the accumulation and flux terms and equating them to the source terms, Equation 6.4 follows:

$$\phi c_t V \frac{dP_1}{dt} + \frac{\int (\rho_1 \bar{u}_1 \cdot \bar{n})\, dA}{\rho_1} + \frac{\int (\rho_2 \bar{u}_2 \cdot \bar{n})\, dA}{\rho_2} + \frac{\int (\rho_3 \bar{u}_3 \cdot \bar{n})\, dA}{\rho_3} = \int (q_1 + q_2 + q_3)\, dV \tag{6.14}$$

The mass balance described in Equation 6.14 is now prescribed quantities for an individual grid cell i,j,k – where i is the index in the x direction, j is the index in the y direction, and k is the index in the z direction, denoting the center of the grid cell. The lengths of cell i,j,k are described by Δx, Δy and Δz. The fluxes in and out of a cell are described by quantities at the face of the cell, and are given half indices, as seen in Equation 6.15.

$$\begin{aligned}
&\left(\phi c_t V \frac{dP_1}{dt}\right)_{i,j,k} + \left(u_x \Delta y \Delta z\right)_{1,i+\frac{1}{2},j,k} - \left(u_x \Delta y \Delta z\right)_{1,i-\frac{1}{2},j,k} \\
&+ \left(u_x \Delta y \Delta z\right)_{2,i+\frac{1}{2},j,k} - \left(u_x \Delta y \Delta z\right)_{2,i-\frac{1}{2},j,k} \\
&+ \left(u_x \Delta y \Delta z\right)_{3,i+\frac{1}{2},j,k} - \left(u_x \Delta y \Delta z\right)_{3,i-\frac{1}{2},j,k} \\
&+ \left(u_y \Delta x \Delta z\right)_{1,i,j+\frac{1}{2},k} - \left(u_y \Delta x \Delta z\right)_{1,i,j-\frac{1}{2},k} \\
&+ \left(u_y \Delta x \Delta z\right)_{2,i,j+\frac{1}{2},k} - \left(u_y \Delta x \Delta z\right)_{2,i,j-\frac{1}{2},k} \\
&+ \left(u_y \Delta x \Delta z\right)_{3,i,j+\frac{1}{2},k} - \left(u_y \Delta x \Delta z\right)_{3,i,j-\frac{1}{2},k} \\
&+ \left(u_z \Delta x \Delta y\right)_{1,i,j,k+\frac{1}{2}} - \left(u_z \Delta x \Delta y\right)_{1,i,j,k-\frac{1}{2}} \\
&+ \left(u_z \Delta x \Delta y\right)_{2,i,j,k+\frac{1}{2}} - \left(u_z \Delta x \Delta y\right)_{2,i,j,k-\frac{1}{2}} \\
&+ \left(u_z \Delta x \Delta y\right)_{3,i,j,k+\frac{1}{2}} - \left(u_z \Delta x \Delta y\right)_{3,i,j,k-\frac{1}{2}} = \left((q_1 + q_2 + q_3)\Delta x \Delta y \Delta z\right)_{i,j,k}
\end{aligned} \tag{6.15}$$

These flux terms with half indices are now redefined in terms of constant transmissibility across the face, *T*, the mobility across the face, λ, and a pressure difference between the adjacent grid cells across which flux is occurring. As an example, the flux from cell i,j,k to cell i+1,j,k is described below in Equation 6.16.

$$\left(u_x \Delta y \Delta z\right)_{1,i+\frac{1}{2},j,k} = \left(T_x\right)_{1,i+\frac{1}{2},j,k} \lambda_{1,i+\frac{1}{2},j,k} \left(P_{1,i,j,k} - P_{1,i+1,j,k} - \gamma_1 \left(D_{1,i,j,k} - D_{1,i+1,j,k}\right)\right) \quad (6.16)$$

In order to describe the interblock mobility, $\lambda_{1,i+\frac{1}{2},j,k}$, the upstream block mobility is be selected and used as the interblock mobility. The term $\gamma_1$is the specific gravity of phase 1 (water). The upstream block is defined by the block with the higher potential across an interblock connection. In order to describe the constant transmissibility at the face between two cells, i,j,k and i+1,j,k, a harmonic mean of the constant transmissibility between the two grid cells, $T_{i+\frac{1}{2},j,k}$, as seen in Equation 6.3.16 and placed into Equation 6.17.

$$\left(T_x\right)_{1,i+\frac{1}{2},j,k} = 2\left(\frac{1}{\left(\frac{k_x \Delta y \Delta z}{\Delta x}\right)_{i,j,k}} + \frac{1}{\left(\frac{k_x \Delta y \Delta z}{\Delta x}\right)_{i+\frac{1}{2},j,k}}\right)^{-1} \quad (6.17)$$

From Equation 6.17, the pore volume of cell i,j,k is redefined in Equation 6.15. Also, the pore volume and total compressibility product is redefined as $B_{i,j,k}$, the volume compressibility of grid cell i,j,k, is Equation 6.19.

$$\left(\phi V\right)_{i,j,k} = \left(\phi \Delta x \Delta y \Delta z\right)_{i,j,k} \tag{6.18}$$

$$B_{i,j,k} = \left(c_t \phi V\right)_{i,j,k} \tag{6.19}$$

The source rate term is multiplied by the volume of the cell in order to arrive at the quantity $Q_{i,j,k}$ in Equation 6.20. Finally, the temporal derivative of the pressure of cell i,j,k is assigned a simple finite difference approximation in Equation 6.21. Please note that the superscripts on the pressure quantities are temporal indices.

$$Q_{1,i,j,k} = \left(q_1 \Delta x \Delta y \Delta z\right)_{i,j,k} \tag{6.20}$$

$$\frac{dP_{1,i,j,k}}{dt} = \frac{\left(P_1^{n+1} - P_1^{n}\right)_{i,j,k}}{\Delta t} \tag{6.21}$$

Employing all of these newly defined quantities from the recent equations, we decrease the number of quantities in the mass balance of Equation 6.3 and assign implicit indices to the flux and sources terms, as seen in Equation 6.20. Equation 6.20 is further simplified by creating matrices of the volume compressibilities and transmissibilities/mobility products as well as vectors of the pressures and source terms of each grid cell in the system to form a system of equations.

$$\begin{aligned}\left(\overline{\overline{\lambda_{rt}}}\,\overline{T} + \frac{1}{\Delta t}\overline{\overline{B}}\right)\overline{P}_1^{n+1} &= \frac{1}{\Delta t}\overline{\overline{B}}\,\overline{P}_1^{n} + \overline{\overline{\lambda_{r1}}}\,\overline{T}\,\overline{\gamma_1 D} \\ &+ \overline{\overline{\lambda_{r2}}}\,\overline{T}\,\overline{\gamma_2 D} + \overline{\overline{\lambda_{r3}}}\,\overline{T}\,\overline{\gamma_3 D} - \overline{Q}_1^{n+1} - \overline{Q}_2^{n+1} - \overline{Q}_3^{n+1}\end{aligned} \tag{6.22}$$

In order to account for various wells that may be simulated, the source term of grid cell i,j,k is defined in terms of the productivity index's constant portion, $J_{i,j,k}$, a relative mobility, and an implicit pressure difference between the grid cell pressure and well flowing pressure of the well. For a constant rate well, the volumetric flow rate may simply be assigned, but a constant bottom-hole pressure well uses the definition assigned in Equation 6.25 to account for volumetric flow rate from the well. Thus for a constant bottom hole pressure well, two terms is be added to the governing equation, one in the source vector and one in the matrix that is multiplying the implicit pressure vector in Equation 6.24.

$$Q_{1,i,j,k} = J_{i,j,k}\lambda_{1,i,j,k}\left(P_{1,i,j,k} - P_{bhp}\right)^{n+1} \tag{6.23}$$

The constant portion of the productivity index of grid cell i,j,k can be described by the relation in Equation 6.25 where r_w is the well radius, s is the skin term, and r_o is the equivalent wellbore radius as described by Peaceman for a vertical well in Equation 6.26.

$$J_{i,j,k} = \frac{2\pi\sqrt{k_{x,i,j,k}k_{y,i,j,k}}\Delta z_{i,j,k}}{\ln\left(\frac{r_o}{r_w}\right) + s} \tag{6.24}$$

$$r_o = 0.28 \frac{\sqrt{\sqrt{\frac{k_x}{k_y}}(\Delta y)^2 + \sqrt{\frac{k_y}{k_x}}(\Delta x)^2}}{\sqrt[4]{\frac{k_x}{k_y}} + \sqrt[4]{\frac{k_y}{k_x}}} \tag{6.25}$$

In order to incorporate the extra term imposed by the constant bottom-hole pressure wells, a constant portion of the productivity index vector, $\bar{J}$, is defined and used only for constant bottom-hole pressure wells – constant rate well values in this vector are equal to zero. Therefore, the Q vector contains only the opposite of the product of the productivity index and the wellbore flowing pressure for constant bottom-hole wells. Please note that production wells is be assigned negative values within the Q vector. The final working equation can be summarized in Equation 6.3.27. λ_{rt} is defined as the total mobility. C_{pwf} and C_{rate} are defined as the markers which determines if a well operates at constant pressure or constant rate, respectively. Finally, WFC is the well flowing condition described in the input file (bottom-hole pressure for constant pressure wells and injection rate for constant rate wells).

$$\begin{aligned}\left(\overline{\overline{\lambda_{rt}}\overline{T}} + \frac{1}{\Delta t}\overline{\overline{B}} + \overline{\overline{J\lambda_{rt}C_{bhp}}}\right)\bar{P}_1^{n+1} = \frac{1}{\Delta t}\overline{\overline{B}}\bar{P}_1^{n} + \overline{\overline{\lambda_{r1}}\overline{T}}\,\overline{\gamma_1 D} \\ + \overline{\overline{\lambda_{r2}}\overline{T}}\,\overline{\gamma_2 D} + \overline{\overline{\lambda_{r3}}\overline{T}}\,\overline{\gamma_3 D} - \overline{C_{rate}w_{rate}}^{n+1} - \overline{J\lambda_{rt}C_{rate}w_{bhp}}^{n+1}\end{aligned} \tag{6.26}$$

Once the pressure equation is solved implicitly, the water and gas saturations may be obtained through explicitly solving Equations 6.28 and 6.29, which have been derived from Equation 6.9.

$$\bar{S}_1^{n+1} = \left(1 + \left(\bar{P}_1^{n+1} - \bar{P}_1^{n}\right)\left(c_1 + c_f\right)\right)\bar{S}_1^{n} - \frac{\Delta t}{V\phi\psi}\begin{pmatrix} -\overline{\overline{\lambda_{r1}T}}\bar{P}_1^{n+1} + \overline{\overline{\lambda_{r1}T}}\,\overline{\gamma_1 D} \\ +\overline{C_{rate}w_{rate}}^{n+1} + \overline{J\lambda_{r1}C_{rate}\left(w_{bhp} - \bar{P}_1\right)}^{n+1} \end{pmatrix} \tag{6.27}$$

$$\bar{S}_3^{n+1} = \left(1 + \left(\bar{P}_1^{n+1} - \bar{P}_1^{n}\right)\left(c_3 + c_f\right)\right)\bar{S}_3^{n} - \frac{\Delta t}{V\phi\psi}\begin{pmatrix} -\overline{\overline{\lambda_{r3}T}}\bar{P}_1^{n+1} + \overline{\overline{\lambda_{r3}T}}\,\overline{\gamma_3 D} \\ +\overline{C_{rate}w_{rate}}^{n+1} + \overline{J\lambda_{r3}C_{rate}\left(w_{bhp} - \bar{P}_1\right)}^{n+1} \end{pmatrix} \tag{6.28}$$

Such that S_1 and S_3 are the water and gas saturations, respectively. The symbol ψ is the number of saturation substep iterations in the improved IMPES solution technique. If ψ is equal to a value of one, the traditional IMPES solution technique is utilized.

REFERENCES

Aronofsky, J. S., Masse, L., & Natanson, S. G. (1958, January 1). A Model for the Mechanism of Oil Recovery from the Porous Matrix Due to Water Invasion in Fractured Reservoirs. Society of Petroleum Engineers.

Babchin, A., Yuan, J., & Nasr, T. (1998, January 1). Generalized Phase Mobilities In Gravity Drainage Processes. Petroleum Society of Canada. doi:10.2118/98-09

Babu, D. K., & Odeh, A. S. (1989, November 1). Productivity of a Horizontal Well (includes associated papers 20306, 20307, 20394, 20403, 20799, 21307, 21610, 21611, 21623, 21624, 25295, 25408, 26262, 26281, 31025, and 31035). Society of Petroleum Engineers. doi:10.2118/18298-PA

Barbu, A., Hicks, P. J., & Grader, A. S. (1999, December 1). Experimental Three-Phase Flow in Porous Media: Development of Saturated Structures Dominated by Viscous Flow, Gravity, and Capillarity. Society of Petroleum Engineers. doi:10.2118/58357-PA

Bertuzzi, A. F., Fetkovich, M. J., Poettmann, F. H., & Thomas, L. K. (1987, January 1). Wellbore Hydraulics (1987 PEH Chapter 34). Society of Petroleum Engineers.

Blunt, M., Zhou, D., & Fenwick, D. (1995). Three-phase flow and gravity drainage in porous media. *Transport in Porous Media*. doi:10.1007/BF00616926

Blunt, M. J., Fenwick, D. H., & Zhou, D. (1994, January 1). What Determines Residual Oil Saturation in Three-Phase Flow? Society of Petroleum Engineers. doi:10.2118/27816-MS

Bonet, E. J., Cunha, C., Correa, A. C. F., & Elias, V. L. G. (2002, January 1). Gravity Drainage-Lab Tests, Relative Permeability Calculation and Field Simulation. Petroleum Society of Canada. doi:10.2118/2002-033

Brooks, R. J., & Corey, A. T. (1964). Hydraulic properties of porous media.

Buckingham, E. (1914). On Physically Similar Systems; Illustrations of the Use of Dimensional Equations. *Physical Review*. doi:10.1103/PhysRev.4.345

Buckley, S. E., & Leverett, M. C. (1942, December 1). Mechanism of Fluid Displacement in Sands. Society of Petroleum Engineers. doi:10.2118/942107-G

Butler, R. M., & Kanakia, V. (1993, January 1). Recovery Of Heavy And Conventional Oils From Pressure-Depleted Reservoirs Using Horizontal Wells. Petroleum Society of Canada. doi:10.2118/SS-93-08

Cardwell, W. T., & Parsons, R. L. (1949, December 1). Gravity Drainage Theory. Society of Petroleum Engineers. doi:10.2118/949199-G

Cardwell, W. T. (1959, January 1). The Meaning of the Triple Value in Noncapillary Buckley-Leverett Theory. Society of Petroleum Engineers.

Carlson, L. O. (1988). Performance of Hawkins Field Unit Under Gas Drive-Pressure Maintenance Operations and Development of an Enhanced Oil Recovery Project. doi:10.2118/17324-MS

Chen, Z. (2007). *Reservoir simulation: Mathematical techniques in oil recovery*. Philadelphia, PA: SIAM/Society for Industrial and Applied Mathematics.

Corey, A. T., Rathjens, C. H., Henderson, J. H., & Wyllie, M. R. J. (1956, November 1). Three-Phase Relative Permeability. Society of Petroleum Engineers. doi:10.2118/737-G

Courant, R., Friedrichs, K., & Lewy, H. (1967). On the Partial Difference Equations of Mathematical Physics. *Ibm Journal of Research and Development*. doi:10.1147/rd.112.0215

Darcy, H. (1856). Les Fontaines Publiques de la Ville de Dijon.

Delshad, M., & Pope, G. A. (1989). Comparison of the three-phase oil relative permeability models. *Transport in Porous Media*. doi:10.1007/BF00134742

Delshad, M., & Nedrud, M. C. (1997, January 1). Residual Oil Saturation in a Pure Gravity Drainage Regime. Society of Petroleum Engineers. doi:10.2118/37556-MS

Dumore, J. M., & Schols, R. S. (1974, October 1). Drainage Capillary-Pressure Functions and the Influence of Connate Water. Society of Petroleum Engineers. doi:10.2118/4096-PA

Dykstra, H. (1978, May 1). The Prediction of Oil Recovery by Gravity Drainage. Society of Petroleum Engineers. doi:10.2118/6548-PA

Dykstra, H., & Dickinson, W. (1992, September 1). Oil Recovery by Gravity Drainage Into Horizontal Wells Compared With Recovery From Vertical Wells. Society of Petroleum Engineers. doi:10.2118/19827-PA

Espie, A. A., & Brown, C. E. (1994, January 1). A Laboratory Investigation of Gravity Drainage/Waterflood Interaction in Prudhoe Bay. Society of Petroleum Engineers. doi:10.2118/28614-MS

Essley, P. L., Hancock, G. L., & Jones, K. E. (1958, January 1). Gravity Drainage Concepts in a Steeply Dipping Reservoir. Society of Petroleum Engineers.

Ghalambor, A., Asadi, M., LeBlanc, J. L., & Hayatdavoudi, A. (1987, January 1). Utilization of Gravity Drainage Holes in Shallow Oil Recovery by Mining: Part II-A Conceptual Model for Drainage Hole Recovery. Society of Petroleum Engineers. doi:10.2118/17077-MS

Gillham, T., Cerveny, B., & Turek, E. (1996). West Hackberry Tertiary Project. Quarterly technical progress report, July 1September 30, 1996. doi:10.2172/453451

Grader, A. S., & O'Meara, D. J. (1988, January 1). Dynamic Displacement Measurements of Three-Phase Relative Permeabilities Using Three Immiscible Liquids. Society of Petroleum Engineers. doi:10.2118/18293-MS

Guzman, R. E., & Fayers, F. J. (1997, September 1). Mathematical Properties of Three-Phase Flow Equations. Society of Petroleum Engineers. doi:10.2118/35154-PA

Guzman, R. E., & Fayers, F. J. (1997, September 1). Solutions to the Three-Phase Buckley-Leverett Problem. Society of Petroleum Engineers. doi:10.2118/35156-PA

Hagoort, J. (1980, June 1). Oil Recovery by Gravity Drainage. Society of Petroleum Engineers. doi:10.2118/7424-PA
Hall, H. N. (1961, September 1). Analysis of Gravity Drainage. Society of Petroleum Engineers. doi:10.2118/1517-G-PA
Hassker, G. L., Brunner, E., & Deahl, T. J. (1944, December 1). The Role of Capillarity in Oil Production. Society of Petroleum Engineers. doi:10.2118/944155-G
Hyatt, J. H., & Hutchison, D. A. (2005, January 1). Enhanced Oil Recovery in East Texas. Society of Petroleum Engineers. doi:10.2118/93631-MS
Jadhawar, P. S., & Sarma, H. K. (2008, January 1). Scaling and sensitivity analysis of Gas-oil Gravity Drainage EOR. Society of Petroleum Engineers. doi:10.2118/115065-MS
Jadhawar, P. S., & Sarma, H. K. (2010, February 1). Numerical Simulation and Sensitivity Analysis of Gas-Oil Gravity Drainage Process of Enhanced Oil Recovery. Society of Petroleum Engineers. doi:10.2118/133373-PA
Johnston, J. R., & Perry, G. E. (1989). Weeks Island gravity stable CO2 pilot: Final report. doi:10.2172/6545286
Juanes, R., & Patzek, T. W. (2003, January 1). Relative Permeabilities in Co-Current Three-Phase Displacements With Gravity. Society of Petroleum Engineers. doi:10.2118/83445-MS
Juanes, R., & Patzek, T. W. (2004, September 1). Three-Phase Displacement Theory: An Improved Description of Relative Permeabilities. Society of Petroleum Engineers. doi:10.2118/88973-PA
Kantzas, A., Chatzis, I., & Dullien, F. A. L. (1988, January 1). Enhanced Oil Recovery by Inert Gas Injection. Society of Petroleum Engineers. doi:10.2118/17379-MS
Kantzas, A., Chatzis, I., & Dullien, F. A. L. (1988, January 1). Mechanisms of Capillary Displacement of Residual Oil by Gravity-Assisted Inert Gas Injection. Society of Petroleum Engineers. doi:10.2118/17506-MS
Kasiri, N., & Bashiri, A. (2009, January 1). Gas-Assisted Gravity Drainage (GAGD) Process For Improved Oil Recovery. International Petroleum Technology Conference. doi:10.2523/13244-MS
King, R. L., & Lee, W. J. (1976). An Engineering Study of the Hawkins (Woodbine) Field. *Journal of Petroleum Technology*. doi:10.2118/5528-PA
Kulkarni, M. M., & Rao, D. N. (2006, January 1). Characterization of Operative Mechanisms in Gravity Drainage Field Projects Through Dimensional Analysis. Society of Petroleum Engineers. doi:10.2118/103230-MS
Kuuskraa, V. A., "Stranded Oil Resources: The New Domestic Oil Prize", Testimony to U.S. House of Representatives, Subcommittee on Energy and Resources on 'Advances in Technology: Innovations in the Domestic Energy and Minerals Sector', Jul 15, 2004.
Lake, L. W. (1989). *Enhanced oil recovery*. Englewood Cliffs, N.J: Prentice Hall.
Lepski, B., Bassiouni, Z., & Wolcott, J. M. (1998). Screening of Oil Reservoirs for Gravity Assisted Gas Injection. doi:10.2118/39659-MS

Leverett, M. C. (1939, December 1). Flow of Oil-water Mixtures through Unconsolidated Sands. Society of Petroleum Engineers. doi:10.2118/939149-G
Leverett, M. C. (1941, December 1). Capillary Behavior in Porous Solids. Society of Petroleum Engineers. doi:10.2118/941152-G
Leverett, M. C., & Lewis, W. B. (1941, December 1). Steady Flow of Gas-oil-water Mixtures through Unconsolidated Sands. Society of Petroleum Engineers. doi:10.2118/941107-G
Leverett, M. C., Lewis, W. B., & True, M. E. (1942, December 1). Dimensional-model Studies of Oil-field Behavior. Society of Petroleum Engineers. doi:10.2118/942175-G
Lewis, J. O. (1944, December 1). Gravity Drainage in Oil Fields. Society of Petroleum Engineers. doi:10.2118/944133-G
Li, K., & Horne, R. N. (2003, January 1). Prediction of Oil Production by Gravity Drainage. Society of Petroleum Engineers. doi:10.2118/84184-MS
Matthews, C. S., & Lefkovits, H. C. (1956, January 1). Gravity Drainage Performance of Depletion-Type Reservoirs in the Stripper Stage. Society of Petroleum Engineers.
Mirzaei, M., DiCarlo, D. A., Ashouripashaki, M., Dehghanpour, H., & Aminzadeh, B. (2010, January 1). Prediction of Three-Phase Gravity Drainage from Two-Phase Capillary Pressure Curves. Society of Petroleum Engineers. doi:10.2118/129945-MS
Moritis, Guntis. 2006. "CO2 Injection Gains Momentum." Oil and gas Journal, v. 104, no. 15
Paidin, W. R., Mwangi, P., & Rao, D. N. (2010, January 1). Economic Evaluation Within the Scope of the Field Development and Application of the Gas-Assisted Gravity Drainage (GAGD) Process in an Actual Northern Louisiana Field. Society of Petroleum Engineers. doi:10.2118/129723-MS
Peaceman, D. W. (1978, June 1). Interpretation of Well-Block Pressures in Numerical Reservoir Simulation(includes associated paper 6988). Society of Petroleum Engineers. doi:10.2118/6893-PA
Purcell, W. R. (1950, August 1). Interpretation of Capillary Pressure Data. Society of Petroleum Engineers. doi:10.2118/950369-G
Ramey, H. J., & Cobb, W. M. (1971, December 1). A General Pressure Buildup Theory for a Well in a Closed Drainage Area (includes associated paper 6563). Society of Petroleum Engineers. doi:10.2118/3012-PA
Rao, D. N., Ayirala, S. C., Kulkarni, M. M., Paidin, W. R., Sequeira, D. S., & Sharma, A. P. (2004). DEVELOPMENT AND OPTIMIZATION OF GAS-ASSISTED GRAVITY DRAINAGE (GAGD) PROCESS FOR IMPROVED LIGHT OIL RECOVERY. doi:10.2172/836737
Ruark, A. E., (1935). Inspectional Analysis: A Method Which Supplements Dimensional Analysis. Journal of the Mitchell Society vol 51: 127-133
Sahni, A., Beeson, D., & DiCarlo, D. A. (2012, January 1). Field Scale Production Decline Characteristics During Gravity Drainage. Society of Petroleum Engineers. doi:10.2118/154327-MS

Sahni, A., Guzman, R., & Blunt, M. (1996, January 1). Theoretical Analysis of Three Phase Flow Experiments in Porous Media. Society of Petroleum Engineers. doi:10.2118/36664-MS
Schilthuis, R. J. (1936, December 1). Active Oil and Reservoir Energy. Society of Petroleum Engineers. doi:10.2118/936033-G
Spanos, T. J. T., De La Cruz, V., Hube, J., & Sharma, R. C. (1986, January 1). An Analysis Of Buckley-Leverett Theory. Petroleum Society of Canada. doi:10.2118/86-01-05
Stahl, R. F., Martin, W. A., & Huntington, R. L. (1943, December 1). Gravitational Drainage of Liquids from Unconsolidated Wilcox Sand. Society of Petroleum Engineers. doi:10.2118/943138-G
Stone, H. L. (1970, February 1). Probability Model for Estimating Three-Phase Relative Permeability. Society of Petroleum Engineers. doi:10.2118/2116-PA
Stone, H. L. (1973, October 1). Estimation of Three-Phase Relative Permeability And Residual Oil Data. Petroleum Society of Canada. doi:10.2118/73-04-06
Templeton, E. E., Nielsen, R. F., & Stahl, C. D. (1962, June 1). A Study of Gravity Counterflow Segregation. Society of Petroleum Engineers. doi:10.2118/186-PA
Terwilliger, P. L., Wilsey, L. E., Hall, H. N., Bridges, P. M., & Morse, R. A. (1951, November 1). An Experimental and Theoretical Investigation of Gravity Drainage Performance. Society of Petroleum Engineers. doi:10.2118/951285-G
Van Everdingen, A. F., & Hurst, W. (1949, December 1). The Application of the Laplace Transformation to Flow Problems in Reservoirs. Society of Petroleum Engineers. doi:10.2118/949305-G
Verlaan, M., & Boerrigter, P. M. (2006, January 1). Miscible Gas-Oil Gravity Drainage. Society of Petroleum Engineers. doi:10.2118/103990-MS
Walsh, M. P., & Lake, L. W. (2003). *A generalized approach to primary hydrocarbon recovery*. Boston, Mass: Elsevier.
Welge, H. J. (1949, December 1). Displacement of Oil from Porous Media by Water or Gas. Society of Petroleum Engineers. doi:10.2118/949133-G
Welge, H. J. (1952, April 1). A Simplified Method for Computing Oil Recovery by Gas or Water Drive. Society of Petroleum Engineers. doi:10.2118/124-G

Permanent Email: cav212@gmail.com

This thesis was typed by Cameron Artigues Vitter.